NTNU

Norwegian University of
Science and Technology

Investigation of RC Structural Behaviour of Wall-Equivalent Dual System through Non-Linear Analyses.

Undersøkelse av den konstruksjonsmessige oppførselen til veggekvivalent dobbeltsystem i armert betong ved hjelp av ikke-lineære analyser

Samson Amanuel Semere

Master of Science in Civil and Environmental Engineering
Submission date: June 2016
Supervisor: Amir Kaynia, KT

Norwegian University of Science and Technology
Department of Structural Engineering

NTNU
Norwegian University of
Science and Technology

Investigation of RC Structural Behaviour of Wall-Equivalent Dual System through Non-Linear Analyses.

Samson Amanuel Semere

Civil and Environmental Engineering

Submission date: June 2015

Supervisor: Professor II Amir Kaynia, NTNU

Co-supervisor: Nina Øystad-Larsen, Ramboll

Norwegian University of Science and Technology
Department of Structural Engineering

Department of Structural Engineering
Faculty of Engineering Science and Technology
NTNU- Norwegian University of Science and Technology

ACCESSIBILITY

Open

MASTER THESIS 2016

SUBJECT AREA:	DATE:	NO. OF PAGES: 139
Structural dynamics	10 June 2015	(18+80+41)

TITLE:

Investigation of RC Structural Behaviour of Wall-Equivalent Dual System through Non-Linear Analyses.
Undersøkelse av den konstruksjonsmessige oppførselen til veggekvivalent dobbeltsystem i armert betong ved hjelp av ikke-lineære analyser.

BY:
Samson Amanuel Semere

SUMMARY:

The purpose of this thesis is to evaluate the non-linear response of a wall-equivalent dual-system structure. The procedure of the analyses follows the guidelines incorporated in the current Norwegian seismic design code NS-EN 1998-1. The investigated structure is detailed for medium ductility in accordance to NS-EN 1998-1. A representative finite element model of the structure (2D) is created with SeismoStruct and OpenSees software packages with emphasis on capturing the non-linear behavior adequately. Both non-linear static analysis and non-linear time history analysis are executed to simulate earthquake for the structure in question.

Over-strength and period-based ductility factors of the structure are assessed in accordance to FEMA P695 and the results confirmed that a conservative approach is incorporated in NS-EN 1998-1. Although the structure is detailed for DCM, the results from non-linear static analysis revealed that the structure response remained in the elastic range. Furthermore, in the latter analysis the software packages give excellent results in terms of target displacements and base shear forces. Non-linear time history analysis confirmed the results obtained from non-linear static analysis for displacements. Moreover, the importance of distribution of stiffness through the structure with regard to inter-storey drifts is demonstrated. The effect of a soft storey is investigated by increasing the height of the first floor. The results reveal that the inter-storey drifts highly increases at the lower stories rather than at the upper stories.

RESPONSIBLE TEACHER: Professor II Amir Kaynia.

SUPERVISORS: Professor II Amir Kaynia, Nina Øystad-Larsen.

CARRIED OUT AT: Department of Structural Engineering.

Preface

This master thesis is written at the Department of Structural Engineering, Norwegian University of Science and Technology (NTNU) in collaboration with Rambøll Norway (Oslo). The thesis accounts 30 credit points and is conducted during the spring semester of 2016. The topic of this thesis is " Investigation of RC Structural Behaviour of Wall-Equivalent Dual System through Non-Linear Analyses ". It is the authors interest to investigate structural behaviour with Performance-Based Seismic Design, which is not covered in the current curriculum of the structural engineering program at NTNU.

On this occasion, I would like to thank my supervisor Professor II Amir M. Kaynia (NTNU), for sharing his extensive knowledge into the theory of earthquake analysis, for tremendous support and encouragement throughout the entire process. Additionally, I would like to thank my co-supervisor PhD Candidate Nina Øystad-Larsen (Rambøll), for sharing her knowledge, for her contributions during our countless meetings and discussions which has been fundamental to the follow-through and outcome of this master's thesis. Last but not least , I want to thank my family and friends for being helpful and supportive.

Trondheim, 10. June 2016
Samson Amanuel Semere

Abstract

Since the introduction of NS-EN 1998-1, seismic design of structures have become a more salient topic in Norway. The code divides structures into classes for DCH (ductility class high), DCM (ductility class medium) and DCL (ductility class low). The ductility class is related to the strength of the structure: the higher the ductility, the lower the design forces, and hence the strength of the structure. DCM allows reduction of forces because of energy dissipation due to plastic deformation.

The purpose of this thesis is to evaluate the non-linear response of a wall-equivalent dual-system structure. The procedure of the analyses follows the guidelines incorporated in the current Norwegian seismic design code NS-EN 1998-1. The investigated structure is detailed for medium ductility in accordance to NS-EN 1998-1. A representative finite element model of the structure (2D) is created with SeismoStruct and OpenSees software packages with emphasis on capturing the non-linear behavior adequately. Both non-linear static analysis and non-linear time history analysis are executed to simulate earthquake for the structure in question.

Over-strength and period-based ductility factors of the structure are assessed in accordance to *FEMA P695* and the results confirmed that a conservative approach is incorporated in NS-EN 1998-1. Although the structure is detailed for DCM, the results from non-linear static analysis revealed that the structure response remained in the elastic range. Furthermore, in the latter analysis the software packages give excellent results in terms of target displacements and base shear forces. Non-linear time history analysis confirmed the results obtained from non-linear static analysis for displacements. Moreover, the importance of distribution of stiffness through the structure with regard to inter-storey drifts is demonstrated. The effect of a soft storey is investigated by increasing the height of the first floor. The results reveal that the inter-storey drifts highly increases at the lower stories rather than at the upper stories.

Keywords: Behaviour factor, Wall-equivalent dual system, 2D seismic response, Over-strength, OpenSees, SeismoStruct.

Sammendrag

Etter innføringen av NS -EN 1998-1 har dimensjonering av konstruksjoner for jordskjelv blitt et aktuelt tema i Norge. Standarden deler konstruksjoner i klasser for DCH (hy duktilitet klasse), DCM (middels duktilitet klasse) og DCL (lav duktilitet klasse). Klassifiseringen i duktilitet er relatert til styrken av strukturen: jo høyere duktilitet, desto lavere dimensjonerende krefter, og følgelig styrken av strukturen. DCM tillater reduksjon av krefter på grunn av energiopptaket knyttet til plastisk deformasjon.

Hensikten med denne rapporten er å evaluere den ikke-lineære responsen til en struktur med vegg-ekvivalent dobbelsystem. Analysemetoden følger retningslinjene som er innlemmet i dagens norske kode NS-EN 1998-1. Den undersøkte strukturen er dimensjonert for middels duktilitet i henhold til NS-EN 1998-1. En numerisk element modell av strukturen (2D) er utarbeidet med SeismoStruct og OpenSees programvarer med hovedfokus på å anslå den ikke-lineære oppførselen i en tilstrekkelig grad. Både den ikke-lineære statiske analysen og den ikke-lineære tidshistorie analysen er utført for å simulere jordskjelv på den evaluerte strukturen.

Konstruksjonens overstyrke og duktilitets-faktorer er vurdert i henhold til *FEMA P695*, og resultatene bekrefter at det er en konservativ metode som er innlemmet i NS-EN 1998-1. Selv om konstruksjonen er dimensjonert for DCM, viser resultatene fra den ikke-lineære statiske analysen at den seismiske responsen forblir i det elastiske området. I tillegg gir den sistnevnte analysen fra programvarene utmerket resultater av påførte forskyvninger og skjærkrefter. Den ikke-lineære tidshistorie analysen bekreftet de oppnådde resultatene for forskyvninger fra den ikke-lineære statiske analysen. Dessuten er viktigheten av stivhet fordelingen gjennom strukturen med hensyn til skadebegrensningen (forskyvning mellom etasjer) det påvist. Effekten av en fleksibel etasje er undersøkt ved å øke høyden av den første etasjen. Resultatene viser at forskyvningen mellom etasjene øker betydelig på de lavere enn på de øvre etasjene.

Nøkkelord: Konstruksjonsfaktor, Vegg-ekvivalent dobbeltsystem, 2D seismisk respons, Overstyrke, OpenSees, SeismoStruct.

Contents

List of Figures

List of Tables

Chapter 1

Introduction

1.1 Background

In Norway, seismic design was not mandatory until the norm, NS 3491-12, was first implemented in 2004. A similar but renewed norm, denoted as NS-EN 1998-1 [31], was re-published in 2010 that deals with seismic loads and classes, as well as effectively specifies and adopts design requirements for all type of structures.

Seismic design allows structural detailing of materials beyond their elastic range due to energy dissipations. Therefore, the deformations in the structure are permanent and should be treated cautiously. The current design code NS-EN 1998-1, for instance, implies requirements and gives simplified guidelines for structures situated in seismic areas. Adopting such simplified methods, i.e. a straight-forward procedure, can hinder junior engineers from deepen their knowledge in the seismic analyses and not think beyond these limitations.

Furthermore, the code contains procedures for linear and non-linear, static or dynamic analysis. However, in practice, considering the financial and time constraints, the simplified methods are mainly used. Contrarily, Performance-Based Seismic Design (PBSD) assesses structural behaviour under seismic loads and tries to maximize the utility of the structure at a minimum expected cost. The avant-garde of PBSD is to evaluate seismic response in terms of displacements and not forces, which are the primary indicators of a structural damage.

In that case, the non-linear methods best approach the correct evaluation of seismic analysis, and in reaching a prominent numerical solution, the finite element based software packages execute the analyses preeminently. However, the accuracy of the solution, based on PBSD method, depends on how analysts's implement the finite element model. In fact, before performing the analyses, a deeper understanding of the problem is necessary and any examiner should accurately be aware of the sensitiveness of the results in correspondence to the methods adopted.

The investigated structure is a four storey RC (reinforced concrete) residential building allocated in Bergen. The structure is a wall-equivalent dual system: columns and beams carry weight (secondary seismic elements), whereas shear walls (primary seismic elements) mainly withstand the horizontal seismic loads. The building is relatively designed according to such a simplified procedure, i.e. the lateral force method in NS-EN 1998-1, for ductility class medium (DCM), and the resulting seismic performance is closely evaluated through non-linear analyses.

1.2 Thesis Objectives

The objectives of this thesis are summarized in the following points:

- Design of a structure in accordance to NS-EN 1998-1.
- Assessment of the non-linear analyses procedures provided in NS-EN 1998-1, i.e. the Pushover Analysis (PA) and the Non-Linear Time-History (Dynamic) Analysis (NLTHA).
- Discuss and compare the results obtained from PA and NLTHA.

1.3 Method

Firstly, the structure is detailed in accordance to the Norwegian norms, including NS-EN 1998-1. The building is characterized with regular geometry and plan to accommodate the use of Lateral Force Method. The design is computed in Robot Structural Analysis (Robot) to determine eigenvalues, shape modes and drift displacements. Then, two different finite element based software packages, i.e. OpenSees and SeismoStruct, are used to compare the results obtained from Robot. The aim is to achieve an accurate numerical model, from 3D to 2D, for the non-linear analyses. The latter software programmes are used to study the structural behaviour and response in non-linear static and dynamic analysis. The results are evaluated to reveal the accuracy and shortcomings of static and dynamic procedures, differences between the software packages and to compare the capacity required in NS-EN 1998-1 versus the acquired results.

1.4 Thesis Outline

The structure of the thesis is as follows:

Chapter 2 - Theoretical background

This chapter contains the theoretical backgrounds needed to utilize the different types of analysis. Furthermore, it provides general knowledge of earthquake and the software packages used.

Chapter 3 - Design

The structure is designed and detailed in accordance to the current Norwegian codes. Lateral force method is adopted for the linear static analysis. The natural periods and modes of the elastic model are determined by Robot [41]. Shear walls are detailed in accordance to NS-EN 1998-1, where over-strength and ductility are accounted for through the so-called behaviour factor.

Chapter 4 - NUMERICAL STRUCTURAL MODEL

This chapter contains the assessment of the numerical models of the structure and the element types utilized in the non-linear analyses. The results are the natural periods and the first four translational modes.

Chapter 5 - Pushover Analysis

This chapter contains the assessment of the non-linear static analysis, i.e Pushover Analysis (PA). The outcome is the determination of the over-strength and period-based ductility of the structure in accordance to *FEMA P695* [17]. In addition, the target displacement is determined in accordance to NS-EN 1998-1 and the chapter concludes with a discussion of the results.

Chapter 6 - Non-linear Time History Analysis

This chapter contains the assessment of the Non-Linear Time-History Analysis. The results are presented and compared with PA's results. The chapter concludes with a discussion of the results.

Chapter 7 - Further Analysis

The chapter contains the investigation of the structural response with regard to soft-storey mechanism. The height of the first floor is increased, ergo, increasing the structure's total height. PA and NLTHA of the new system are computed and the results are compared with the results of the original model. Furthermore, the effect of modelling approach, fibre-section versus shell element model, is investigated.

Chapter 8 - Conclusion

Main conclusion and remarks are presented.

Chapter 2

Theoretical background

2.1 Seismology

Earthquake engineering is an interdisciplinary branch of engineering that deals with the effects of earthquakes on people and their environment. The core aim is to built structures more resistant to such event and reduce damages. However, it requires an advanced knowledge and contribution from different fields, i.e. seismology and engineering. The field of seismology, a Greek word *seismos* for earthquake and *logos* for science, studies the internal structure and behaviour of the earth related to earthquake phenomena [22]. The earth's crust is composed of various plates denoted continental (African, American, Antarctic, Australia-Indian, Eurasian and Pacific) and about 14 subcontinental plates (e.g., Caribbean, Cocos, Nazca, Philippine, etc.). Figure 2.1 illustrates earth's plate tectonics [22].

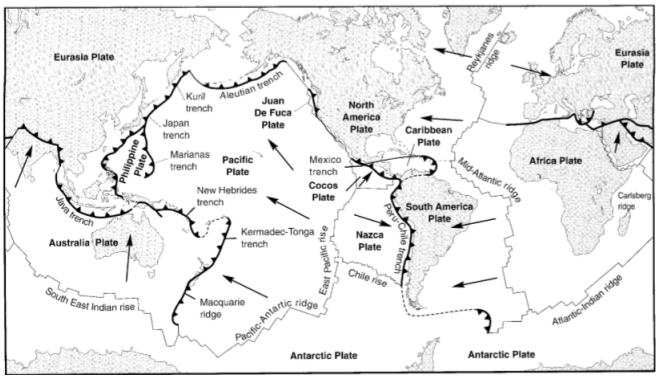

Figure 2.1: The major tectonic plates, mid-oceanic ridges, trenches and transform faults of the earth. The Figure is a replication from Kramer [22].

Three types of boundaries confines such plate tectonics: spreading-ridges or spreading rifts boundaries, subduction zone boundaries, transform fault boundaries, and influences the nature of the earthquakes. In geological terms, the movement between two portions of the crust is known as faults. Thus, they can extend both in length and depth. Faults classification depends on the movement and direction of the strike and dip.

An earthquake results from a rupture of the rock along a fault where its starting point is known as focus or hypo-centre. Thus, it originates at a focal depth below the ground surface. The point

on the ground surface directly above the focus is known as an epicentre. The distance between the epicentre and a site is known as the epicentre distance and the focal distance is the space between the site and the focus. Figure 2.2 gives a better insight of the aforementioned facts.

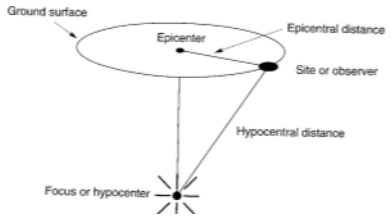

Figure 2.2: Notation for description of earthquake location. The Figure is a replication from Kramer [22].

When an earthquake occur, an elastic energy is released in the Earth's crust that creates seismic waves [22]. There are two types of seismic waves: body and surface waves. P- and S- waves are the two main types of body waves, that denote as pressure and shear waves, and travels through the interior part of the earth. Surface waves, however, results from the interaction between body

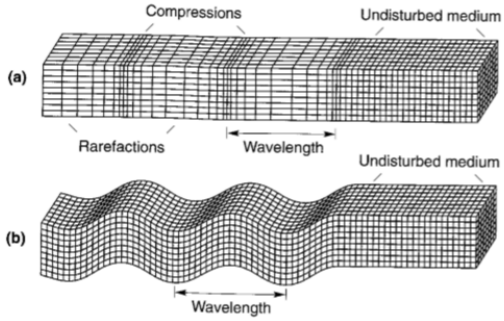

Figure 2.3: Deformations produced by body waves:(a)P-waves;(b)SV-waves. The Figure is a replication from Kramer [22].

waves and the surface layers of the earth. The two most common surface waves are Rayleigh and Love waves that travel either in a vertical or parallel direction to the surface. Figure 2.3 and 2.4 illustrates the four above-mentioned types of waves.

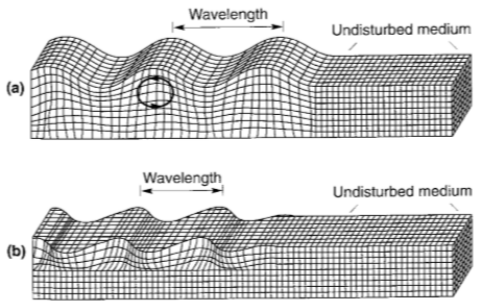

Figure 2.4: Deformations produced by surface waves:(a)Rayleigh wave;(b)Love wave [22].

2.1.1 Size of earthquakes

The oldest measurement of an earthquake size is the quake intensity. It is a qualitative description of the effects of an earthquake, by observing the damages and human reactions, at a particular place. The intensity is generally greatest in the vicinity of the epicentre. Figure 2.5 highlights different intensity classes and their respective descriptions, according to Mercalli [22].

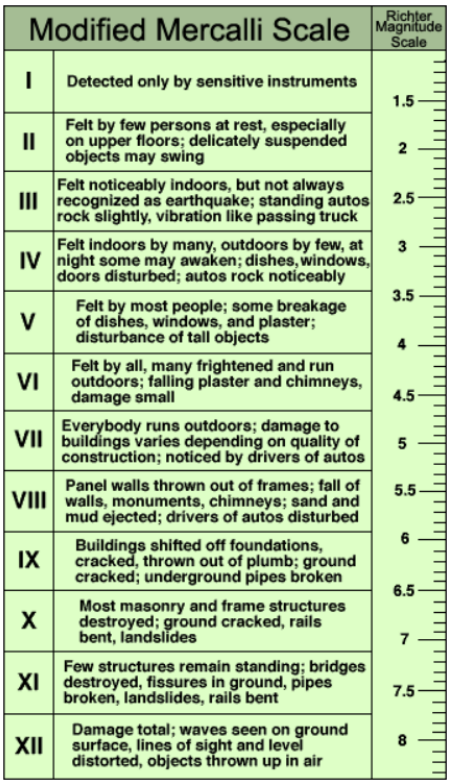

Figure 2.5: Modified Mercalli Intensity Scale versus Richter Scale. The Figure is a replication from Missouri department of geology [2].

During an earthquake, the energy released increases without necessarily increasing the rate of the ground-shaking. This phenomenon is known as saturation [22]. Similarly, Moment Magnitude describes the size of a large quake without depending on the ground-shaking levels and saturation. Thus, it is based on the seismic moment, which is a direct measure of the factors that produce rupture along a fault. The Moment Magnitude is given by

$$\mathrm{M_w} = \frac{\log \mathrm{M_0}}{1.5} - 10.7 \tag{2.1}$$

Here, $\mathrm{M_0}$ is the seismic moment.
The traditional way of measuring the strength of an earthquake is through Richter Scala. A scale based on the amplitude of the ground motion recorded on seismographs and the distance to the earthquake (see Figure 2.6). Richter Scala is logarithmic measure, meaning that an increase of one unit on the scale corresponds to an increase of 10 times in the ground motion and circa 32 times in the energy released by the earthquake.

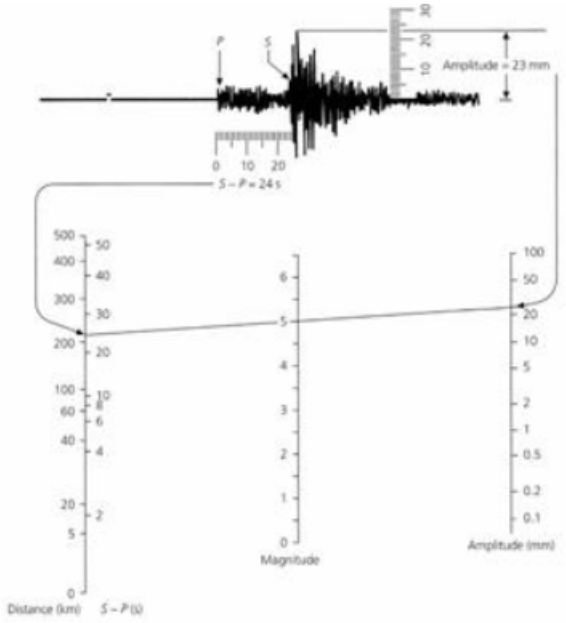

Figure 2.6: Richter scale measurement. The Figure is a replication from NNSN [29].

2.2 Earthquake in Norway

According to NORSAR [37], Norway is not known as a place that is most prone to earthquakes; however, it is the area in northern Europe that is experiencing the most earthquake nowadays. The largest earthquake that attracted most attention dates to 1904 when a 5.4 magnitude quake struck the southern part of Oslo and was felt in many parts of Scandinavia and Northern Europe. As a result, there were some ascertained damages to buildings but no data was gathered for injuries. Figure 2.7 shows earthquake discoveries from 1979 until 2015, where red symbols are earthquake felt by humans and yellow ones are earthquakes with a magnitude of 4 or higher.

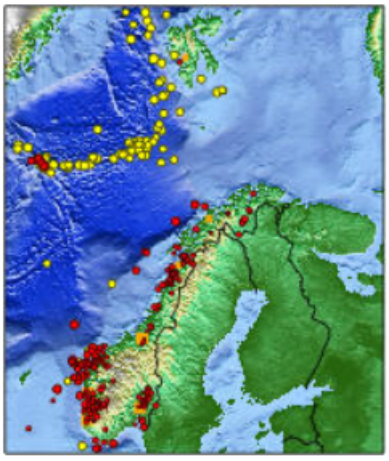

Figure 2.7: Earthquake in Norway from 1979 until 2015. This Figure is a replication from NORSAR [37].

It is clear that the most active zones are in the western part of Norway and in the North

Sea. However, the eastern part of Norway, Nordland and Finnmark are experiencing frequent earthquakes as well.

The investigated structure in this report is a residential building in Bergen. In Bergen, the most recent major earthquake event dates on December 2000 with strength of 3.2 Richter Scala. Recently in 2012, another happening took place with a strength of 2.9. Figure 2.8 shows earthquake activities that have occurred in Bergen and surrounding areas since 2010 [37].
The peak ground acceleration or PGA of an earthquake is the largest acceleration recorded by

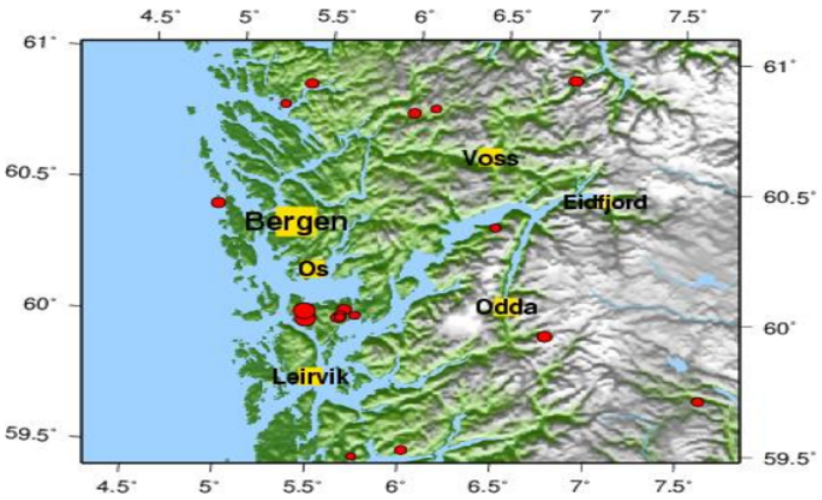

Dato	Kl. (Lokal tid)	Bredde-grad	Lengde-grad	Styrke	Sted
10/02/2010	07:04:36	59.80	6.46	2.2	Ca. 18 km nord-nordoest for Sauda
16/01/2011	23:43:04	59.89	5.48	1.7	Ca. 13 km nord for Leirvik
13/11/2011	03:39:17	60.44	5.29	2.0	Ca. 9 km vest-nordvest for Bergen
14/03/2012	20:22:28	59.52	5.58	3.2	Ca. 20 km nordoest for Haugesund
24/03/2012	07:05:19	60.82	4.88	2.9	Ca. 57 km vest-nordvest for Bergen
24/03/2012	12:06:30	60.64	6.40	3.0	Ca. 1 km nordvest for Voss
02/07/2012	09:03:33	60.44	6.04	3.0	Ca. 29 km soervest for Voss
03/06/2013	18:37:28	59.44	5.73	2.5	Ca. 25 km oest for Haugesund
21/01/2014	07:39:04	61.05	4.56	2.3	Ca. 43 km soervest for Askvoll
23/07/2015	12:31:22	59.70	5.88	2.7	Ca. 22 km oest-soeroest for Leirvik

Figure 2.8: Seismic activities in Bergen and vicinity. The Figure is re-plotted from NORSAR [37].

a seismograph. For the Bergen region, the design PGA is $0.85\mathrm{m/s^2}$, which is determined by using a formula from NS-EN 1998-1 [31]:

$$\mathrm{a_g} = \gamma_\mathrm{I} \times\ 0,8 \times\ \mathrm{a_{g40Hz}} \tag{2.2}$$

where, $\mathrm{a_{40Hz}}$ is the PGA and γ_I is an importance factor. The value of $\mathrm{a_{40Hz}}$ can be read in NS-EN 1998-1 NA3.2.1. Figure 2.9 presents different contours of $\mathrm{a_{40Hz}}$, in the southern part of Norway, with an annual exceedance probability of $2.1 \cdot\ 10^{-3}$. Bergen is located $60^0 20'\mathrm{N}$ and $5^0 20'\mathrm{E}$, as latitude and longitude respectively.

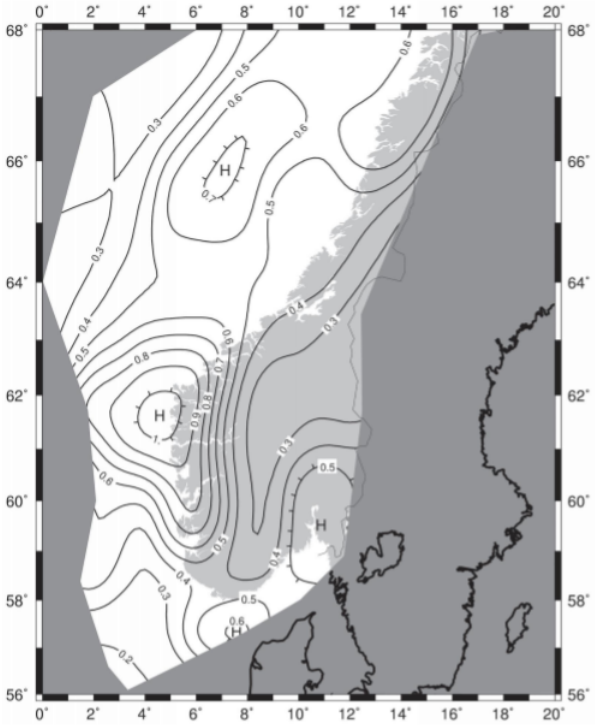

Figure 2.9: Seismic zones in the southern part of Norway and $\mathrm{a}_{40\mathrm{Hz}}$ in $\mathrm{m/s^2}$ according to NS-EN 1998-1 [31].

2.3 Earthquake response analysis

Seismic analysis consists of the determination of structural response during an earthquake. Different methods applied throughout this report are described below.

2.3.1 Linear static analysis

Introduction

The standard design procedure applied in NS-EN 1998-1 [31] is the modal response spectrum analysis. This report uses the Lateral force method, because it is a relatively easy and less time-consuming approach that can be adopted for all types of structures within its limitation. Furthermore, it is a straight-forward method for determining forces and displacements of structures excited by the earthquake. Moreover, the contribution of the higher modes are not accounted without affecting the global response, i.e. the base shear and overturning moment.

Limitation of the procedure

The lateral force method is only applied when the effects of higher modes are insignificant and the fundamental translational mode in the direction of the applied lateral forces governs the response. NS-EN 1998-1 gives the following restrictions:

- the fundamental period of the building is less than 2 s or 4 times the corner period $\mathrm{T_C}$
- the building must fulfil the requirement for regularity (see NS-EN 1998-1 clause 4.2.3.3).

Fundamental Period and Base shear

NS-EN 1998-1 promotes different approaches to find the fundamental period, $\mathrm{T_1}$, which estimate or define its determination analytically. It must be noted that the linear static method can only be used on an elastic building model.
The seismic shear above the foundation or the top of a rigid basement (base shear), $\mathrm{F_b}$, is separately determined in horizontal directions X and Y, on the basis of the 1^{st} translational mode period and direction of interest. Thus,

$$\mathrm{F_b} = \mathrm{S_d}(\mathrm{T_1}) \cdot \mathrm{m} \cdot \lambda \tag{2.3}$$

Here, $\mathrm{S_d}(\mathrm{T_1})$ is the design spectral acceleration, m is the total mass of the building and λ is a correction factor defined by the number of stories in the building and the fundamental period.

Pattern of Lateral Loads

The base shear defined by Eq. (2.3) is the resultant of a set of inertia forces on the masses $\mathrm{m_i}$ associated with degree of freedom *i* in the horizontal direction. Those lateral forces are defined as

$$\mathrm{F_i} = \mathrm{F_b} \cdot \frac{\mathrm{h_i} \cdot \mathrm{m_i}}{\sum(\mathrm{h_i} \cdot \mathrm{m_i})} \tag{2.4}$$

Here $\mathrm{m_i}$ is the floor mass and $\mathrm{h_i}$ is the height of the floor.

Disadvantages

The linear static analysis is implemented when the contribution of higher modes are insignificant and the structural response is dominated by the first translational mode. Moreover, the analysis can only be applied in the elastic domain. Generally, seismic analysis is more reliable when non-linear methods are applied and deformations post-elastic domain are determined. Furthermore, the linear static analysis does not account for the variation of the modal properties when the structure responds in the post-elastic domain.

2.3.2 Non-linear static (Pushover) analysis

Introduction

The prime use of non-linear static analysis is for the assessment and evaluation of seismic performance of new designs. This analysis method is a practice procedure that estimates the structural capacity of buildings in the post-elastic range. It is commonly denoted as *Pushover Analysis* , (PA), and enhances the lateral force procedure into the non-linear regime. PA is conducted with constant gravity loads and monotonically increasing lateral loading applied on the masses of the structural model until the displacement of interest is reached [15].

In this report, the structural behaviour is observed until the value of roof displacement equivalent to $0.8\mathrm{F_{max}}$ is obtained, in accordance to *FEMA P695* [17]. The most significant result of the analysis is the characteristic non-linear force- displacement relationship, also denoted *capacity curve*, of the multi-degree of freedom (MDOF) system. In principle, any force and displacement could be chosen. In this thesis, for instance, base shear - roof (top) displacement relationship is used as representative of force and displacement (see Figure 2.10). Moreover,

the PA-method is also applied to quantify the over-strength and period-based ductility in the inelastic domain, which are discussed in accordance to *FEMA P695* (Federal Emergency Management Agency). The reason is it provides an easy and explicit procedure for assessment of the afore-stated factors rather than NS-EN 1998-1.
In order to account for P-δ effects, all the gravity loads must clearly be included in the analysis, [9]. As a reference to control displacement point, the centre of the mass at the roof level is chosen.

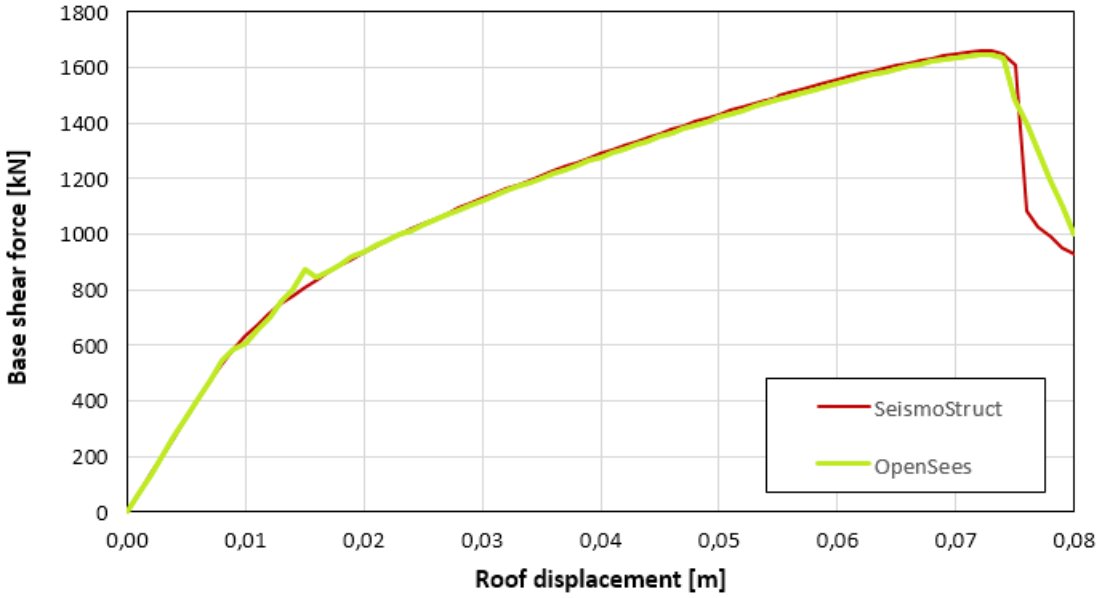

Figure 2.10: Non-linear static curves.

Lateral Load Vector

The load vectors must simulate the inertia forces due to a horizontal component of the seismic action. According to NS-EN 1998-3 [32], two different lateral load patterns should be applied. The first one is based on a modal pattern corresponding to the inertia forces of the 1^{st} mode, i.e. purely translational, in the horizontal direction. The second one is uniform lateral pattern based on mass distribution regardless of elevation, which is not used in this report to avoid underestimation (in upper stories) and overestimation (in lower stories) of the drifts according to a study conducted by G. Rakesh K and A.ChopraK [18].

Displacement

A mathematical model of a single degree-of-freedom system, SDOF, is implemented to represent the lateral force- displacement relationship. This method is also known as the N2-method [15] and is incorporated in NS-EN 1998-1. The N2-procedure is proposed by P.Fajfar [13] and is briefly described below.
The equation of motion of a planar multi degree-of-freedom (MDOF) system that explicitly accounts only lateral translational degrees of freedom is

$$\mathbf{M\ddot{u} + Ku = MT\ddot{u}_g} \tag{2.5}$$

Here, **M** is the diagonal mass matrix, **Ku** represents the internal forces, **T** is a unit vector, $\ddot{u}_g$ and **ü** are representing the ground acceleration and the motion of the system, respectively. It is worth mentioning that damping is not included for simplicity, but its influence is accounted in the design spectrum. The most critical assumption is that the mode shape $\mathbf{\Phi}$ is constant, i.e that remains unmodified during the structural response due to excitation. In addition, $\mathbf{\Phi}$ is normalized, for convenience, resulting that the component at top is 1. The displacement vector **u** is given as

$$\mathbf{u} = \mathbf{\Phi} d_n \tag{2.6}$$

Here, d_n is the time-dependent roof displacement. From statics it follows that the internal forces are equal to the lateral loads **F** . Thus,

$$\mathbf{F} = \mathbf{Ku} = p\mathbf{M\Phi} \tag{2.7}$$

Here, p controls the magnitude of the lateral loads. By substituting Eq. (2.7) and (2.6) into Eq. (2.5) and by multiplying from the left side with $\mathbf{\Phi}^T$, it is obtained

$$\mathbf{\Phi}^T\mathbf{M\Phi}\ddot{d}_n + \mathbf{\Phi}^T\mathbf{M\Phi}p = -\mathbf{\Phi}^T\mathbf{MT}\ddot{u}_g \tag{2.8}$$

Subsequently, by multiplying and dividing the left hand side with $\mathbf{\Phi}^T\mathbf{MT}$, the equation of the equivalent SDOF system is

$$m^*\ddot{d} + F^* = -m^*\ddot{u}_g \tag{2.9}$$

Here, the equivalent mass of the SDOF system m^* is

$$m^* = \Phi^T\mathbf{MT} = \sum m_i \cdot \Phi_i \tag{2.10}$$

where, m_i is the lumped storey mass and Φ_i is the value of the normalized mode shape at storey *i*. Its force, F^*, and displacement, d^*, are

$$F^* = \frac{F_b}{\Gamma} \tag{2.11}$$

$$d^* = \frac{d_n}{\Gamma} \tag{2.12}$$

where:

$$\Gamma = \frac{m^*}{\sum m_i \cdot \Phi_i^2} \tag{2.13}$$

Here, F_b is the base shear force, d_n is the displacement at the control point (roof) and Γ is the transformation factor of that mode in the direction of the lateral forces. The base shear force and control displacement curve is converted to an idealized bi-linear curve by requiring that the deformation energy up to the target displacement is equivalent for both curves. The elastic period, T^*, of the idealized equivalent SDOF system is given as

$$T^* = 2\pi \cdot \sqrt{\frac{m^* \cdot d_y^*}{F_y^*}} \tag{2.14}$$

The yield force, F_y^*, of the elastic-perfectly plastic model is the value of base shear force, F^*, at the first formation of the plastic mechanism for both the modelled and idealized system. Furthermore, the yield displacement, d_y^*, is determined by requiring that the deformation energy

of the idealized bi-linear curve at the displacement of the equivalent SDOF system when the plastic mechanism forms, d_m^*, is equal to the actual capacity-curve at the same point, E_m^* :

$$d_y^* = 2(d_m^* - \frac{E_m^*}{F_y^*}) \tag{2.15}$$

The maximum displacement induced by the earthquake at the control node is denoted the *target displacement* and depends on the response domain. According to NS-EN 1998-1 Appendix B.5, the target displacement, d_t , is calculated as follows:

a) For short periods, i.e. $T^* \leq T_c$, the response is elastic if

$$\frac{F_y^*}{m^*} \geq S_e(T^*) \tag{2.16}$$

Here, $S_e(T^*)$ is the elastic acceleration response spectrum at the period T^*. The target displacement of SDOF is then given by the *"equal displacement rule"*

$$d_t = d_{et}^* \tag{2.17}$$

where,

$$d_{et}^* = S_e(T^*) \cdot \ (\frac{T^*}{2\pi})^2 \tag{2.18}$$

The response is inelastic if

$$\frac{F_y^*}{m^*} \leq S_e(T^*) \tag{2.19}$$

and the target displacement is defined as

$$d_t^* = \frac{d_{et}^*}{q_u} \cdot \ (1 + (q_u - 1) \cdot \ \frac{T_c}{T^*}) \geq d_{et}^* \tag{2.20}$$

Here, q_u is the ratio between the acceleration in the structure with unlimited elastic behaviour $S_e(T^*)$ and in the structure with limited strength $\frac{F_y^*}{m^*}$. Thus,

$$q_u = \frac{S_e(T^*) \cdot \ m^*}{F_y^*} \tag{2.21}$$

b) For long periods, i.e. $T^* \geq T_c$, the target displacement is equal to Eq. (2.13).

If the assumed displacement differs significantly from the target displacement of the SDOF, an iterative approach is required until they are equivalent. In that case, d_m^* can be used as an initial displacement .
For the real MDOF system, the target or expected displacement is

$$d_t = \Gamma \cdot \ d_t^* \tag{2.22}$$

Over-strength and period-based ductility

As afore-stated, pushover analysis is used to quantify the maximum base shear, $\mathrm{F_{max}}$, and roof displacement, $\mathrm{d_u}$. Those parameters are further used to compute the over-strength, Ω, and period based ductility, μ_T. In order to quantify these values, the lateral loads are applied monotonically until a loss of 20% of the base shear capacity ($0.8\mathrm{F_{max}}$) is achieved. According to *FEMA P695* [38], the over-strength and period-based ductility are defined as

$$\Omega = \frac{\mathrm{V_{max}}}{\mathrm{V}} = \frac{\mathrm{F_{max}}}{\mathrm{F_{el}}} \tag{2.23}$$

$$\mu_\mathrm{T} = \frac{\delta_\mathrm{u}}{\delta_\mathrm{y,eff}} = \frac{\mathrm{d_u}}{\mathrm{d_{eff}}} \tag{2.24}$$

Here, $\mathrm{F_{max}}$ is the maximum base shear resistance, $\mathrm{F_{el}}$ is the elastic base shear, $\mathrm{d_u}$ is the ultimate

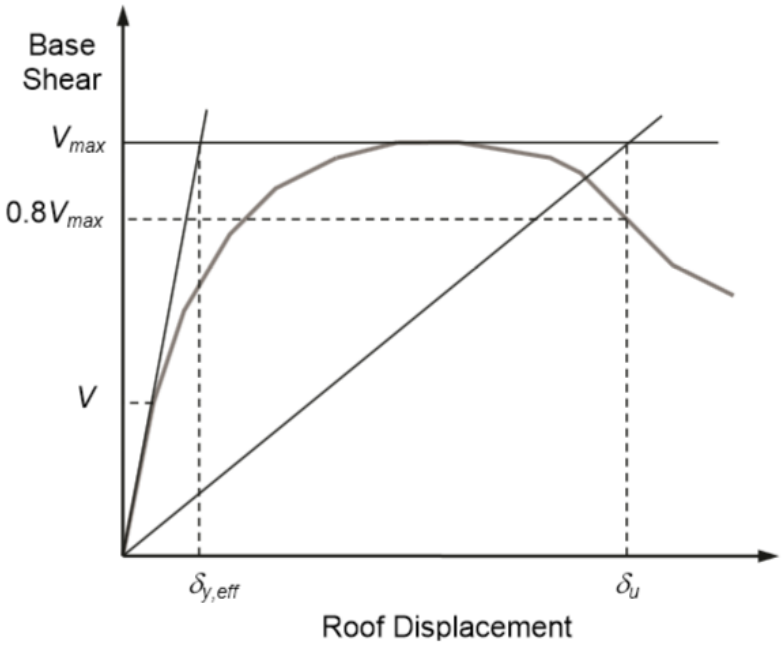

Figure 2.11: Idealized non-linear static pushover curve. The Figure is re-plotted from *FEMA P695* [38].

roof displacement respective to $0.8\mathrm{F_{max}}$, and $\mathrm{d_{eff}}$ is the effective yield roof drift displacement. The parameter $\mathrm{d_{eff}}$ is defined as

$$\mathrm{d_{eff}} = \Gamma \cdot \frac{\mathrm{F_{max}}}{\mathrm{W}} \cdot \frac{\mathrm{g}}{4\pi^2} \cdot \mathrm{T_1^2} \tag{2.25}$$

Here, Γ is the transformation factor defined by Eq. (2.13), $\mathrm{F_{max}}$ is the maximum base shear resistance, W is the building weight, g is the gravity constant and $\mathrm{T_1}$ is the fundamental period computed using eigenvalue analysis. Figure 2.11 illustrates the aforesaid parameters according to $\mathrm{FEMAP695}$.

Disadvantages

In a performance-based seismic design, the use of this method will not exhibit the behaviour of the model after the formation of the first mechanism. As a result, the weakness of the structure

can not be detected in the inelastic domain due to unchanged modal properties. Since PA is based on a SDOF system, the response is dominated by a single mode shape, and can be only suitable for structures governed by one mode. Furthermore, the material degradation in both stiffness and strength is not accounted due to the static nature of the method [5].

2.3.3 Non-linear time history analysis

Introduction

The non-linear time history analysis (NLTHA) provides a more realistic model of structural response to ground shaking. In fact, it provides a more reliable assessment of earthquake performance than non-linear static analysis. Its main practical application is for the retrofit of existing structures. Furthermore, the analysis is also adopted when the effects of higher modes and structural behaviour after the first mechanism are of interest [17]. Additionally, NLTHA provides estimates not only of the peak deformations but of residual ones. The peak deformation is important for the overall safety and integrity of the structure. The residual deformations are the meaningful measure of damage and important for performance-based design.
In NLTHA, the non-linear properties of the structure are considered as part of a time domain analysis. This is performed by incorporating the non-linear material properties into the numerical model.

Seismic Input Motions

For a NLTHA, time histories of the ground motions are needed. Those records will be adopted to simulate the earthquakes in the numerical model [11]. To achieve a reliable data of the structural response, several ground motions must be applied. In fact, NS-EN 1998-1 clause 4.3.3.4.3 [31] requires the application of at least seven ground motions and the average response must be applied in the design. It also states, if only three ground motions are implemented, the result from the most unfavourable one must be used.

The choice and scaling of earthquake ground motions is an essential step in defining the seismic loads that will be applied to a structure during structural analysis. In addition, the selection of historic records must be representative for the site in question, i.e. soil conditions for measurements should match to the soil of the structure analysed [19]. Nowadays, it is preferable to use intensity-based method to scale ground motions rather than spectral matching approach, which modifies the frequency content to match its response spectrum to the interested spectrum. Contrarily, intensity-based scaling technique preserves the original content and only modifies its amplitude [21]. Since the analyses in this thesis are two dimensional due to regularity of the structure, the selected ground motions are individually scaled such that their peak ground acceleration (PGA) matches on average the value $\mathrm{a_g S}$ of the elastic design spectrum [17]. The parameter $\mathrm{a_g}$ represents the design ground acceleration, whereas S is soil factor that depends on the ground in question.

Disadvantages

One of the main disadvantages of NLTHA is the sensitivity of results to the choice of input ground motions. Furthermore, it is a complicated and time requiring approach. In addition,

NLTHA does not explicitly give the overview of the stiffness, strength and ductility of the structure, thereby, it should be supplemented with Pushover analysis.

2.4 Finite element software

2.4.1 Robot

Robot Structural Analysis Professional software provides engineers with advanced BIM (Building Information Modelling) integrated analysis and design tools to understand the behaviour of any structure type and verify code compliance. Moreover, the programme is also used to compute modal and seismic analysis of structures. In this thesis, the software package is only used for the elastic analysis.

2.4.2 OpenSees

The Open System for Earthquake Engineering Simulation (OpenSees) is a software framework for simulating the seismic response of structures. OpenSees [27] has been developed as the computational platform for research in performance-based earthquake engineering at the Pacific Earthquake Engineering Research Centre. It has different material models, elements and solution algorithms. The software is based on finite element methods and interprets scripts of Tcl (Tool command language). Furthermore, it is an open-source and gives access to all earthquake engineering researchers and students. The main advantage is that the user must create the model manually and define all the steps throughout the procedures. This improves the theoretical background and skills of the users. The disadvantages are it lacks a graphical user interface (GUI) and some material models does not perform as they should, i.e. confined elements. Figure 2.12 shows the user interface of the software.

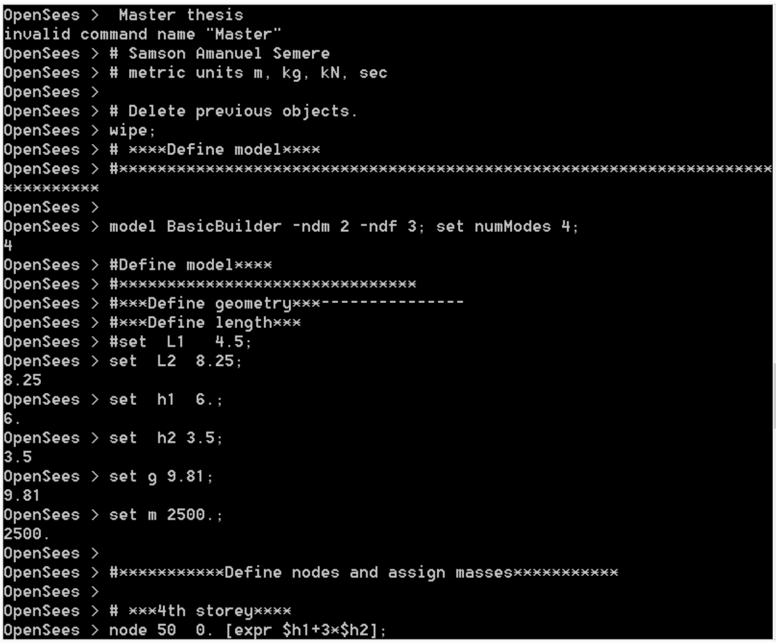

Figure 2.12: OpenSees user interface.

2.4.3 SeismoStruct

SeismoStruct [40] is also a finite element package capable of predicting the large displacement behaviour of structures under static or dynamic loading and accounts both geometric non-linearities and material inelasticity. Concrete and steel models are available, together with a large library of 3D elements that may be used with a wide variety of pre-defined steel and concrete configurations. Due to academic purpose in SeismoStruct, the author has only access to partially-functional package (2D version). The main advantages of this software is it incorporates a visual interface, which reduces the configuration time of models. Other aspects are that SeismoStruct has a full integration with Windows programs, i.e. Excel. Furthermore, it contains eight different types of analysis: dynamic and static time-history, conventional and adaptive pushover, incremental dynamic analysis, eigenvalue, non-variable static loading, and response spectrum analysis. Finally, it has an advanced post-processing facility, including the ability to user-format plots and deformed shapes, which increasing the productivity of users. Figure 2.13 illustrates an example of a shear wall in 2D-configuration. The main disadvantages are computational-time costs, i.e. NLTHA, few possibilities of material and element configurations, and limited informations in the user's manual.

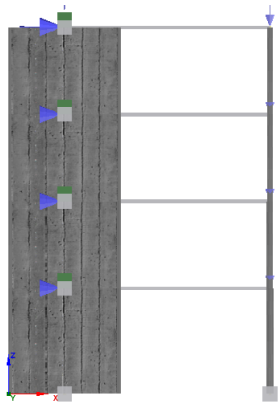

Figure 2.13: SeismoStruct user interface.

Chapter 3

Design

3.1 General

This chapter presents the design of a building with prefabricated hollow core slabs, shear walls, beams and columns elements. The edifice is located in Bergen and is designed for both wind and seismic loads. The chosen ductility class of the structure in the seismic analysis is medium, denoted DCM. The utility of the building is for residential purposes and its geometry is illustrated in Figure 3.1. Furthermore, Figure 3.2 shows the structures model in 3D. The choice of the building and its geometry is performed in collaboration with Nina Øystad-Larsen. The design is performed according to NS-EN 1990 [33], NS-EN 1992-1-1 [30], NS-EN 1991-1-3 [34], NS-EN 1991-1-4 [36], NS-EN 1993-1-1 [35] and NS-EN 1998-1 [31]. According to NS-EN 1998-1 Table 4.1, the building fulfils the requirements of both regularity and elevation criteria. Therefore, the Lateral Force Method can be applied when assessing seismic analysis. The structure is modelled in 3D, to minimize the accidental torsion, and computed by using Robot Structural Analysis [41]. The shear walls mainly withstands the lateral forces, while the beams and columns are secondary seismic members since they are hinged at ends.

3.2 Materials

The material properties that are permitted for DCM structures are of Class B or C for reinforcement and Class $\mathrm{C16/20}$ or higher for concrete [12]. Furthermore, the exposure class of the building is an aspect that must be accounted in the choice of the material properties. Hence, hollow core slabs are of $\mathrm{C45/55}$, whereas $\mathrm{C30/37}$ for walls and columns reinforced with $\mathrm{B500NC}$. Beam elements are of steel quality $\mathrm{S355}$. Hollow core slabs and columns are prefabricated, while the walls are cast in-site. The RC elements belong to$\mathrm{XC3/M60}$ with $25 + / - 10\ \mathrm{mm}$ cover.

3.3 Loads

The dimensions of the hollow core slabs were selected from the Betong-Elementer Bind A book. The choice is made in accordance to the live load, concrete levelling ($50\ \mathrm{mm}$) and span width in the serviceability limit state (SLS). The maximum span is 6 m. Hence, the thickness of the hollow core is 200 mm, denoted HD200. For detailed information, the reader is referred

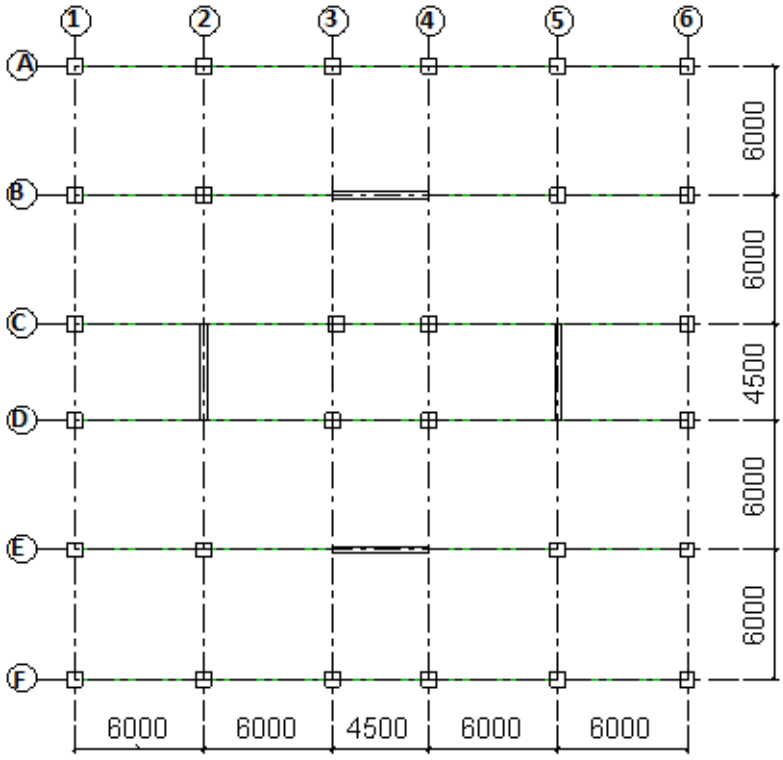

Figure 3.1: Plan view of the building, [41].

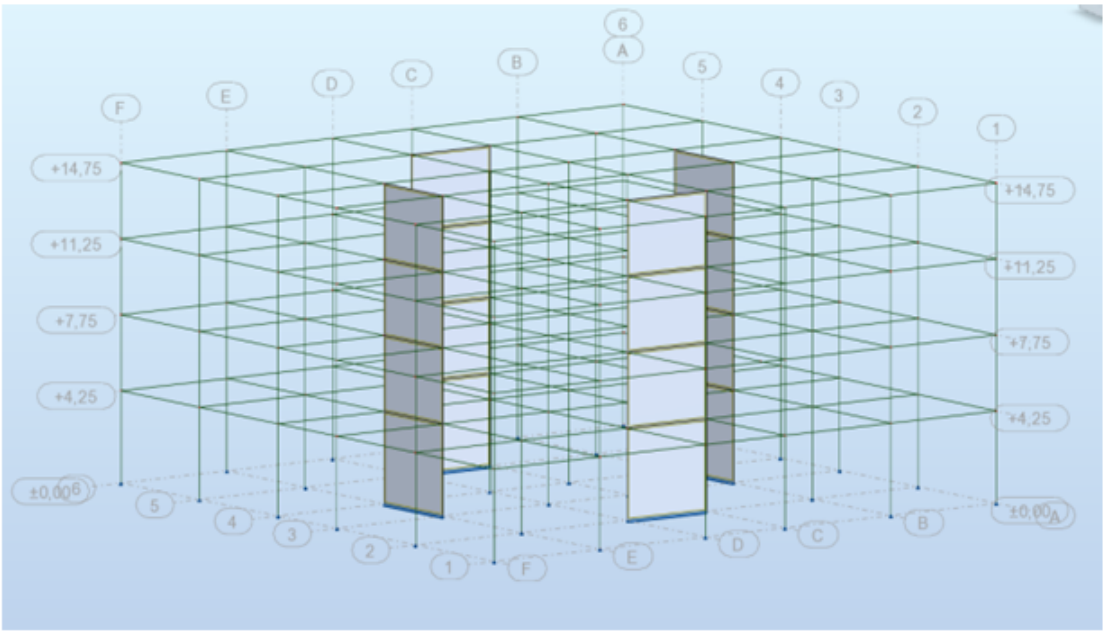

Figure 3.2: Structures model in 3D, [41].

to Appendix A.1.
Dead loads, including the self-weight of the hollow core and $50\ \mathrm{mm}$ concrete levelling, are equal to $\mathrm{Q_{dead}} = 3.85\ \mathrm{kN/m^2}$ (floors) and $2.6\ \mathrm{kN/m^2}$ (roof). The live load, $\mathrm{Q_{live}} = 2.0\ \mathrm{kN/m^2}$, is taken from NS-EN 1990. Both the snow and wind loads are calculated by using the Last-Ec software programme. Thus, calculations are performed in accordance to NS-EN 1991-

1-3 and NS-EN 1991-1-4. Hence, the snow load is $Q_{snow} = 1.6\ kN/m2$ and wind load $Q_{wind} = 0.77\,kN/m^2$ (see Appendix A.1). Before seismic analysis are performed, the structure is designed and controlled with regard to the wind load. Table 3.1 shows the load combinations according to NS-EN 1990.

3.4 Geometric imperfection

According to NS-EN 1992-1-1 clause 5.2(2), imperfections shall be taken into account in ultimate limit states and accidental design situations (earthquake). The imperfections are represented by an inclination, ϑ_i, given in NS-EN 1992-1-1 clause 5.2(5) as

$$\vartheta_i = \vartheta_0 \cdot \alpha_h \cdot \alpha_m \tag{3.1}$$

Here, ϑ_0 is the basic value equal to 1/200, α_h is the reduction factor for height and α_m is the reduction factor for number of members (see Appendix A.2). Thus,

$$\vartheta_i = (1/200) \cdot (2/3) \cdot 0.72 = 0.0024. \tag{3.2}$$

The geometrical imperfection loads are 0.24% of the gravity loads (see Appendix A.2). Initially, the structure is designed and computed with Robot [41] for gravitational loads, wind-induced loads and geometric imperfections. Table 3.1 presents load combinations in accordance to NS-EN 1990 for the latter mentioned loads. The geometric imperfections induced forces, denoted H, are calculated in Appendix A.2. The maximum shear force at base is equal to $555kN$ (see Appendix A.3). Subsequently, seismic loads are introduced instead of wind loads. The respective shear forces at base results $865kN$ (see section 3.6.3). Therefore, this document will focus on seismic analysis including geometric imperfections.

Table 3.1: Load Combination Eq.(6.10b) according to NS-EN 1990 [33].

Load Combination	Dead Load	Snow Load	Live Load	Wind Load
1	1.2 or 1.0	1.5	1.05	0.9
2	1.2 or 1.0	1.5	1.05	-
3	1.2 or 1.0	1.05	1.5	0.9
4	1.2 or 1.0	1.05	1.5	-
5	1.2 or 1.0	1.05	1.05	1.5

3.5 Design for gravity loads

The structure is symmetric in both directions with hinged joints at beam-column ends. The load combinations for gravity loads, in the ultimate limit state (ULS), are taken from EN 1990 table A1.2(B):

$$Q_{G,(6.10a)} = \gamma_{Gj,sup} \cdot G_{kj,inf} + \gamma_{Q,1} \cdot \psi_{0,1} \cdot Q_{k,1} \tag{3.3}$$

$$Q_{G,(6.10b)} = \zeta \cdot \gamma_{Gj,sup} \cdot G_{kj,inf} + \gamma_{Q,1} \cdot Q_{k,1} \tag{3.4}$$

Here, Q_G is the gravity load, γ is a partial factor, $\gamma_{Gj,sup} = 1.35$ and $\gamma_{Q,1} = 1.5$, $G_{kj,inf}$ is the characteristic dead load. The parameter ψ_0 is a factor for combination value of a variable

action, thereby, $\psi_{0,1} = 0.7$. $Q_{k,1}$ is the characteristic value of the leading variable action, and ζ is a reduction factor. Here, $\zeta = 0.89$. Hence,

$$Q_{G,(6.10a)} = 1.35 \cdot G_{kj,inf} + 1.05 \cdot Q_{k,1} \tag{3.5}$$

$$Q_{G,(6.10b)} = 1.2 \cdot G_{kj,inf} + 1.5 \cdot Q_{k,1} \tag{3.6}$$

3.5.1 Hollow core slabs

According to NS-EN 1998-1 clause 5.11.3.5(3), a minimum of 40mm concrete levelling shall be used for a span width less than 8m. In this report, 50mm reinforced concrete levelling is used, which is recommended from suppliers and commonly used in Norway. Moreover, the capacity should be calculated in accordance to NS-EN 1992-1-1. The choice of HD200 satisfies this requirement.

3.5.2 Design of secondary seismic elements

NS-EN 1998-1 clause 4.2.2 states that beams and columns may be designed as secondary seismic members, since they do not withstand to the seismic actions. The reason is that the beams and columns are connected with moment releaser hinges at both ends. Nonetheless, these members are designed to maintain support of gravity loads. The shear walls are designed to withstand lateral seismic forces and gravity loads.

Beams

The design of the beams are detailed by using Beam EC3 [6], which is a computer programme based on NS-EN 1993-1-1. For the border and interior beams HSQ profile type is chosen, while for shear walls and hollow core connections L profile beam is selected. According to NS-EN 1998-1 clause 5.11.2.1, the design load for beams is obtained from the design capacity of the hollow core slabs multiplied by a factor of 1.1 and/or 1.2, for HSQ and L beams respectively. This is to account for over-strength in the joints and thus prevents collapse. Figure 3.3 and Table 3.2 shows the cross sections, given in mm, quality of the steel and Table 3.3 illustrates the capacities of the beams.

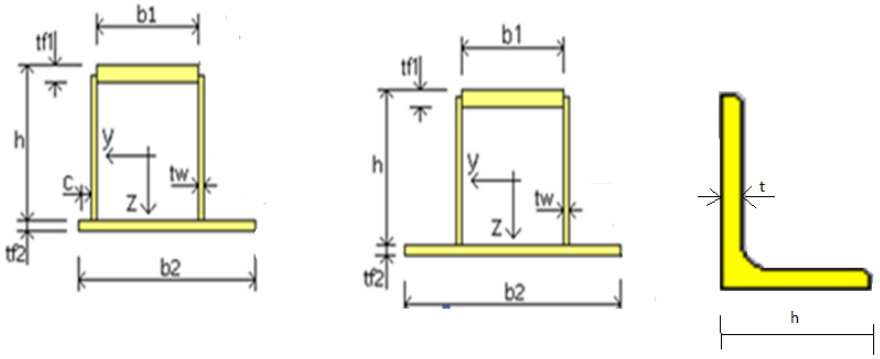

Figure 3.3: Cross sections of border and interior beams

Table 3.2: Dimensions and qualities of beams.

Beam	S355	h	b_1 (mm)	b_2 (mm)	t_w (mm)	t_{f1} (mm)	t_{f2} (mm)	c (mm)
Border	HSQ	180	100	150	10	25	15	15
Interior	HSQ	180	200	200	25	25	15	-
Wall-HD	L	180	180	-	16	-	-	-

Table 3.3: Design capacities of beams [6].

Beam	S355	V_{Rd} (kN)	M_{Rd} (kNm)	V_{Ed}/V_{Rd}	M_{Ed}/M_{Rd}
Border	HSQ	836	198	0.12	0.73
Interior	HSQ	1906	350	0.10	0.81
Wall-HD	L	562	80	0.12	0.80

Column

According to Figure 3.1, the columns in axis 2/B, 2/E, 5/B and 5/E carry the highest gravity loads. The maximum axial force acting on those columns at each storey from gravity and seismic loads are shown in Table 3.4 and Appendix A.3. The buckling length is set to the length of the column, since the columns are hinged at both ends. The columns are designed for gravity loads in Bt-Snitt [7] and the resulting cross section (dimension and reinforcement) are shown in Table 3.4. Additionally, the M/N diagram of the first floor is depicted in Figure

Table 3.4: Columns properties [7]

Column	Storey (kN)	Comb.6.10a (kN)	Comb.6.10b (kN)	Dimensions (mm)	Vert. Reinf. B500C	$N, M/N_d, M_d$
Interior	4	187	199	$240 \cdot 240$	$4\varphi16$	0.3
	3	462	473	$240 \cdot 240$	$4\varphi16$	0.7
	2	736	747	$260 \cdot 260$	$8\varphi16$	0.7
	1	1010	1021	$300 \cdot 300$	$8\varphi16$	0.9
Border	4	93	99	$240 \cdot 240$	$4\varphi16$	0.12
	3	230	236	$240 \cdot 240$	$4\varphi16$	0.28
	2	367	373	$240 \cdot 240$	$4\varphi16$	0.45
	1	504	510	$240 \cdot 240$	$4\varphi16$	0.65

3.4 to illustrate the capacity versus the design loads. In Table 3.4, the utility of the interior columns in the 4th floor is very low. The reason of the bars chosen, is to fulfil the requirements of the minimum reinforcement in accordance to NS-EN 1992-1-1. Furthermore, the dimensions and their respective reinforcement of the columns is controlled with requirement imposed by TEK10 [1]. The structure corresponds to fire-class II and is detailed for R90 (see Appendix A.4).

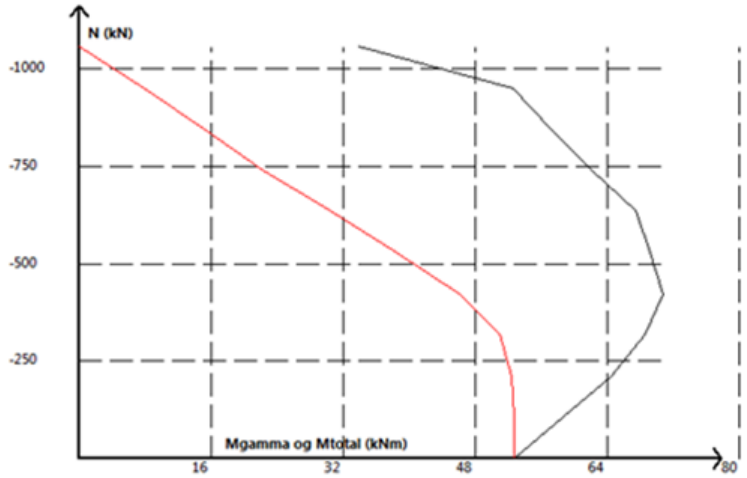

Figure 3.4: M/N diagram for interior column in the 1st floor [7].

3.6 Seismic Analysis

This section describes the design based on the lateral force method conducted according to NS-EN 1998-1. The seismic design is performed in Robot and material factors, for persistent and transient situations, are included in the seismic design. The stiffness is reduced by 50% to fulfil the demand in NS-EN 1998-1 clause 4.3.1(7). The partial factor for concrete $\gamma_C = 1.5$ and for steel $\gamma_S = 1.15$, are set respectively in accordance to NS-EN 1992-1-1. Accidental torsion is accounted by introducing a 5% eccentricity to the horizontal load in each storey. Thus, the load is applied at 1.425 m from the centre of the storey. Due to bidirectional shaking, 30% of the seismic load is applied perpendicularly to the main direction in compliance with NS-EN 1998-1.

3.6.1 Behaviour factor

According to NS-EN 1998-1 clause 5.11.1.4, the behaviour factor q_p for pre-cast structures is given by

$$q_p = k_p \cdot q \tag{3.7}$$

Here, q is the behaviour factor according to clause 5.2.2.2, and k_p is the reduction factor depending on the energy dissipation capacity of the pre-cast structure. The value of k_p is equal to 1 since the shear walls are designed to have ductile behaviour. For simpler notation in this report, it will be exploited that $q_p = q$. Thus,

$$q_p = q = q_0 \cdot k_w \tag{3.8}$$

Here, q_0 is the basic value of the behaviour factor, dependent on the structural system and on its regularity in elevation. The factor k_w is a factor that reflects the prevailing failure mode in structural systems with walls and depend on the ratio between the height and length of the walls [12]. The structure in this report is a wall equivalent dual system. Thus, $q_0 = 3.6$, and $k_w = 1.0$, according to clause 5.2.2.2(2), (5) and (11)P (see Appendix A.5). The factor k_w = 1.0 implies that there is no reduction of the q-factor due to the failure mode of the walls. Hence,

$$q_p = q = 3.6 \cdot 1.0 = 3.6 \tag{3.9}$$

3.6.2 Load Combinations for seismic mass

Load combinations are set according to EN 1998-1 clause 3.2.4, i.e.,

$$\mathrm{Q_G} = \sum \mathrm{G_{k,j}} + \sum \psi_{2,\mathrm{i}} \cdot \ \mathrm{Q_{k,i}} \tag{3.10}$$

Here, $\mathrm{Q_G}$ is the gravity load, $\mathrm{G_{k,j}}$ are dead loads, $\psi_{2,\mathrm{i}}$ is a reduction factor that considers the permanent part of variable loads. Thus, $\psi_{2,\mathrm{i}}$ = 0.3 for live load and 0.2 for snow load. $\mathrm{Q_{k,i}}$ is live and snow load as determined in section 3.3.

$$\mathrm{Q_G} = \mathrm{Q_{dead}} + 0.3\mathrm{Q_{live}} + 0.2\mathrm{Q_{snow}} \tag{3.11}$$

This results in a total gravity load, $\mathrm{Q_G}$=4.45 $\mathrm{kN/m^2}$ at the floors and 2.92 $\mathrm{kN/m^2}$ at the roof level. The mass at each storey is calculated according to EN 1998-1 clause 3.2.4 and 4.2.4, which state that the seismic mass should be determined from the gravity loads combined as:

$$\mathrm{Q_G} = \sum \mathrm{G_{k,j}} + \sum \varphi \cdot \ \psi_{2,\mathrm{i}} \cdot \ \mathrm{Q_{k,i}} \tag{3.12}$$

where, $\mathrm{G_{k,j}}$ are dead loads (section 3.3), φ is a reduction factor that allows for the incomplete coupling between the structure and its live load. For residential buildings, φ = 1.0 according to NS-EN 1998-1 N.A.4.2.4. The reduction factor $\psi_{2,\mathrm{i}}$ considers the permanent part of variable loading, and $\mathrm{Q_{k,i}}$ is live load as determined in section 3.3. Values are inserted:

$$\mathrm{m_{roof}} = \frac{\mathrm{Q_{dead}} + 0.2\mathrm{Q_{snow}}}{\mathrm{g}} = \frac{(2.6 + 0.2 \cdot \ 1.6)\ \mathrm{kN/m^2} \cdot \ 28.5^2\mathrm{m^2}}{9.81\mathrm{m/s^2}} = 242\ \mathrm{tons} \tag{3.13}$$

$$\mathrm{m_{3rd}} = \mathrm{m_{2nd}} = \mathrm{m_{1st}} = \frac{(3.85 + 0.3 \cdot \ 2)\ \mathrm{kN/m^2} \cdot \ 28.5^2\mathrm{m^2}}{9.81\mathrm{m/s^2}} = 369\ \mathrm{tons} \tag{3.14}$$

The masses determined in Eq. (3.13) and (3.14) accounts the contribution of the hollow core and variable loads. The mass of the columns and beams are accounted in the Robot model, to get the complete mass. However, they will be negligible compared to the mass of the over accounted elements.

3.6.3 Seismic loading

The peak ground acceleration (PGA) in Bergen is $0.85\ \mathrm{m/s^2}$, according to NS-EN 1998-1:2004 NA. 3.2.1 and ground type C. This results in the control periods and soil factors given in Table 3.5. Figure 3.5 illustrates the response spectrum.

Table 3.5: Soil factor and control periods, [31].

S	$\mathrm{T_B}$ (s)	$\mathrm{T_C}$ (s)	$\mathrm{T_D}$ (s)
1.15	0.2	0.6	2.0

Natural frequencies and mode shapes are executed in Robot with CQC (Complete Quadratic Combination) method. Relevant parameters and rules, with regard to NS-EN 1998-1, are selected and inserted before taking any types of calculations. Figure 3.6 shows the natural frequencies and effective mass percentage. The translational mode shapes, i.e. 1, 3, 5 and 6 are illustrated in Appendix A.6, whereas mode 2 and 4 are torsion.

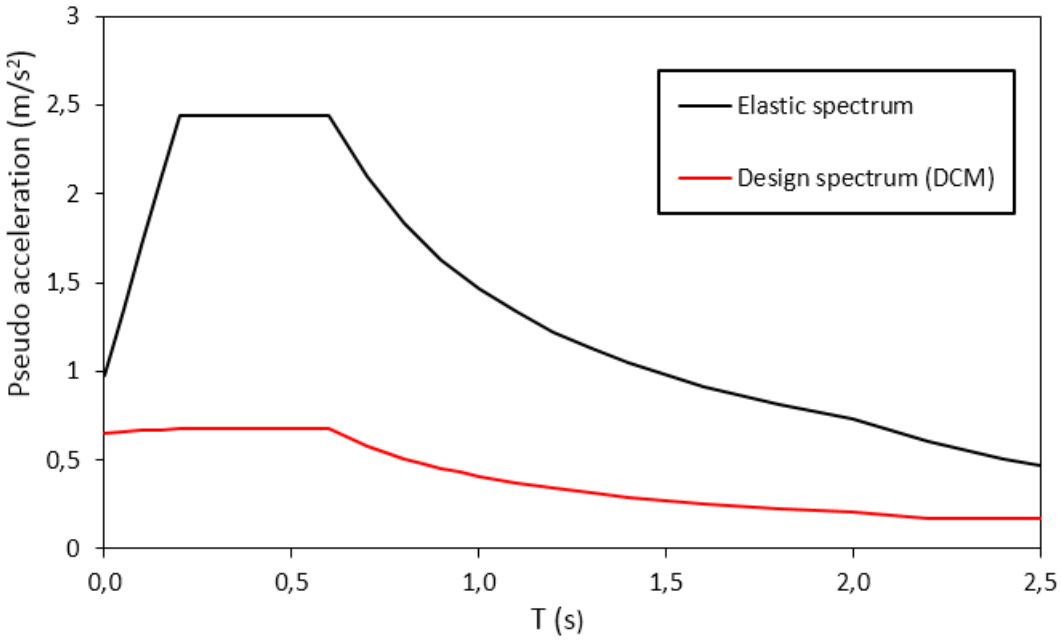

Figure 3.5: Elastic and design response spectrum.

Case/Mode	Frequency (Hz)	Period (sec)	Rel.mas.UX (%)
6/ 1	1,63	0,61	73,90
6/ 2	2,28	0,44	73,90
6/ 3	7,05	0,14	94,18
6/ 4	9,84	0,10	94,18
6/ 5	13,44	0,07	98,75
6/ 6	16,77	0,06	99,22

Figure 3.6: Natural frequencies and periods [41].

Seismic forces and displacements

Figure 3.6 shows that the first natural period is 0.61 s and the design spectrum $\mathrm{S_d(T)}$ is determined in accordance to NS-EN 1998-1 clause 3.2.2.5(4) Eq (3.15). Thus,

$$\mathrm{S_d(T_1)} = \frac{0.85 \cdot\ 1.15 \cdot\ 2.5 \cdot\ 0.6}{3.6 \cdot\ 0.61} = 0.67\ \mathrm{m/s^2} \tag{3.15}$$

By lumping the structure masses in their equivalent stories we get the following inputs, for the calculation of the base shear force:
$\mathrm{m_{roof}}$ = 250 tons, $\mathrm{m_{3rd}}$ = 384 tons, $\mathrm{m_{2nd}}$ = 386 tons and $\mathrm{m_{1st}}$ = 393 tons.
The total mass of the structure is $\mathrm{m_{total}}$ = 1413 tons. For detailed calculations, the reader is referred to Appendix A.5. The seismic base shear force $\mathrm{F_b}$, in both the horizontal directions, is determined in compliance with NS-EN 1998-1 clause 4.3.3.2(1)P. Hence,

$$\mathrm{F_b} = \mathrm{S_d(T_1)} \cdot\ \mathrm{m_{total}} \cdot\ \lambda \tag{3.16}$$

Here, $S_d(T_1)$ is the design spectral acceleration, m_{total} is the total mass of the building. λ = 0.85 for $T_1 < 2T_c$ and for building that has more than two stories, λ = 1.0 otherwise. Therefore, the base shear force due to seismic loading is equal to $805\ \mathrm{kN}$. Meanwhile, the total shear force at base, equivalent to seismic and geometric imperfection loads, results $865\ \mathrm{kN}$. Furthermore, the seismic load is distributed between the stories according to NS-EN 1998-1 clause 4.3.3.2.3(3) and are depicted in Table 3.6. More detailed calculation are reported in Appendix A.5. Thus,

$$F_i = \frac{F_b \cdot z_i \cdot m_i}{\sum z_j \cdot m_j} \tag{3.17}$$

The displacements, δ, of the elastic model are computed with Robot. The actual displacements are obtained by multiplying the values with the behaviour factor q = 3.6, according to NS-EN 1998-1 clause 4.3.4. The results are shown in Table 3.6.

Table 3.6: Force and displacement results.

Storey	F_i(kN)	δ_{Robot} (mm)	δ_{Real}(mm)
4	234	19	69
3	275	13	47
2	190	7	25
1	106	3	11

$P-\delta$ **effects**

NS-EN 1998-1 clause 4.4.2.2(2) states that $P-\delta$ effects (second order effect of gravity loads on laterally deformed structures) must be checked by evaluating the sensitivity factor, ϑ, defined as

$$\vartheta = \frac{P_{tot} \cdot d_r}{V_{tot} \cdot h_i} \tag{3.18}$$

Here, P_{tot} is the gravity load over and above the storey, d_r is the average deformation between the stories, V_{tot} is the total seismic shear load at the storey and h_i is the storey height. The value of ϑ is divided into four different categories and are presented in Table 3.7.

Table 3.7: Categories of ϑ for determination of $P-\delta$ effects,[31].

$\vartheta < 0.1$	$P-\delta$ effect can be neglected.
$0.1 < \vartheta < 0.2$	$P-\delta$ effects must be considered with a factor 1/(1- ϑ)
$0.2 < \vartheta < 0.3$	$P-\delta$ effects must be considered.
$\vartheta > 0.3$	The structure must be made stiffer.

As is evident from Table 3.8, the sensitivity factor is less or equal to 0.1 in all stories and the $P-\delta$ effects is disregarded.

3.6.4 Design of the Shear Walls

The walls are designed in accordance to NS-EN 1998-1 clause 5.4.1.2.3 which states a minimum thickness of the web, b_{w0},

$$b_{w0} = \max(150; h_s/20) \tag{3.19}$$

Table 3.8: $\mathrm{P}-\delta$ effects and ϑ at each storey.

Storey	$\mathrm{P_{tot}}$(kN)	$\mathrm{d_r}$(mm))	$\mathrm{V_{tot}}$(kN)	h (mm)	ϑ
4	2453	22	246	3500	0.06
3	6220	22	537	3500	0.07
2	10006	14	743	3500	0.04
1	13862	11	865	4250	0.05

Here $\mathrm{h_s}$ is the maximum free storey height. Therefore, the thickness of the walls are 175 and 220 mm, for the $4^{\mathrm{th}}-3^{\mathrm{rd}}-2^{\mathrm{nd}}$ and 1^{st} floor, respectively. The normalized axial force in the primary seismic elements should not exceed the value of 0.4, in accordance to NS-EN 1998-1 clause 5.4.3.4.1(2). Moreover, clause 5.4.3.4.2(12) states that if the normalized axial force is less than 0.15, the shear walls can be designed by using NS-EN 1992-1-1. Thus,

$$\mathrm{v_d} = \frac{\mathrm{N_{Ed}}}{\mathrm{h_c}\cdot\ \mathrm{b_c}\cdot\ \mathrm{f_{cd}}} < 0.15 \tag{3.20}$$

Here, $\mathrm{h_c}$ and $\mathrm{b_c}$ are the wall cross section. Table 3.9 illustrates walls dimensions with corresponding results. It is evident that $\mathrm{v_d} < 0.15$ in all stories. More detailed calculations

Table 3.9: Walls properties and normalized axial force.

Storey	$\mathrm{b_c}$ (mm)	$\mathrm{h_c}$ (mm)	$\mathrm{N_{Ed}}$ (kN)	$\mathrm{v_d}$
4th	175	3500	348	0.03
3rd	175	3500	829	0.06
2nd	175	3500	1310	0.1
1st	220	4250	1791	0.1

are included in the Appendix A.5. The design base shear force in the seismic analysis is 865 kN as per calculation (section 3.6.3). NS-EN 1998-1 clause 5.4.2.4 states that walls with height to length ratio greater than 2, the design bending moment must be increased due to uncertainties of the moment distribution along the wall. Thus,

$$\frac{\mathrm{h_w}}{\mathrm{l_w}} = \frac{14.75\mathrm{m}}{4.5\mathrm{m}} = 3.3 > 2 \tag{3.21}$$

The result obtained from Eq.(3.21) implies the increase of the bending moment and is performed as stated by NS-EN 1998-1. Walls must act as a vertical cantilever allowing the formation of a single plastic hinge at the base. In order to avoid yielding above the base hinge, the design bending moment diagram along the height of the wall is given by an envelope bending diagram vertically displaced (tension shift). Figure 3.7 illustrates the design envelope for bending moments for wall systems [31].

The parameter $\mathrm{a_l}$ represent the vertical tension shift and is defined as [12]:

$$\mathrm{a_l} = \mathrm{d}\cdot\ \mathrm{cot}\vartheta \tag{3.22}$$

Here, d is the effective depth at base of the wall and $\mathrm{cot}\vartheta$ is determined in accordance to NS-EN 1992-1-1. Thus, $\mathrm{a_l} = 4.5\mathrm{m}\cdot\ 1 = 4.5$ m.
The lateral forces per wall are reported in Fig 3.8 (a). The design overturning moment at the base due to the seismic forces and geometric imperfections per wall is

$$\mathrm{M_{Ed}} = 123\cdot\ 14.75 + 145.5\cdot\ 11.25 + 103\cdot\ 7.75 + 61\cdot\ 4.25 = 4606\ \mathrm{kNm} \tag{3.23}$$

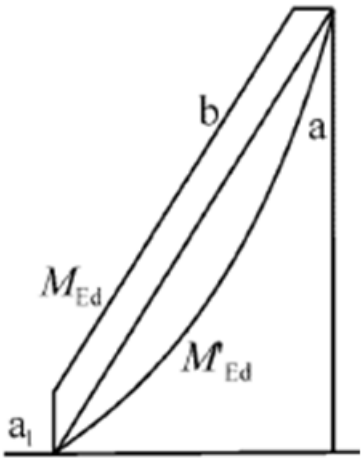

Key

a	moment diagram from analysis
b	design envelope
a_l	tension shift

Figure 3.7: Design envelope for bending moments in wall systems. The Figure is re-plotted from NS-EN 1998-1 [31].

Shear forces must be multiplied by a factor of 1.5, in accordance to NS-EN 1998-1 clause

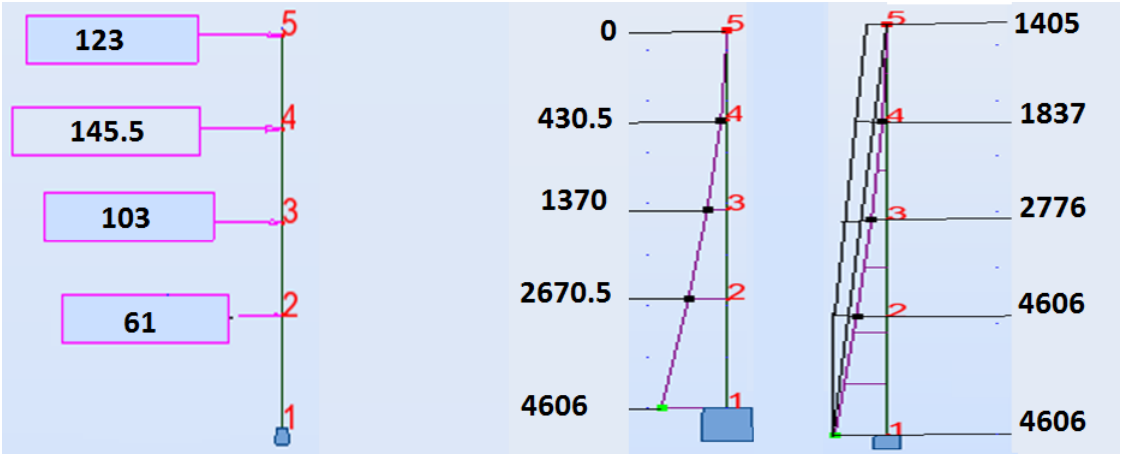

Figure 3.8: (a)Lateral forces, bending moment diagram(kNm), (b) before and (c) after envelope design.

5.4.2.4.(7), to take into account the possible increase of shear forces after yielding at the base of shear walls. Thus, the total design shear at the base level is equal to $865 \cdot 1.5 = 1298$ kN and 649 kN per wall in one direction. The design control is computed with Bt-Snitt [7] and the results are shown in Table 3.10.

Table 3.10: Reinforcement of the walls [7].

Storey	b_c (mm)	Vert.Reinf.	Hor.Reinf.	V_{Ed}/V_{Rd}	M_{Ed}/M_{Rd}	Stirrups
4^{th}	175	φ16c250	φ10c250	0.6	0.4	φ10c250
3^{rd}	175	φ16c250	φ10c250	0.9	0.5	φ10c250
2^{nd}	175	φ20c275	φ10c250	0.9	0.6	φ10c250
1^{st}	220	φ20c275	φ10c250	0.8	0.6	φ10c250

3.6.5 Hollow core slabs

The maximum lateral force acting in plane is at the 3^{rd} floor, according Figure 3.8(a). The maximum bending moment due to this force is

$$M_{slabs} = \frac{F_{4^{th}} \cdot l_{slab}}{4} = \frac{145.5\ \text{kN} \cdot (28.5-12)\text{m}}{4} = 600\ \text{kNm} \tag{3.24}$$

Here, l_{slab} is the distance between the walls. Figure 3.9 illustrates the moment diagram for the hollow cores at the 3^{rd} floor. The design is detailed in accordance to Betongelement Bind B [4] and NS-EN 1998-1 clause 5.11.3.5(4). The required tension force is given by

$$S = \frac{M_{slab}}{z} \tag{3.25}$$

where, z is the lever arm, obtained from Figure B12.4 [4]. Thus, $z = 0.7 \cdot 28.5\text{m} = 19.95\text{m}$. Inserting the values,

$$S = \frac{600\ \text{kNm}}{19.95\ \text{m}} = 30\ \text{kN} \tag{3.26}$$

The tension forces are withstood by the steel beams, where the minimum tension capacity is

$$S_{beams} = A_{profile_L} \cdot \frac{f_{yd-S355}}{\gamma_S} = 6180\ \text{mm}^2 \cdot \frac{355\ \text{N/mm}^2}{1.15} = 1908\ \text{kN} \tag{3.27}$$

Here, $A_{profile_L}$ is the area of the cross section of L-beam (see Fig. 3.3), and $f_{yd-S355}$ is the design tensile capacity of steel S355.

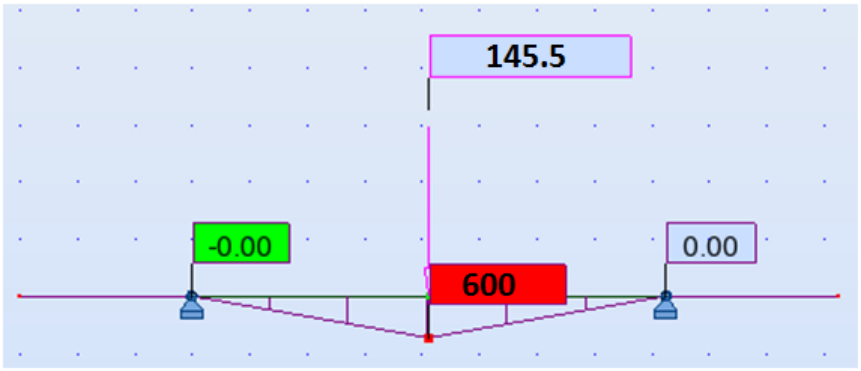

Figure 3.9: Moment diagram of HD (kNm), Robot.

According to NS-EN 1998-1 clause 5.11.3.5(6), shear force acting in plane must be increased with a factor of 1.3 and are detailed in accordance to Betongelement Bind B [4].

Figure 3.8(a) shows that the maximum shear force acts at the first floor and is equivalent to 432.5 kN. The respective shear force for hollow core slabs is

$$\mathrm{V_{slab}} = 1.3 \cdot \frac{432.5 \text{ kN}}{2} = 281 \text{ kN} \tag{3.28}$$

The respective shear forces acting on beam-hollow core slabs joints, along HD width, and their respective orthogonal reinforcements are:

$$\mathrm{V_h} = \mathrm{V_{slab}} \cdot \frac{\mathrm{b}}{\mathrm{z}} = 281 \text{ kN} \cdot \frac{1.2 \text{ m}}{19.95 \text{ m}} = 17 \text{ kN} \tag{3.29}$$

$$\mathrm{A_{sb}} = \frac{\mathrm{V_h}}{0.6 \cdot \mathrm{f_{yd}}} = \frac{17 \text{ kN}}{0.6 \cdot 435 \text{ N/mm}^2} = 66 \text{ mm}^2 \tag{3.30}$$

The equivalent reinforcement is $\varphi 10$ at each beam-HD slab interface. The maximum bending moment and shear due to gravity loads acting on the HD are:

$$\mathrm{M_{gravity}} = \frac{(1.2 \cdot 3.85 + 1.5 \cdot 2)\text{kN/m}^2 \cdot 6^2}{8} = 34 \text{ kNm/m} \tag{3.31}$$

$$\mathrm{V_{gravity}} = \frac{(1.2 \cdot 3.85 + 1.5 \cdot 2)\text{kN/m}^2 \cdot 6}{2} = 23 \text{ kN/m} \tag{3.32}$$

According Betongelement book Bind A [42], HD200 with 4 pre-stressed strands has a capacity of 70 kNm/m and 42 kN/m, for moment and shear respectively, hence, the demand is met.

3.6.6 Shear transfer to walls

The required shear capacity in order to transfer the shear forces to the walls is detailed in accordance to Betongelement book Bind B [4]. Shear forces are directly transferred at wall-HD connection through the reinforcement welded to the steel beams. This type of transmission demands a reinforcement of

$$\mathrm{A_s} = \frac{\mathrm{V_{slab}}}{0.6 \cdot \mathrm{f_{yd}}} = 1078 \text{ mm}^2 \tag{3.33}$$

At the transmission state, the maximum number of HD that can be adopted is 3, thereby, a reinforcement of $\varphi 25$ is welded to the beams and anchored inside the holes of the HD-slabs.

Chapter 4

NUMERICAL STRUCTURAL MODEL

Finite element model (FEM) is an advanced modelling approach for design and analysis of load-bearing structures. The main task is to detect and adopt an accurate and reliable numerical structural model to perform linear and non-linear analysis. The structure is modelled with two software packages: OpenSees and SeismoStruct. In order to verify the accuracy of the FEM's, the natural frequencies of both the elastic and inelastic numerical models are determined and compared (see section 4.2). Indeed, the outcome gave a good agreement between the models.

4.1 Model

4.1.1 Geometry

As presented in section 3.1, the building is symmetric in x and y directions, and regular in plan view. Therefore, the choice of 2D (two-dimensional) model is justified in the light of NS-EN 1998-1 Table 4.1 [31]. 2D analyses are only undertaken in one direction (x-direction) of the structure. The model consists of shear wall elements, where masses from half part of the building and correspondent gravity loads acting on the wall are applied. A lean-on column is included in the numerical model and connected to the wall elements by rigid links, to account the $P-\delta$ effects (global second-order) of the remaining gravity loads. The resultant model is illustrated in Figure 4.1.

4.1.2 Material

The material model adopted for concrete is Mander et al. (1988) [20] approach for stress-strain relationship. The reason is that this method takes into account the high strain rate through an increase, in both strength and stiffness, of the concrete when loads are applied rapidly. Furthermore, it can be used for all current reinforcement configurations and in unconfined concrete. The main parameters in the Mander's concrete model are

- f'_{co} and ε_{c0}: unconfined concrete compressive strength and corresponding strain
- f'_{cc} and ε_{cc}: confined concrete compressive strength and corresponding strain

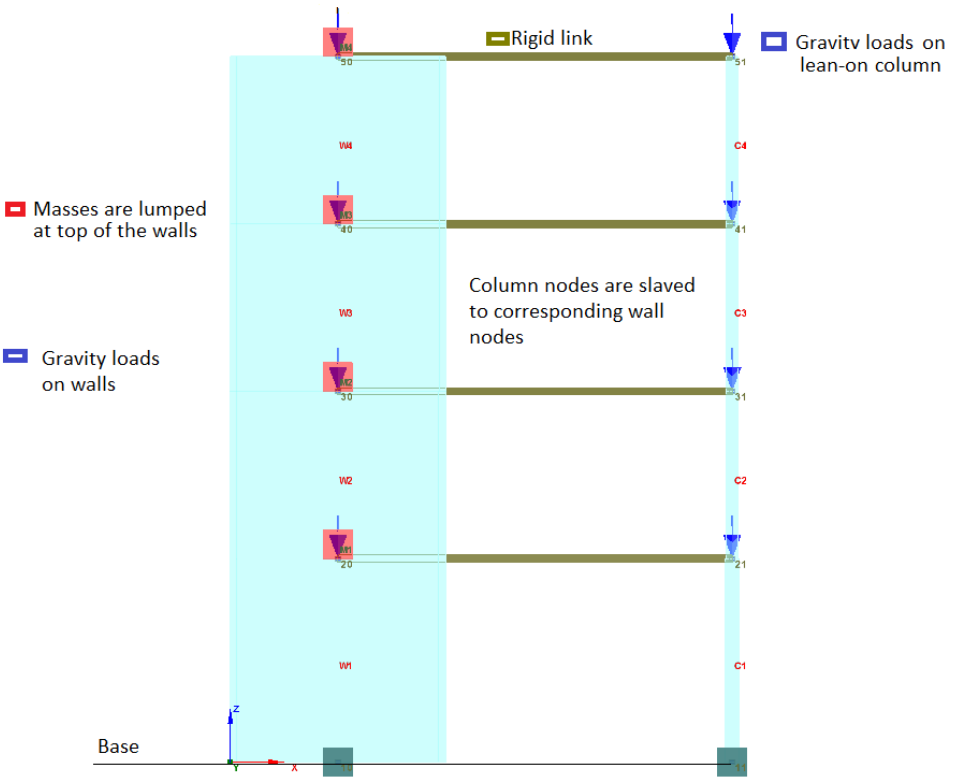

Figure 4.1: 2D FEM model of the structure, [27].

- ε_{cu}: concrete compressive strain at first fracture of the transverse reinforcement
- E_c: tangent modulus of elasticity defined as $E_c = 5000\sqrt{f'_{co}}$
- E_{sec}: secant modulus defined as $E_{secc} = \frac{f'_{cc}}{\varepsilon_{cc}}$.

According to NS-EN 1998-1, the values for f'_{co} and ε_{c0} are 30 MPa and 0.0022 respectively. For the calculation of the ultimate compression strain, ε_{cu}, a conservative estimate is adopted, following the study conducted by T. Paulay and M.J.N. Priestley [39]. Thus,

$$\varepsilon_{cu} = 0.0004 + 1.4 \cdot \rho_s \cdot \frac{f_{yh} \cdot \varepsilon_{sm}}{f'_{cc}} \tag{4.1}$$

where, ε_{sm} is the steel strain at maximum tensile stress, f_{yh} is tensile yield strength of steel B500NC (500 MPa) and ρ_s is the volumetric ratio of confining steel. In order to account the increase of the strength, stiffness and strain at the peak stress of the concrete, dynamic amplification factors are applied [20]. Thus,

$$(f'_{co})_{dyn} = D_f \cdot f'_{co} \tag{4.2}$$

$$(E_c)_{dyn} = D_E \cdot E_c \tag{4.3}$$

$$(\varepsilon_{co})_{dyn} = D_\varepsilon \cdot \varepsilon_{co} \tag{4.4}$$

where, $\mathrm{D_f}$ is the dynamic magnification factor for strength, $\mathrm{D_E}$ is the magnification factor for stiffness and $\mathrm{D_\varepsilon}$ is for the strain at the peak stress. The factors are determined as follow:

$$\mathrm{D_f} = \frac{1 + [\frac{\varepsilon_c}{0.0035 \cdot (f'_{co})^{\mathbf{2}}}]^{1/6}}{1 + [\frac{0.00001}{0.0035 \cdot (f'_{co})^{\mathbf{2}}}]^{1/6}} \tag{4.5}$$

Here, ε_c is the strain rate in $\mathrm{s^{-1}}$ and a value of $0.167\ \mathrm{s^{-1}}$ is used, following the research conducted by Scott et al. (1982). For the stiffness, the dynamic magnification factor, $\mathrm{D_E}$ is given by

$$\mathrm{D_E} = \frac{1 + [\frac{\varepsilon_c}{0.0035 \cdot (f'_{co})^{\mathbf{3}}}]^{1/6}}{1 + [\frac{0.00001}{0.0035 \cdot (f'_{co})^{\mathbf{3}}}]^{1/6}} \tag{4.6}$$

The dynamic magnification factor for the strain at peak stress is given by

$$\mathrm{D_\varepsilon} = \frac{1}{\mathrm{D_f}} \cdot (1 + \sqrt{1 + \frac{3 \cdot \mathrm{D_f^2}}{\mathrm{D_E}}}) \tag{4.7}$$

The walls cross sections, with their respective longitudinal and transversal reinforcements are inserted in the afore-stated formulas to calculate the concrete properties. As a result, the dynamic compression strength, stiffness and strain at peak compressive stress are $35.6\ \mathrm{MPa}$, $32838\ \mathrm{MPa}$ and 0.002, respectively. The confinement ratio, which is the ratio of $\frac{f'_{cc}}{f'_{co}}$ is 1 (see Appendix B.1), meaning that the core of the walls are unconfined with ultimate compressive strain equal to 0.006. Figure 4.2 illustrates the stress-strain results from the aforementioned calculations, where the red and blue line shows the properties of the concrete according to Mander (theoretical) and OpenSees (*Concrete04*), respectively.

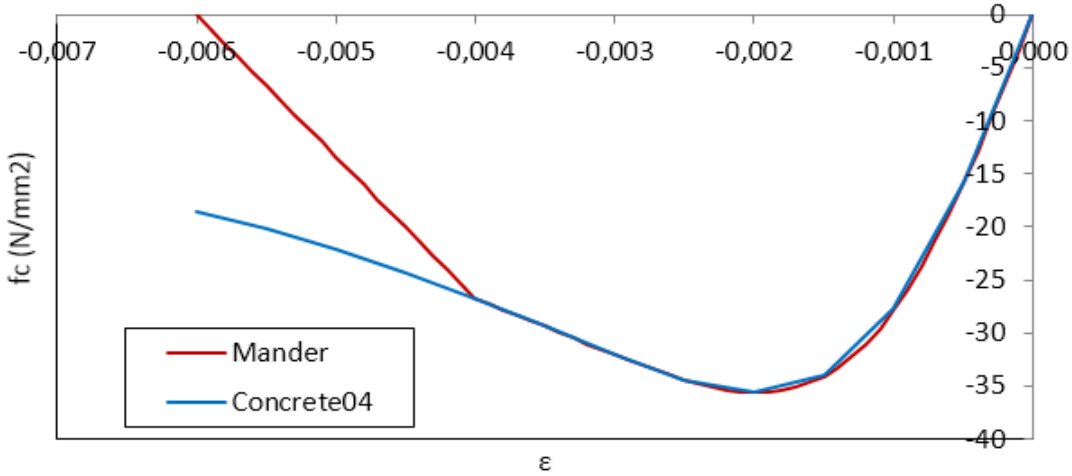

Figure 4.2: Stress-Strain relationship for the wall sections.

SeismoStruct incorporates a material model in accordance to Mander, where input parameters, i.e. compressive and tensile strength, strain at peak stress, etc., are user defined. Figure 4.3 illustrates the concrete material model (SeismoStruct) implemented in this thesis. Contrarily, in OpenSees, the user must model the material properties manually. Indeed, *Concrete04* is adopted and gives an appropriate match with Mander's concrete model (see Figure 4.2).
The reinforcing steel is represented in OpenSees with *Steel02* material model, whereas $\mathrm{stl-mp}$

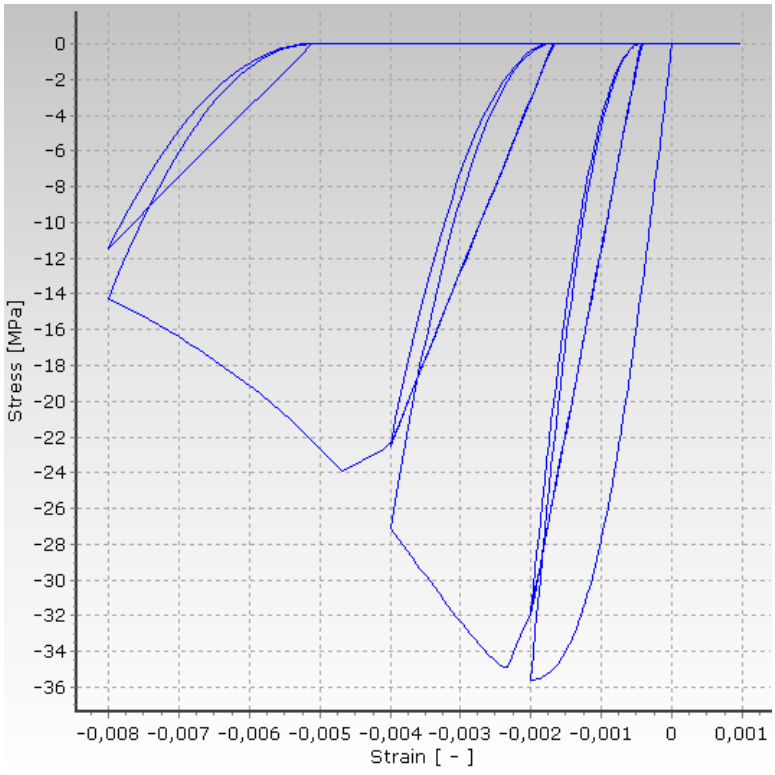

Figure 4.3: Concrete material model, SeismoStruct.

is implemented in SeismoStruct and are illustrated in Figure 4.4. They corresponds to a uniaxial $\mathrm{Giuffre-Menegotto-Pinto}$ [27] and $\mathrm{Menegotto-Pinto}$ [40] steel material models with isotropic strain hardening effect, to account a non-linear transition from the elastic range to strain hardening stage. The input parameters used in both software packages are: 1) yield strength 500 MPa, 2) E-modul $2 \cdot 10^5$ MPa, 3) strain hardening parameter 0.005.

4.1.3 Elements

The elements that are implemented in the elastic analyses are *Beam-Column* elements with six degrees of freedom that accounts for bending and axial deformations. In OpenSees, the cross sections properties, E (modulus of elasticity), I_z (second moment of inertia), A (cross-sectional area), reinforcement and element type are defined manually. Contrarily, in SeismoStruct the element type is assigned through *elfrm* after the cross section is defined.

Inelastic system relies on the non-linear fuse concept to control the level of forces the structure exposed for. In order to perform analysis accounting for material non-linearity, two main approaches are usually used: lumped (point-hinge) and distributed (fibre model) inelasticity elements. The first one is dependent on the length of the plastic hinge defined from several parameters, i.e. axial load, concrete strength, reinforcement, etc. and is inaccurate compared to fibre model [28]. Nowadays, especially due to increase of computational tools, distributed inelasticity elements are the standard approach. In addition, the latter one has the feature of representing the spread of inelasticity within the element cross-section and along the element length. The main advantage of such model is the non-existence of a predetermined length nor calibration of empirical response parameters [8]. Each fibre is associated with a

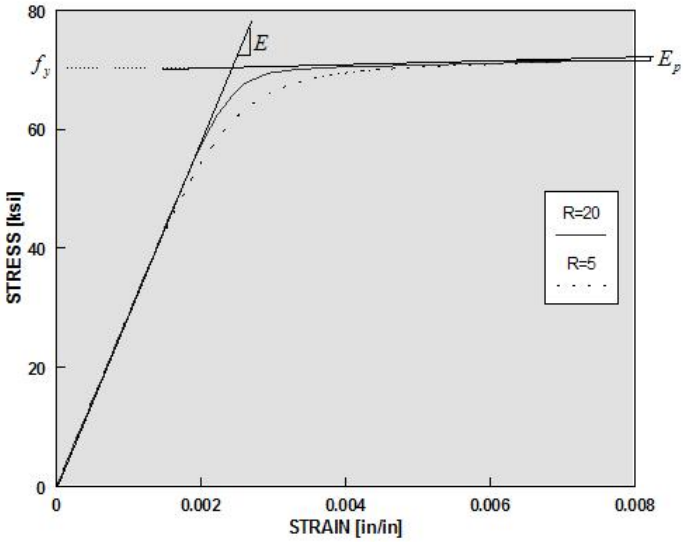

(a) Steel02 material model in OpenSees.

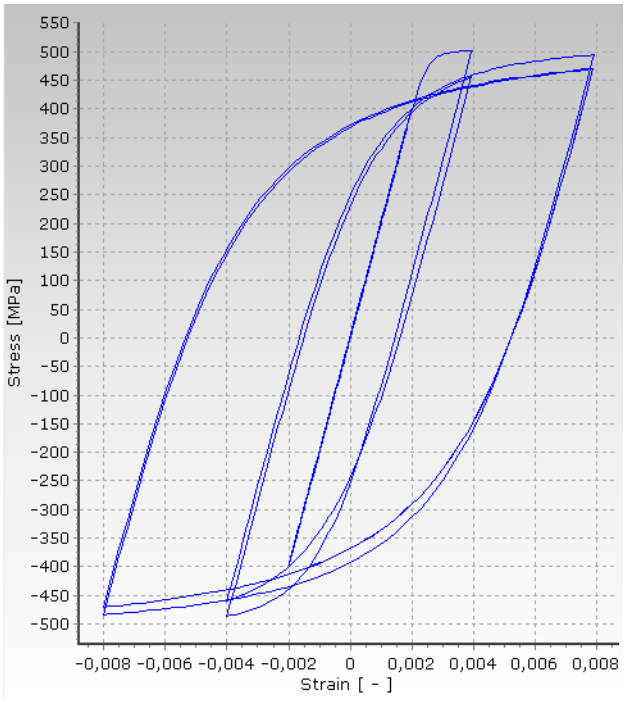

(b) Steel $\mathrm{stl-mp}$ material in Seismostruct.

Figure 4.4: Stress-strain relationship of steel material model.

uniaxial stress-strain relationship to represent the cross-section behaviour and the sectional stress-strain state of the element is obtained through the integration of the individual fibres. Figure 4.5 depicts the discretisation of a typical reinforced concrete cross-section. Fibre-based elements are modelled with two different methods depending on the interpolation functions adopted. The displacement-based formulation (DB) assigns displacement shape function to a finite element and the governing equations are solved based on the element's stiffness. In addition, it is based on a linear variation of curvature along the element. On the other hand, the force-based (FB) formulation imposes a force field and is built on the element's flexibility. According to a study presented by Calabrese et al. (2010) [8], a FB method is more accurate

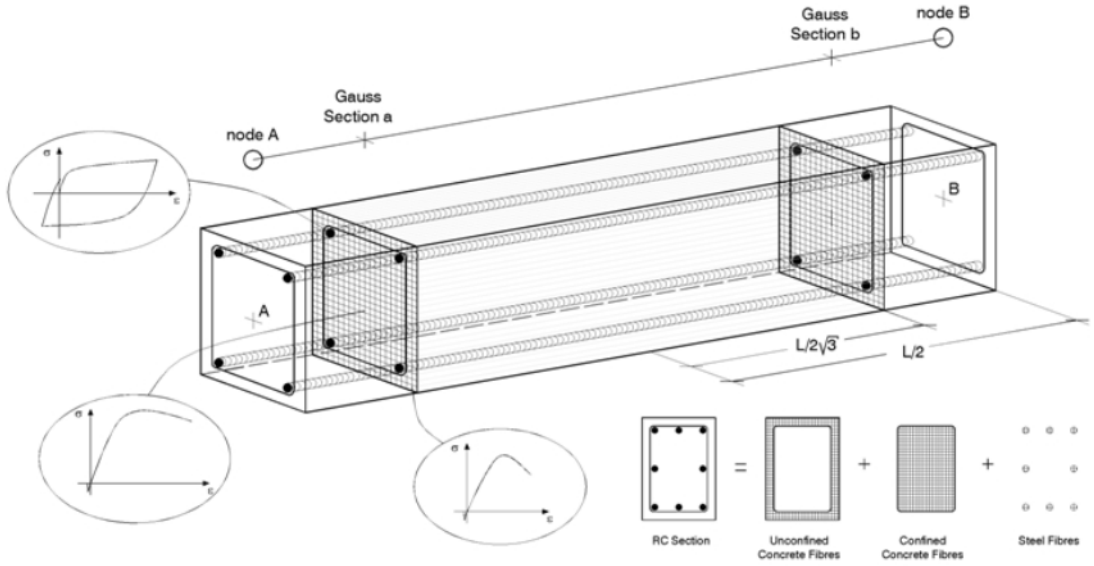

Figure 4.5: Discretisation of a reinforced concrete cross-section. The Figure is re-plotted from SeismoStruct.

than DB approach. The main reason is that the DB-method can not capture the real deformation shape when material inelasticity is accounted. In FB-approach, the solution is approximated by the discrete number of controlling sections along the element that are used for the numerical integration. The lower bond of integration points (IP) is 4 to provide reliable results at the global level [8]. In addition, a Gauss-Lobatto integration scheme (see Figure 4.6) is recommended for FB elements.

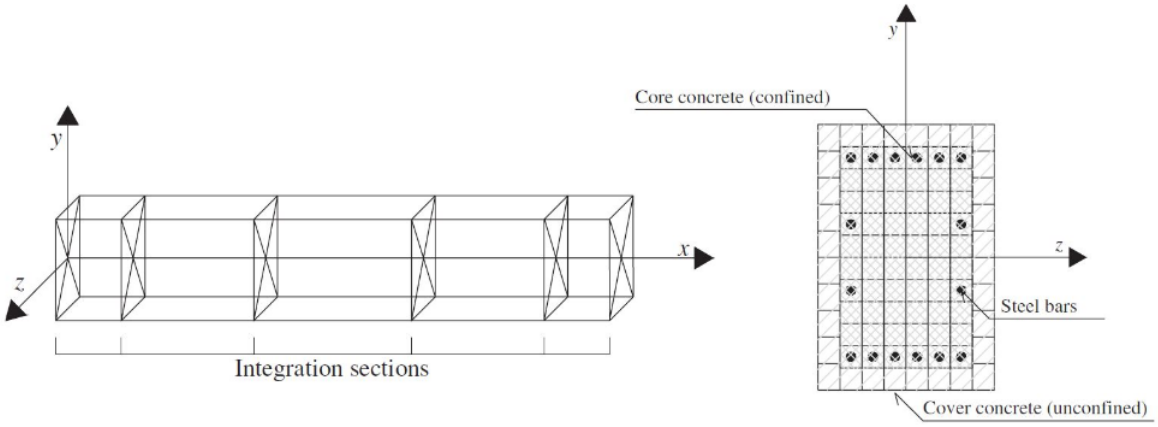

Figure 4.6: Gauss-Lobatto integration sections. This Figure is a replication from SeismoStruct.

In this thesis, force-based beam column elements are adopted in both software packages. The number of section fibres used is 160 per wall in both SeismoStruct and OpenSees (see Figure 4.7), which is recommended in SeismoStruct's user manual. Four IP with Gauss-Lobatto quadrature rule (per wall) are also adopted to ensure numerical stability of the models. In addition, the choice of IP is made to avoid the so-called Localization issue, i.e. increase of local strains at the base integration point exhibiting spurious global response [8]. As a result, no-convergence issue is experienced. Finally, the $\mathrm{P}-\delta$ effects at a global level are accounted

for.

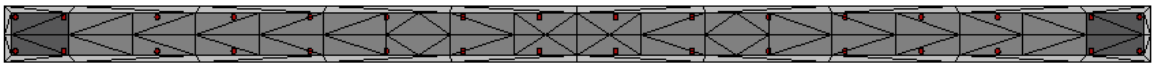

Figure 4.7: DiSection discretisation pattern of the wall in the first floor, SeismoStruct.

4.1.4 Numerical Solution Algorithms

The Newton-Raphson method is adopted for the iterative solution approaches in both SeismoStruct and OpenSees (see Appendix D). The algorithm is implemented with prescribed displacement increments, which gave the most rapidly converging process to determine the structural response. In the non-linear time-history analysis, the Hilber-Hughes-Taylor method is used. This algorithm suppresses high frequency modes without degradation of the second order accuracy [10].

4.1.5 Damping

In non-linear time-history analysis, Rayleigh damping is included to represent viscous damping of the structure. The damping matrix of the MDOF-system, $\mathbf{C}$, is given by [9]

$$\mathbf{C} = \alpha \mathbf{M} + \beta \mathbf{K} \tag{4.8}$$

Here, $\mathbf{M}$ and $\mathbf{K}$ are the mass and stiffness matrices of the system, respectively, α and β are constants of proportionality. These latter parameters are defined as

$$\alpha = \frac{2(\zeta_i \omega_j - \zeta_j \omega_i)\omega_i \omega_j}{\omega_j^2 - \omega_j^2} \tag{4.9}$$

$$\beta = \frac{2(\zeta_i \omega_j - \zeta_j \omega_i)}{\omega_j^2 - \omega_j^2} \tag{4.10}$$

Here, ω_i and ω_j are two of the eigenfrequencies of the system, ζ_i and ζ_j are their corresponding damping ratios. In this thesis, damping ratios of 4% and 6% at the first and fourth mode are used. The Rayleigh scale factors, α and β, are calculated with SeismoStruct and resulted to be 0.859 and 0.0014, respectively.

4.2 Natural periods and Mode shapes

Natural periods and mode shapes for both the elastic and inelastic models are computed. The gravity loads are included and converted into masses. Figure 4.8 and Table 4.1 illustrates the results of the natural periods. Shell elements, which account for shear deformations, are used to model the walls in Robot. Figure 4.9 illustrates the first four mode shapes obtained with SeismoStruct, which complies with the one previously realized from Robot (see Appendix A.6). It is worth to mention that the natural periods are determined without any reduction of the stiffness, ergo, the periods are shorter compared to Figure 3.6.

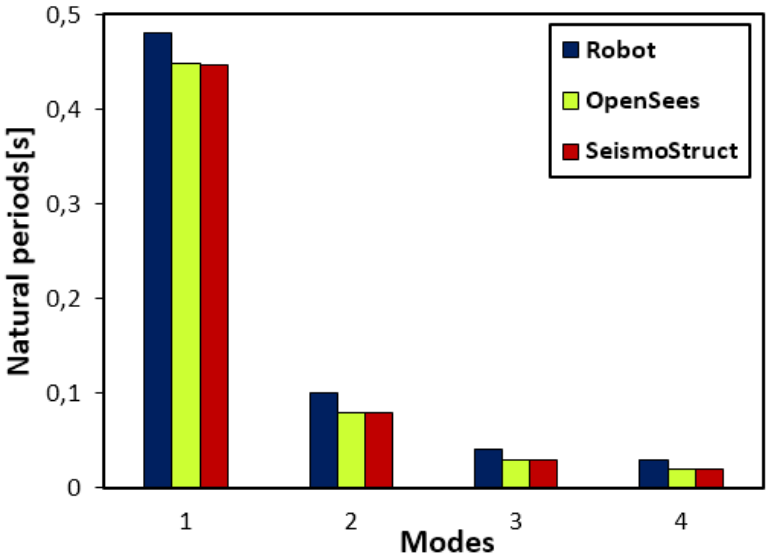

(a) Elastic models.

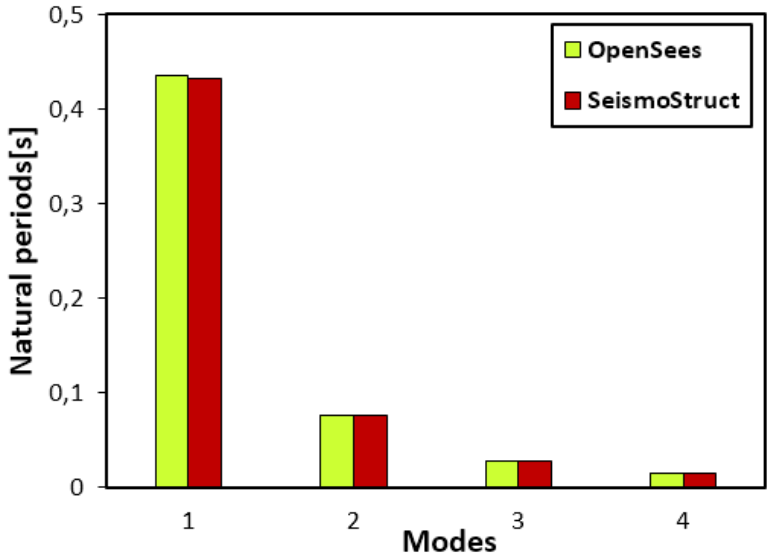

(b) Inelastic models.

Figure 4.8: Natural periods of the numerical models.

Table 4.1: Natural periods of the different numerical models.

		Natural Periods			
Software	Model	T_1 (s)	T_2(s)	T_3 (s)	T_4(s)
Robot	Elastic	0.480	0.100	0.040	0.030
SeismoStruct	Elastic	0.447	0.080	0.030	0.020
OpenSees	Elastic	0.448	0.080	0.030	0.020
Difference (%)		7	25	33	50
SeismoStruct	Inelastic	0.432	0.076	0.028	0.015
OpenSees	Inelastic	0.435	0.076	0.028	0.015

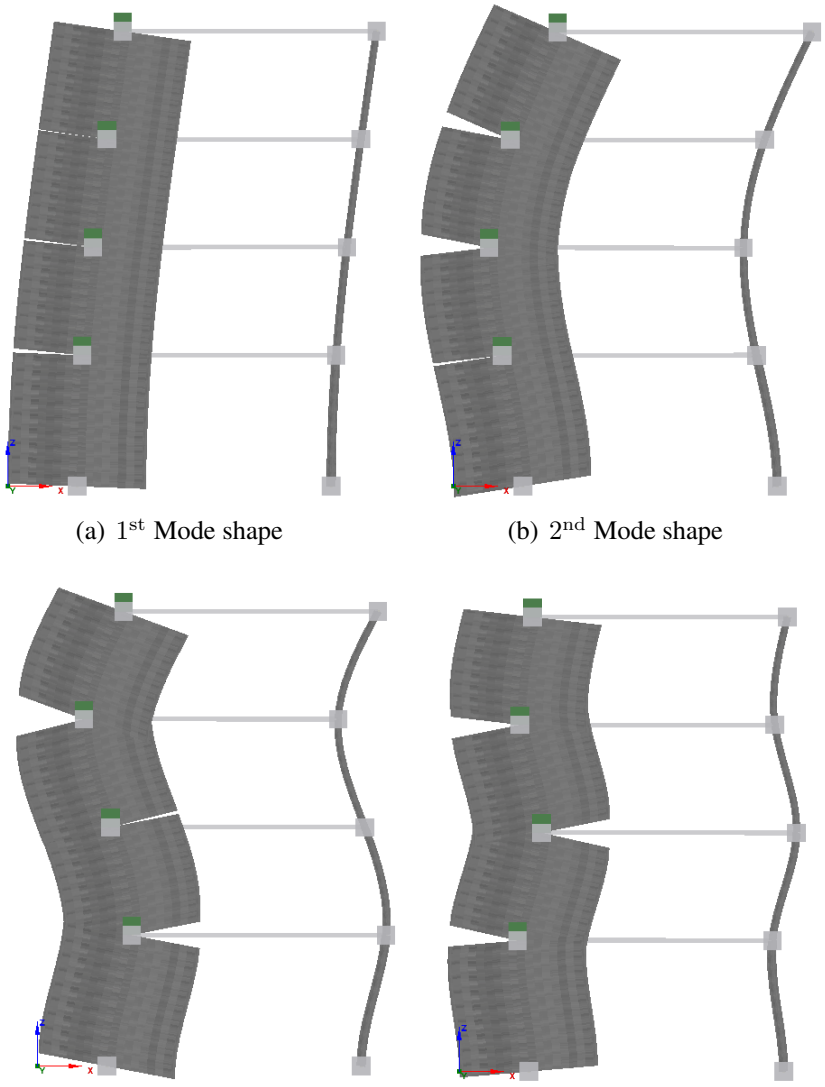

(a) 1^{st} Mode shape (b) 2^{nd} Mode shape

(c) 3^{rd} Mode shape (d) 4^{th} Mode shape

Figure 4.9: First four mode shapes of the numerical model, SeismoStruct.

4.3 Remarks

The results shows that an appropriate model is implemented both in SeismoStruct and OpenSees with regard to the first natural period. A 4% difference in the first or fundamental natural period between the elastic and inelastic models is observed (SeismoStruct and OpenSees). This result was expected since the walls are unconfined. Furthermore, in SeismoStruct, the contribution of the reinforcement to the stiffness is not included and shell elements are not incorporated. In OpenSees, the contribution is low and shear deformations are not accounted. Even though shell elements are adopted in Robot, the results of the first natural period of the elastic model does not differ more than 7% from the other software packages, but significant discrepancies are observed in the higher modes. Therefore, the results from Robot will be compared with OpenSees when the latter one is configured with shell elements (see section 7.2). Since one of the aim of this study is to compare SeismoStruct and OpenSees, the numerical model with fibre-section will be used for non-linear analyses.

Chapter 5

Pushover Analysis

5.1 General

The theoretical background for Pushover Analysis is reported in section 2.3.2. This chapter emphasizes the assessment of Pushover Analysis and discusses the results thoroughly.
The Non-Linear Static Analysis (PA) is executed with OpenSees and SeismoStruct software packages. The performance requirements, according NS-EN 1998-3 [32], refers to the state of damage in the structure. It includes three limit states defined as
a) Near Collapse (NC): the structure is heavily damaged.
b) Significant Damage (SD): the structure is significantly damaged and uneconomic to repair.
c) Damage Limitation (DL): the structure is only lightly damaged, moderate permanent drifts are present and economically repairable.
Moreover, NS-EN 1998-1 NA 4.4.3.2 [31] states that such control is not mandatory in Norway. Therefore, in this thesis the inter-storey drifts will be determined at different stages and evaluated in accordance to the study presented by AM. Mwafy and AS. Elnashai [28], where complete collapse of a structure is considered once the inter-storey drift exceeds the value of 3% (SEAOC-Vision 2000).

The response spectrum adopted in the PA is based on NS-EN 1998-1 [31] and is illustrated in Figure 3.5. This report discusses over-strength and ductility factors in accordance to *FEMA P695* [38]. The reason is it provides an easy and explicit procedure for assessment of the aforementioned factors rather than NS-EN 1998-1. The target displacement is achieved as stated by NS-EN 1998-1.

5.2 Single degree of freedom system (SDOF)

The fundamental or first mode shape of the elastic numerical model determined with OpenSees is

$$\Phi_1 = \begin{bmatrix} 1 & 0.66 & 0.35 & 0.11 \end{bmatrix}^{\mathrm{T}} \tag{5.1}$$

The total lumped masses at each storey are determined in section 3.6.3 and the model of the analysis is reported in section 4.1. Hence, the mass matrix is

$$\mathbf{m} = \mathrm{diag} \begin{bmatrix} 125 & 192 & 193 & 196.5 \end{bmatrix} \mathrm{tons} \tag{5.2}$$

The control node is assessed at the top middle of the roof. The key parameter, which are the equivalent mass m^* and the transformation factor Γ, of the SDOF-system are determined in accordance to NS-EN 1998-1. Hence, the equivalent mass m^* of the SDOF-system is

$$m^* = \sum m_i \cdot \Phi_i = 125 \cdot 1 + 192 \cdot 0.66 + 193 \cdot 0.35 + 196.5 \cdot 0.11 = 341 \text{ tons} \tag{5.3}$$

and the transformation factor is

$$\Gamma = \frac{m^*}{\sum m_i \cdot \Phi_i^2} = \frac{341\text{tons}}{(125 \cdot 1^2 + 192 \cdot 0.66^2 + 193 \cdot 0.35^2 + 196.5 \cdot 0.11^2)\text{tons}} = 1.453 \tag{5.4}$$

5.3 Pushover curves

The capacity curves are determined by computing non-linear static analyses of the numerical models. The analyses are conducted with constant gravity loads and monotonically increasing lateral loads that are applied on the masses of the structure until 20% loss of the capacity is reached. The obtained results are presented in Figure 5.1. The maximum base shear capacities

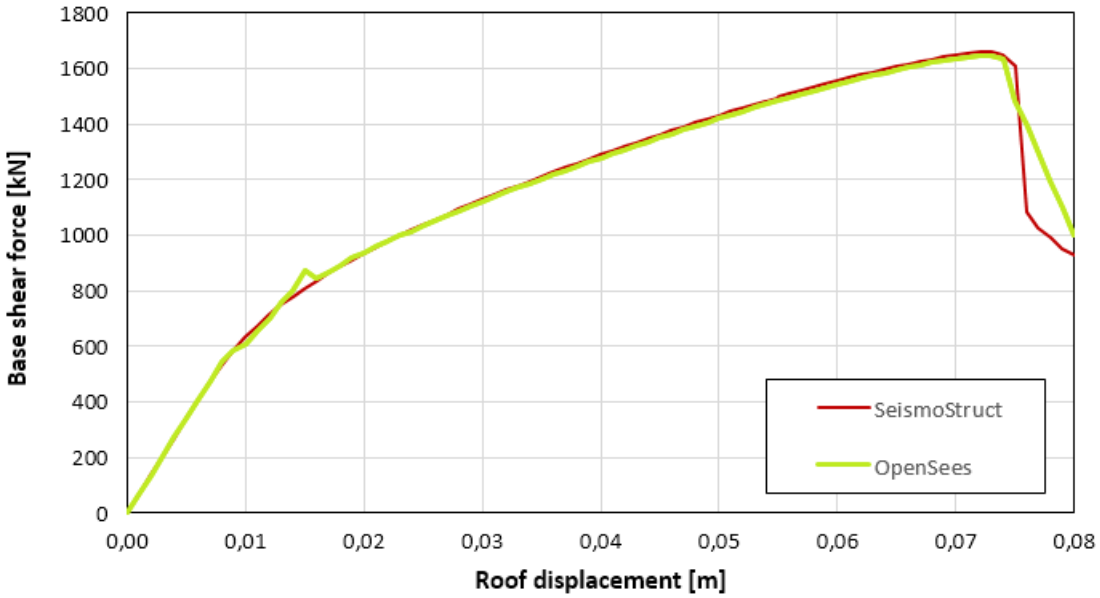

Figure 5.1: Non-linear static curves.

from SeismoStruct and OpenSees resulted to be 1660 kN and 1648 kN, respectively. This illustrates that a correct numerical models are implemented to exhibit the structures behaviour. In order to estimate the period-based ductility of the system, it is necessary to determine the yield displacement. It is also worth to mention that the effective roof displacement is directly proportional to the maximum base shear normalized by the buildings weight and to the square of the fundamental period T_1 [38]. As afore-stated in section 2.3.2, Eq. (2.25) defined the effective yield roof drift displacement, d_{eff}. The natural periods, as seen in section 4.2, are founded by computing the eigenvalue analyses of the numerical models. The results of the first natural periods are: T_1 = 0.432 and 0.435 s, for SeismoStruct and OpenSees, respectively. In addition, Figure 5.2 gives an insight of the normalized base shear versus roof drift ratio (%), which is the ratio between the maximum displacement at the roof and total height of the structure. The yield

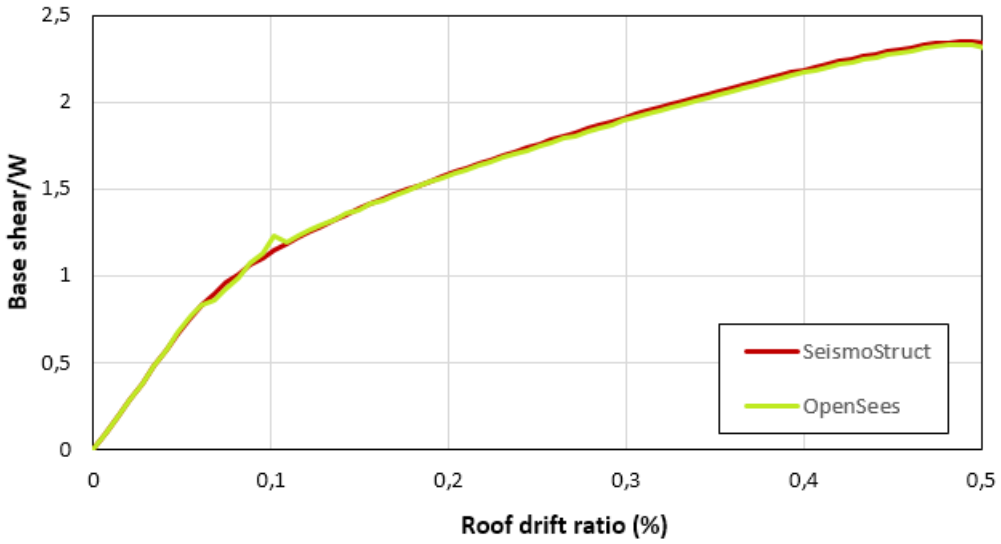

Figure 5.2: Normalized base shear-roof drift ratio relationship.

displacement d_{eff} at the roof level is

$$\text{SeismoStruct}: d_{eff} = 1.453 \cdot \frac{1660 \text{ kN}}{341 \text{ tons} \cdot 9.81 \text{ m/s}^2} \cdot \frac{9.81 \text{ m/s}^2}{4\pi^2} \cdot (0.440 \text{ s})^2 = 0.033 \text{ m} \quad (5.5)$$

$$\text{OpenSees}: d_{eff} = 1.453 \cdot \frac{1648 \text{ kN}}{341 \text{ tons} \cdot 9.81 \text{ m/s}^2} \cdot \frac{9.81 \text{ m/s}^2}{4\pi^2} \cdot (0.435 \text{ s})^2 = 0.034 \text{ m} \quad (5.6)$$

As it could be observed, both software packages render similar results.

5.4 Over-strength and period-based ductility

Both the over-strength and period-based ductility factors are assessed in accordance to *FEMA P695* [38]. The over-strength factor, Ω, is determined in accordance to Eq.(2.23) and repeated here for convenience

$$\Gamma = \frac{F_{max}}{F_{el}}$$

Here, F_{max} is the maximum base shear force and its value is plotted from Figure 5.1, whereas the design base shear force F_{el} per wall is previously determined in section 3.6.4 (see Figure 3.8). The results are presented in Table 5.1.

Table 5.1: Over-strength factor.

Software	F_{max} [kN]	F_{el} [kN]	Ω
SeismoStruct	1660	432.5	3.84
OpenSees	1648	432.5	3.81

The period-based ductility, μ_T, is calculated in accordance to Eq. (2.24), repeated here for convenience,

$$\mu_T = \frac{d_u}{d_{eff}}$$

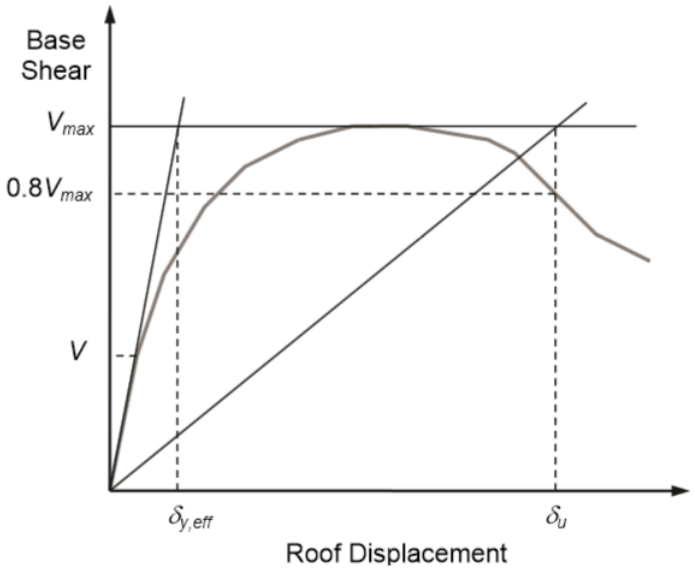

Figure 5.3: Idealized non-linear static pushover curve. The Figure is re-plotted from *FEMA P695* [38].

Here, the roof displacement $\mathrm{d_u}$ at $0.8\mathrm{F_{max}}$, while the yield roof displacement, $\mathrm{d_{eff}}$, is defined in section 5.3 (see Figure 5.3 for better understanding). The results are presented in Table 5.2.

Table 5.2: Period-based ductility.

Software	$0.8\mathrm{F_{max}}$ [kN]	$\mathrm{d_u}$ [m]	$\mathrm{d_{eff}}$ [m]	μ_T
SeismoStruct	1328	0.076	0.033	2.30
OpenSees	1318	0.077	0.034	2.26

It is evident that the software packages gives reliable results for both over-strength and ductility factors.

5.5 Target displacement

The theoretical background of the target displacement is reported in section 2.3.2. First, the capacity curves determined in the previous section are scaled by the transformation factor Γ in order to embark the so-called idealized bi-linear concept.

Prior to finding the target displacement, different parameters are required to be defined: $\mathrm{d_m^*}$, the displacement at the formation of a plastic mechanism, and $\mathrm{T^*}$, the elastic period of the SDOF system. These parameters are determined with an idealized bi-linear force-displacement relationship, usually known as the elastic-perfectly plastic concept. These force-displacement relationships are acquired in accordance to NS-EN 1998-1, for both curves, and are presented in Figure 5.4.

In accordance to Figure 5.4, the values of the yield forces, $\mathrm{F_y^*}$, and their respective displacements, $\mathrm{d_m^*}$ (assumed target displacement), are reported in Table 5.3.

The deformation energy, $\mathrm{E_m^*}$, is determined by requiring equivalences of the areas below the actual and idealized curves as stated by NS-EN 1998-1. Hence, the result for SeismoStruct

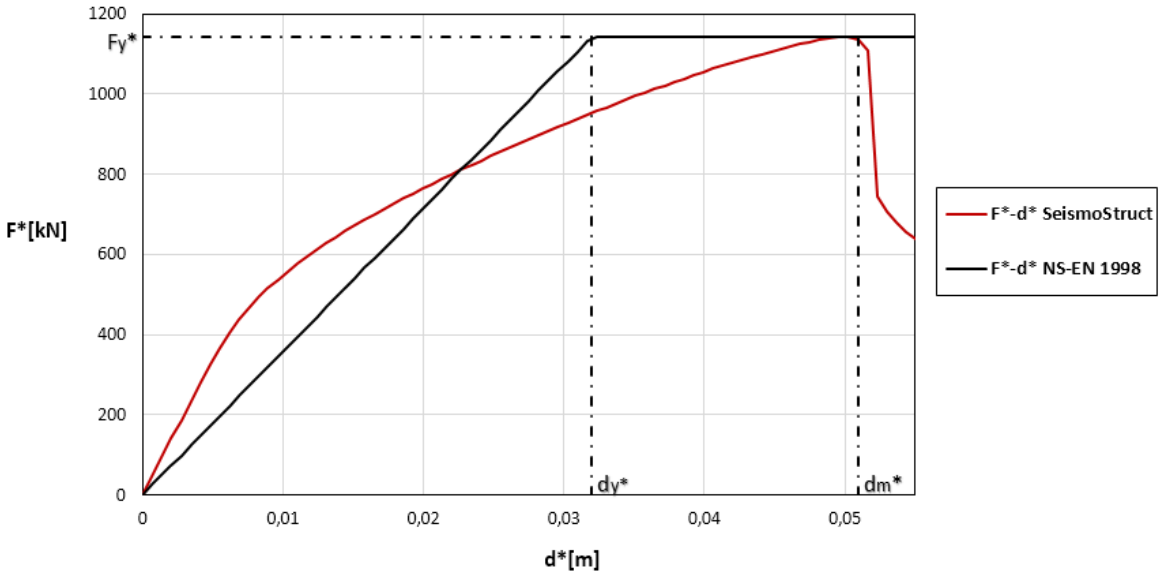

(a) SeismoStruct.

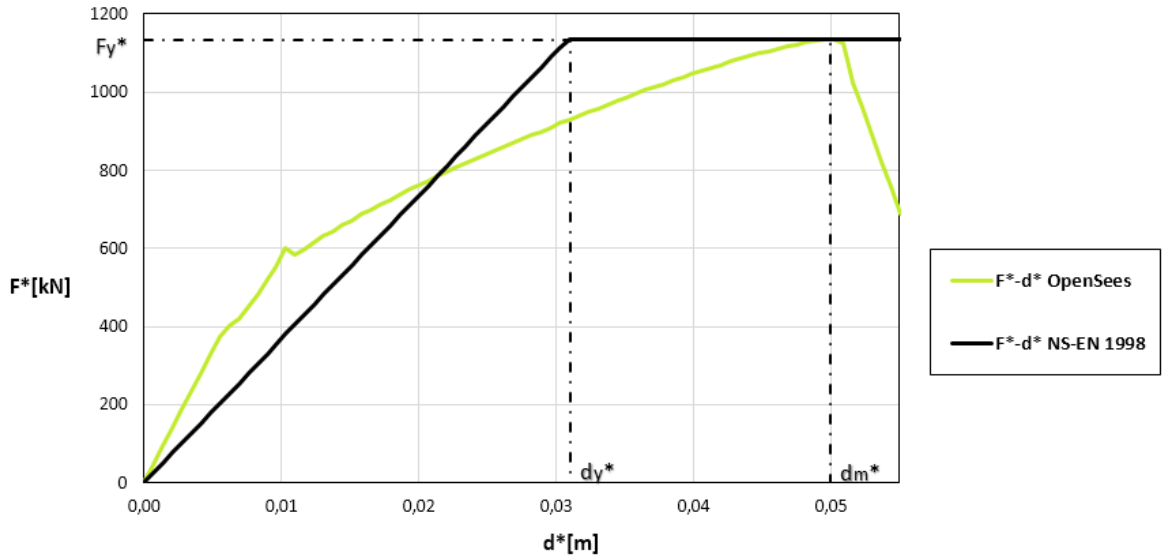

(b) OpenSees.

Figure 5.4: $F^* - d^*$ relationships.

and OpenSees, is 40 and 39 kNm, , respectively. The yield displacement, d_y^*, is defined by Eq. (2.15) and repeated here for convenience,

$$d_y^* = 2(d_m^* - \frac{E_m^*}{F_y^*})$$

and equals to

$$d_{y-\text{SeismoStruct}}^* = 2(0.051\ \text{m} - \frac{40\ \text{kNm}}{1142\ \text{kN}}) = 0.032\ \text{m} \tag{5.7}$$

$$d_{y-\text{OpenSees}}^* = 2(0.050\ \text{m} - \frac{39\ \text{kNm}}{1134\ \text{kN}}) = 0.031\ \text{m} \tag{5.8}$$

Table 5.3: Yield forces and displacements according to NS-EN 1998-1.

Software	F_y^* [kN]	d_m^* [m]
SeismoStruct	1142	0.051
OpenSees	1134	0.050

The elastic period of the idealized SDOF system, T^*, defined by Eq. (2.14) and is

$$T^*_{\text{SeismoStruct}} = 2\pi \cdot \sqrt{\frac{341 \text{ tons} \cdot 0.031 \text{ m}}{1094 \text{ kN}}} = 0.61 \text{ s} \tag{5.9}$$

$$T^*_{\text{OpenSees}} = 2\pi \cdot \sqrt{\frac{341 \text{ tons} \cdot 0.030 \text{ m}}{1125 \text{ kN}}} = 0.61 \text{ s} \tag{5.10}$$

Both the software packages rendered exact result for the elastic period of the system. According to NS-EN 1998 Table 3.2, the corner period T_c of the elastic spectrum is 0.6 s. Since the acquired elastic period T^* is greater than T_c, the target displacement of the SDOF system d_t^* is equal to d_{et}^*, also known as the *equal displacement rule* (see Eq. (2.18)). The elastic acceleration response spectrum at the period T^* is obtained as stated by NS-EN 1998-1 clause 3.2.2.2 and equals to

$$S_e(T^*) = 0.85 \text{ m/s}^2 \cdot 1.15 \cdot 2.5 \cdot \frac{0.6}{0.61} = 2.40 \text{ m/s}^2 \tag{5.11}$$

The target displacement, d_t^*, of the idealized SDOF-system, for both software packages is

$$d_t^* = d_{et}^* = 2.40 \text{ m/s}^2 \cdot [\frac{0.61 \text{ s}}{2\pi}]^2 = 0.023 \text{ m} \tag{5.12}$$

It is clear that the assumed target displacement d_m^* differs significantly from the determined displacement d_t^*, ergo, an iterative process is required where a new idealized bilinear-curve must be defined. Table 5.4 and 5.5, shows the results acquired for SeismoStruct and OpenSees, respectively.

Table 5.4: Target displacement of SDOF according to NS-EN 1998-1, SeismoStruct.

Iteration	d_m^* [m]	F_y^* [kN]	E_m^* [kNm]	d_y^* [m]	T^* [s]	d_t^* [m]
0	0.051	1142	40	0.032	0.61	0.023
1	0.023	1065	13	0.022	0.52	0.017
2	0.017	900	8	0.016	0.49	0.015
3	0.015	844	6	0.015	0.49	0.015

Table 5.5: Target displacement of SDOF according to NS-EN 1998-1, OpenSees.

Iteration	d_m^* [m]	F_y^* [kN]	E_m^* [kNm]	d_y^* [m]	T^* [s]	d_t^* [m]
0	0.050	1125	38	0.031	0.61	0.023
1	0.023	1068	13	0.022	0.52	0.017
2	0.017	881	8	0.016	0.49	0.015
3	0.015	840	6	0.015	0.49	0.015

The real target displacement of the structure (MDOF system), i.e. the expected displacement during the earthquake, is defined by Eq. (2.22) and repeated here for convenience

$$\mathrm{d_t} = \Gamma \cdot \mathrm{d_t^*}$$

This results to be $\underline{0.021}$ m for both SeismoStruct and OpenSees. According to Figure 5.1, the corresponding base shear forces at the target displacements are 957 kN and 956 kN, for SeismoStruct and OpenSees, respectively. Furthermore, the inter-storey drifts (the difference between displacements of stories normalized by the storey height at each floor), shear forces and displacements at the target point are acquired and presented in Figure 5.5.

5.6 Discussion

For the Pushover analysis (PA), both SeismoStruct and OpenSees gives a good agreement in the results obtained in Figure 5.1. This reveals that an accurate numerical model is implemented to exhibit the structure response. Additionally, it is observed that the base shear capacity reduces steeply after the maximum value is reached as for the unconfined material model with an ultimate compressive strain equal to 0.006 (see Figure 5.6). It is also worth to mention that excessive drifts in the stories coupled with P-δ effects on the walls limits the maximum capacity and induces the collapse of the structure.

In the linear static analysis, the structure was designed in accordance to NS-EN 1998-1, by using the lateral force method (see section 3.6.4). Here, a modification or behaviour factor, q, equal to 3.6 is applied. According to NS-EN 1998-1, the behaviour factor depends on the structure types (for example wall system, frames, etc.) and accounts for over-strength and ductility of the structure. The over-strength factor, from PA, for SeismoStruct and OpenSees is equal to 3.84 and 3.81, respectively. Here, a similar result with negligible differences (1%) is obtained. The ratio between the over-strength factor defined by NS-EN 1998-1 and the one determined according to *FEMA P695*, for SeismoStruct and OpenSees, is 3.6/3.84= 0.94 and 3.6/3.81= 0.94, respectively. This reveals that NS-EN 1998-1 adopts a relatively conservative value (94%) of the behaviour factor. Moreover, the elastic design base shear force of the structure is found to be 432.5 kN as per calculation (see section 3.6.4), where the stiffness is reduced by 50%. After computing the PA, the base shear at the target displacement resulted to be 957 kN and 956 kN, from SeismoStruct and OpenSees, respectively (see Figure 5.5(a)). These values are much greater than the elastic design base shear force and endorses that the walls have reserved shear capacity (see Figure 5.5(a)). If the assessed over-strength factor (OpenSees) is implemented in the linear design, the corresponding design base shear force becomes

$$\mathrm{F_b} = 432.5\mathrm{kN} \cdot \frac{3.6}{3.81} = 409 \text{ kN}. \tag{5.13}$$

As it is observed, the design base shear force is reduced by 6%, thereby, it can be concluded that a conservative over-strength factor is adopted in the linear seismic design of the wall-equivalent dual-system.

The period-based ductility factor, μ_T, determined in accordance to *FEMA P695*, is equal to 2.30 and 2.26 for SeismoStruct and OpenSees, respectively (see Table 5.2). This factor represents the ratio between the maximum displacement at 20% loss of the shear capacity and the yield

displacement. NS-EN 1998-1 assesses the ductility of a wall in DCM, by multiplying the base shear force with a magnification factor, ε, of 1.5, ergo, by increasing the overturning moment at the base. The reason is to develop the formation of plastic hinges only at the base section [15]. The result obtained for the ductility factor is 2.26/1.5=1.51 (OpenSees) higher than that required in NS-EN 1998-1. This demonstrates that the walls have seemingly reserves for both capacity and ductility.

The target displacement is assessed in accordance to NS-EN 1998-1+B3 and an exact result, which is 0.021 m, between the software packages is obtained. The displacement pattern of the system at the target point, as shown in Figure 5.5(b), reveals that the structure primarily vibrates in the first mode and the sway motion follows the distribution of the lateral loads. When assessing the target displacement, a relevant observation is made. The yield forces $\mathrm{F}_{\mathrm{y}}^{*}$ calculated in this report are found to be 1142 and 1134 kN, for SeismoStruct and OpenSees (see Table 5.3), respectively. Conversely, the base shear forces at the target displacement according to Figure 5.1 and Figure 5.5(a) are 957kN and 956 kN for SeismoStruct and OpenSees, respectively. This exhibits that the response of the structure is elastic and hinders to capture the performance of the wall-equivalent dual-system in the plastic domain.

According to SEAOC (Vision 2000) [28], the state of complete collapse is reached when the inter-storey drift ratio (IDR) exceeds the value of 3%. The IDR (%) are assessed at the target displacement and are presented in Figure 5.5(c). A this stage, the structure designed in this report illustrates a peak of IDR of 0.2% and therefore emphasizes that non-structural damage has occurred. In addition, such result is expected due to the nature of the response (elastic). In the $4^{\mathrm{th}}\mathrm{floor}$, however, it is observed that SeismoStruct renders slightly higher (3%) IDR compared to OpenSees, whereas in the lower stories a contrary result is obtained. This result is due to a slightly differences in the estimation of the displacements (see Figure 5.5(b)) at each storey which are negligible for further purposes. In addition, the maximum IDR are exhibited when the permanent displacement reaches values of 0.076m and 0.073, for SeismoStruct and OpenSees respectively. It is worth to mention that the latter values are in the plastic domain and are presented in Figure 5.7. It is noticed that IDR at the fourth floor is 0.68 and exceeds by a factor of 0.68/0.2= 3.4 compared to the value acquired at the target displacement (SeismoStruct). This indicates that the structure is highly deformed at its maximum capacity, but still non-structural damage has occurred.

Pushover analysis captures only the effect of a single mode and its application is limited. However, it is a major tool for assessing the basic relations between seismic demand and capacity. Furthermore, the analysis explores the main structural parameters such as deformation, overstrength and ductility factors by determining the structural response [14]. Since the response of a structure due to an earthquake is a dynamic problem and usually inelastic, the theoretical correct method is the non-linear time-history (dynamic) analysis. In addition, the response of the structure in PA is elastic, thus, it is interesting to investigate the performance of the wall-equivalent dual-system in the post-elastic range through non-linear dynamic analysis, where the contribution from higher modes are accounted.

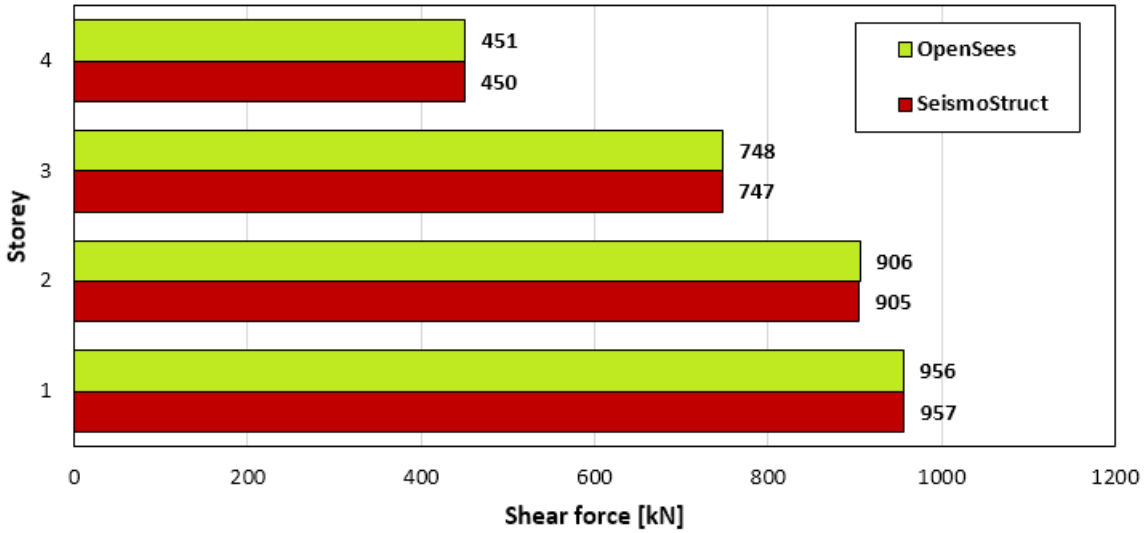

(a) Shear forces at the target displacement.

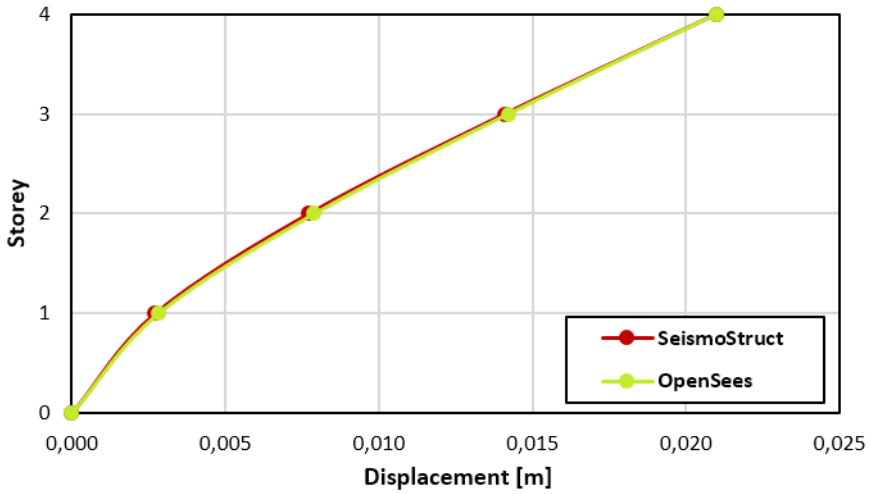

(b) Displacement pattern at the target displacement.

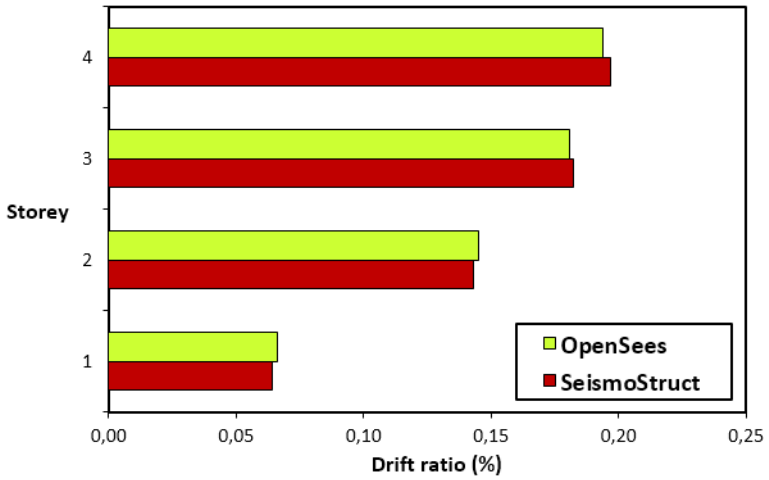

(c) Inter-storey drifts (%)from Pushover analysis.

Figure 5.5: Results from Pushover analysis (PA).

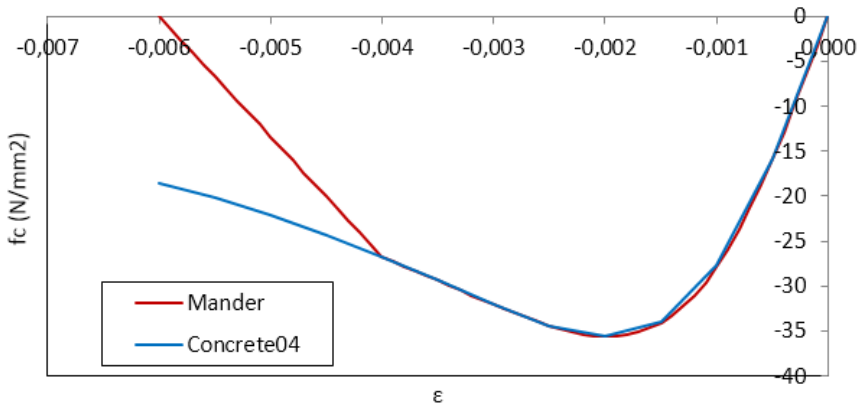

Figure 5.6: Stress-Strain relationship for the wall sections.

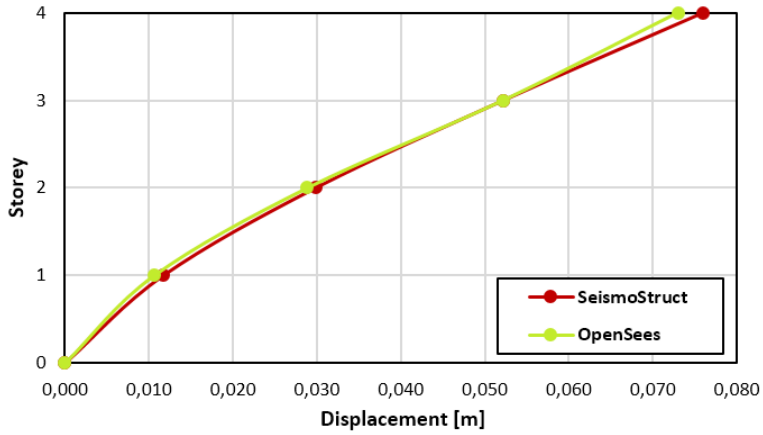

(a) Permanent displacement.

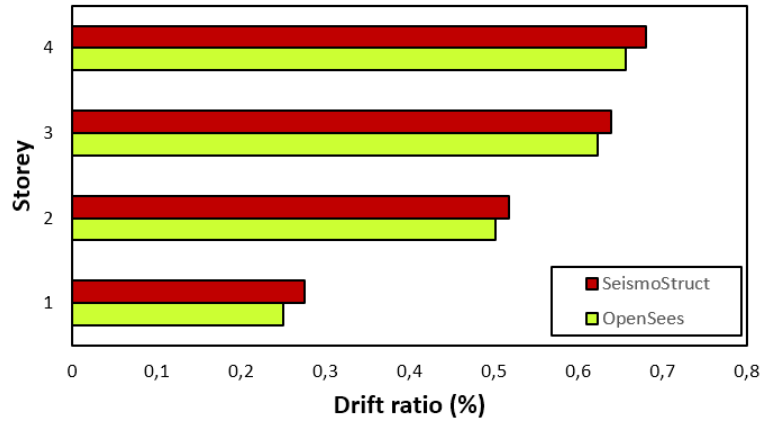

(b) Maximum IDR(%).

Figure 5.7: Maximum IDR(%) from PA.

Chapter 6

Non-linear Time-History Analysis

6.1 Introduction

The theoretical background of the Non-Linear Time-History analysis (NLTHA) is reported in section 2.3.3. This chapter contains the assessment of the NLTHA and rigorously discusses the results (see section 6.4). The numerical model of the structure is executed with both SeismoStruct and OpenSees.

6.2 Seismic Input Motions

6.2.1 Selection of ground motions

Seven ground motions are selected from the Pacific Earthquake Engineering Research Centre (PEER) Ground Motion Database [3] to fulfil the requirement of NS-EN 1998-1 [31]. They are illustrated in Figure 6.1 and Table 6.1. The choice of those ground motions is not a straightforward process, hence, it is made in cooperation with my supervisors. For the selection of the ground motions, the following benchmarks are used:

- PGA $\geq 2.0\ \mathrm{m/s^2}$,
- Moment magnitude greater than 6.5,
- Solely horizontal far-fault recordings are considered, i.e. $\mathrm{R_{rup}} \leq 20\ \mathrm{km}$,
- Shear wave velocity, $240\ \mathrm{m/s} \leq \mathrm{V_{s30}} \leq 360\ \mathrm{m/s}$,
- No pulse-like excitation,
- To prevent bias, only one recording from each event was chosen.

The ground motions are applied at the base of the numerical models as a uniform lateral load pattern of excitation.

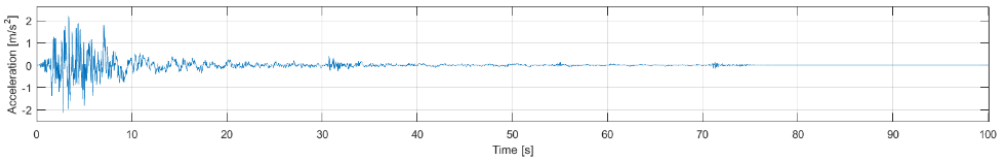

(a) San Fernando.

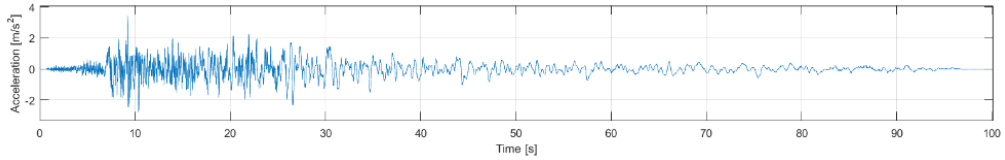

(b) Imperial Valley.

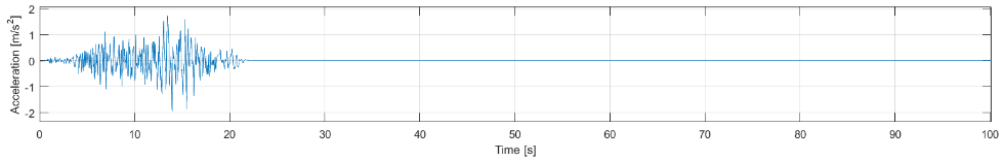

(c) Superstition Hills.

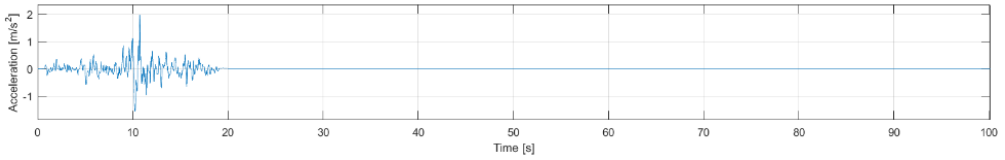

(d) Spitak.

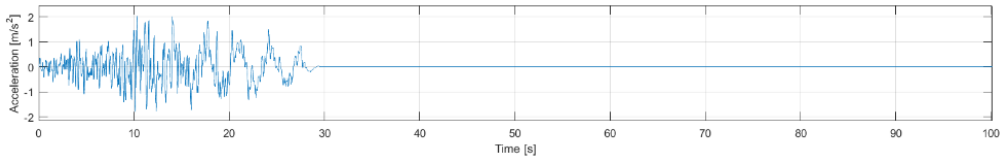

(e) Manjil.

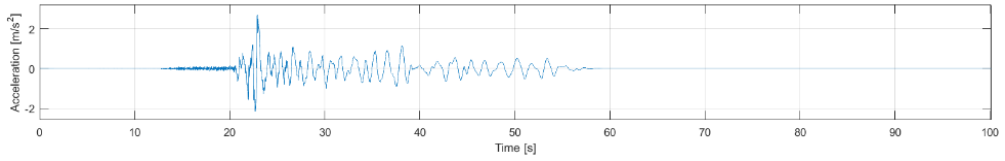

(f) Joetsu City.

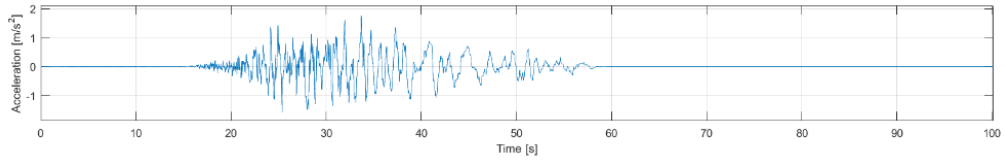

(g) Iwate

Figure 6.1: Non-scaled ground motion time histories.

Table 6.1: Selected ground motions from the PEER Ground Motion Database.

RSN	Earthquake	Date	M	R_{jb}(kM)	R_{rup}(kM)	V_{s30} (m/s)	PGA (m/s^2)
68	San Fernando (S.F.)	09.02.1971	6.6	23	23	316	3.04
169	Imperial Valley (I.V)	15.10.1979	6.5	22	22	242	4.21
724	Superstition Hills (S.H.)	24.11.1987	6.5	27	27	317	2.16
730	Spitak (S.)	07.12.1988	6.8	24	24	355	2.65
1634	Manjil (M.)	20.06.1990	7.4	76	76	303	2.45
4853	Joetsu City (J.C.)	16.07.2007	6.8	26	28	295	3.43
5786	Iwate (I.)	13.06.2008	6.9	35	35	300	2.45

Table 6.2: Scaling factors for the selected ground motions.

San Fernando	Imperial Valley	Superstition Hills	Spitak	Manjil	Joetsu City	Iwate
0.812	0.401	0.420	0.654	0.329	0.378	0.886

6.2.2 Scaling of the time histories

In order to fit the elastic response spectrum shown in Figure 6.2, the selected ground motion inputs are scaled to the first natural period of the elastic model computed with Robot ($T_1 = 0.48$ s, see Table 4.1). The methodology of scaling to the first natural period follows the dominance of the first mode of the structure. The scaling factor is the ratio between the spectral accelerations given by NS-EN 1998-1 and the spectral acceleration of the selected input motions, both at the first natural period. As an example, the spectral acceleration defined by NS-EN 1998-1 at the first natural period is 2.44 m/s^2 (see Figure 6.2), while the spectral acceleration for the Imperial Valley ground motion input file is 6.083 m/s^2. Therefore, the corresponding scaling factor is 2.440/6.083 = 0.401. The input file for the analysis is the original one multiplied by the scaling factor. The scaled and non-scaled response spectrum of the selected ground motions are computed in Matlab [26] following Newmark method and the script is reported in Appendix C. The resulting spectra are presented in Figure 6.2 and the scaling factors for each ground motion are shown in Table 6.2.

6.3 Responses

As for the Pushover analysis, the control node in the NLTHA is assessed at the roof. The results from NLTHA, for displacement and base shear force, are presented in Figure 6.3 and Figure 6.5 respectively. In order to reveal inconsistencies among the software programmes, the displacement at the roof and base shear force are plotted in the time range of interest. Those are highlighted in Figure 6.4 and Figure 6.6, where high discrepancies are observed in the time range between 6-14 s and 13-35 s, for San Fernando and Imperial Valley ground motions due to high frequency content. Table 6.3 depicts the maximum displacement at the control node and base shear force obtained in the NLTHA. In addition, differences between the obtained values are also presented to highlight dissimilarities between the software packages. The hysteric curves, control node displacement versus base shear force, are presented in Figure 6.7. Furthermore, the maximum inter-storey drift ratio (IDR) from each ground motion and the average IDR are presented in Figure 6.8.

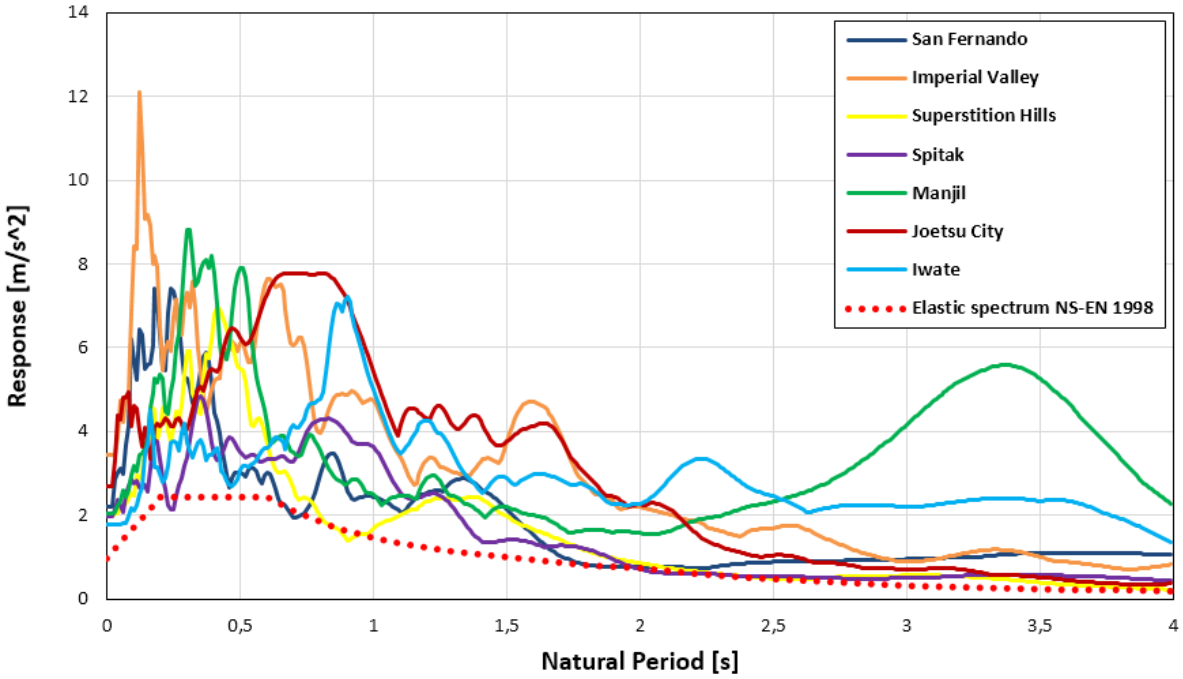

(a) Non-fitted response spectrum.

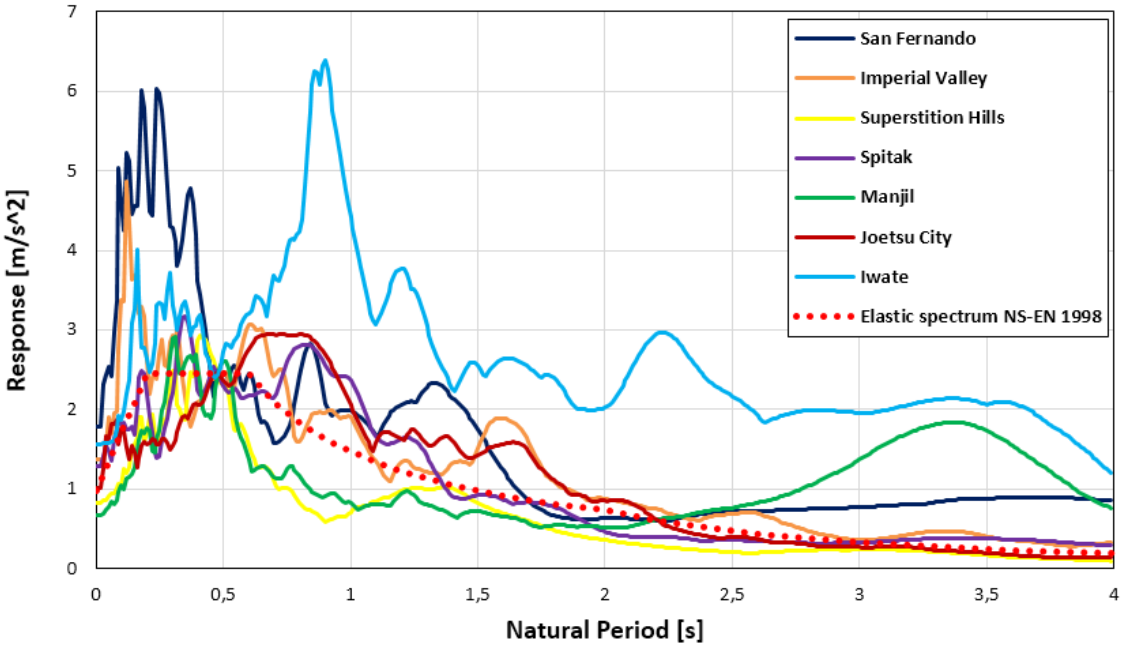

(b) Fitted response spectrum.

Figure 6.2: Response spectrum of ground motions.

As aforementioned in section 2.3.3, the design values for displacement and base shear force must be the average response parameter from the seven analysis, according to NS-EN 1998-1 clause 4.3.3.4.3. Therefore, the resulting maximum displacements of the control node (roof) are

$$\text{SeismoStruct} : \mathrm{d_{max}} = 0.019 \text{ m}$$

$$\text{OpenSees} : \mathrm{d_{max}} = 0.020 \text{ m}$$

Table 6.3: Maximum control node displacement and base shear force from NLTHA.

Software	Response	S.F.	I.V.	S.H.	S.	M.	J.C	I.
SeismoStruct	$\mathrm{d_{max}}$ (m)	0.019	0.019	0.021	0.016	0.017	0.018	0.025
OpenSees	$\mathrm{d_{max}}$ (m)	0.021	0.021	0.023	0.017	0.016	0.018	0.026
Difference (%)		11	11	10	6	6	-	4
SeismoStruct	$\mathrm{F_{b,max}}$ (kN)	1216	1041	1108	1064	960	1208	1292
OpenSees	$\mathrm{F_{b,max}}$ (kN)	1391	1212	1266	1181	1060	1356	1429
Difference (%)		14	16	14	11	10	12	11

and the maximum base shear forces are

$$\mathrm{SeismoStruct} : \mathrm{F_{b,max}} = 1127 \ \mathrm{kN}$$

$$\mathrm{OpenSees} : \mathrm{F_{b,max}} = 1271 \ \mathrm{kN}$$

The maximum base shear versus the control node displacement is depicted in Figure 6.10 together with the obtained average parameters and PA results. It is crucial to denote that the maximum values of these parameters does not occur simultaneously due to non-linear behaviour and contribution from higher modes [25]. Finally, the maximum base shear force, roof displacements and roof drift ratios (%) from each ground motions are presented in Figure 6.9 and discussed in section 6.5.

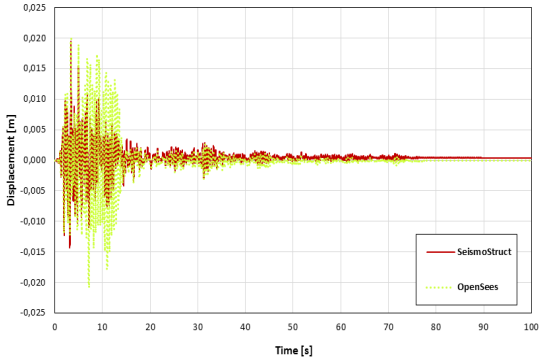

(a) San Fernando.

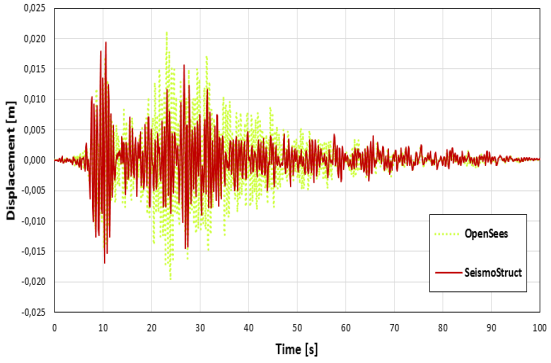

(b) Imperial Valley.

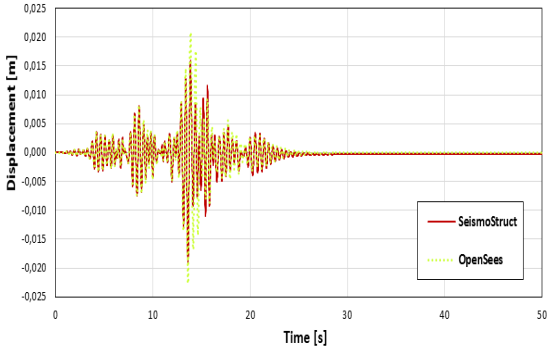

(c) Superstition Hills.

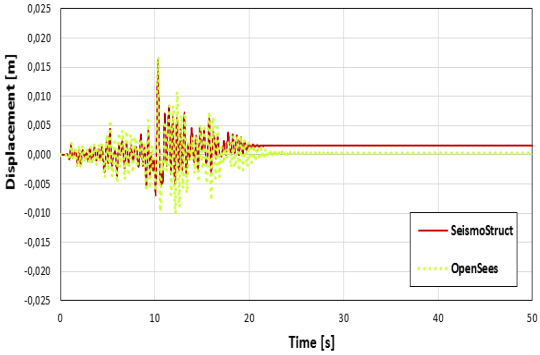

(d) Spitak.

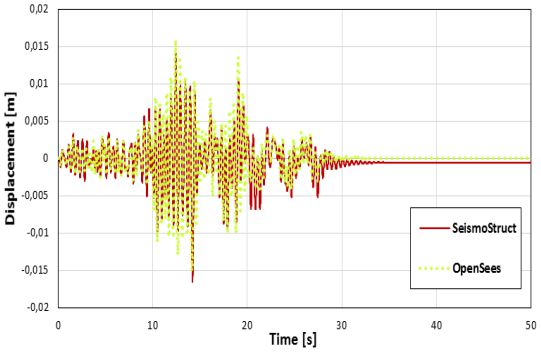

(e) Manjil.

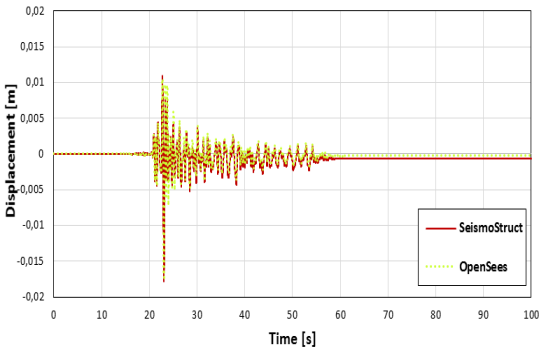

(f) Joetsu City.

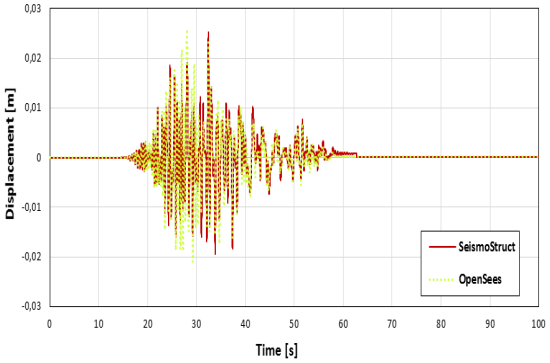

(g) Iwate.

Figure 6.3: Displacement of the control node.

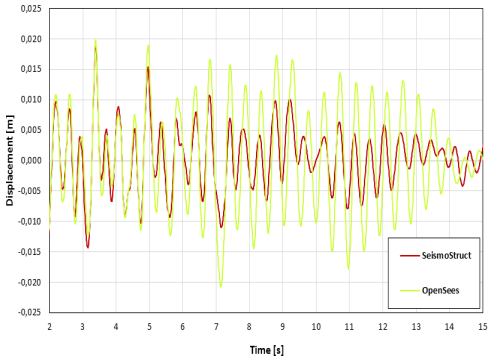

(a) San Fernando.

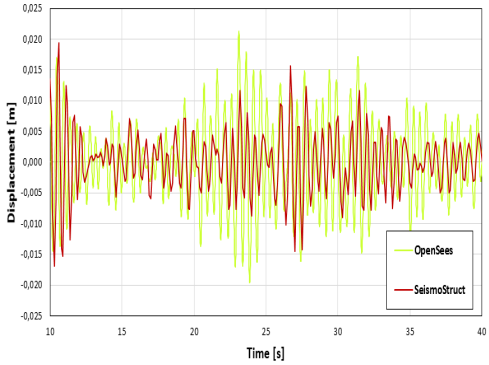

(b) Imperial Valley.

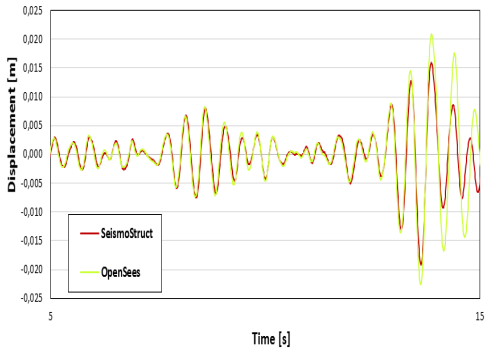

(c) Superstition Hills.

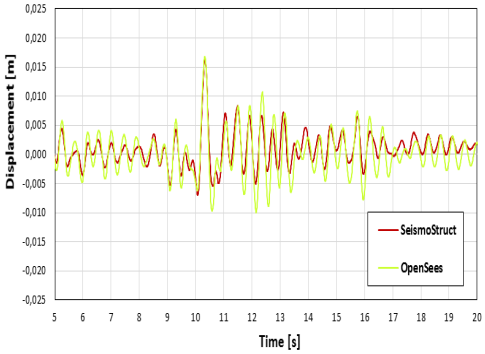

(d) Spitak.

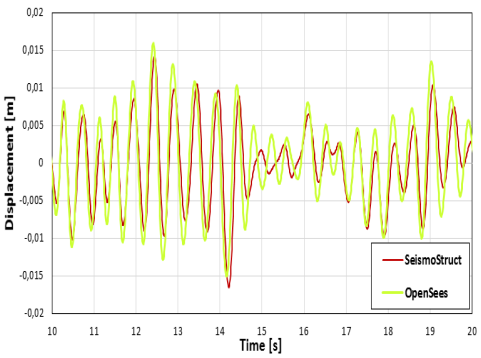

(e) Manjil.

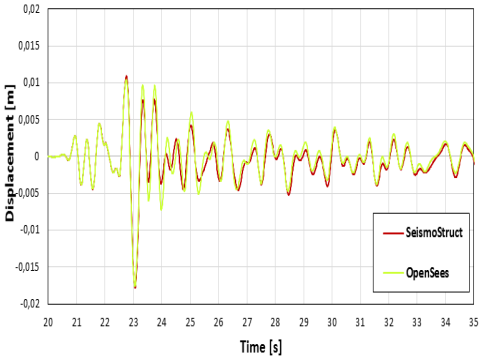

(f) Joetsu City.

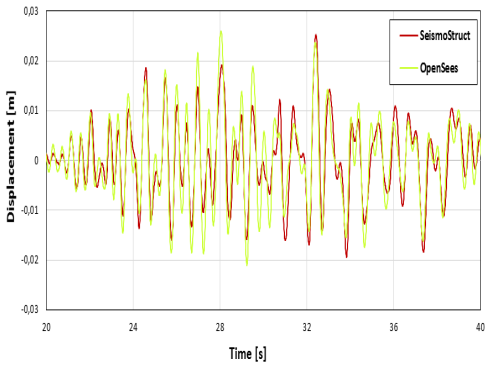

(g) Iwate.

Figure 6.4: Displacement of the control node in the time range of interest to reveal discrepancies.

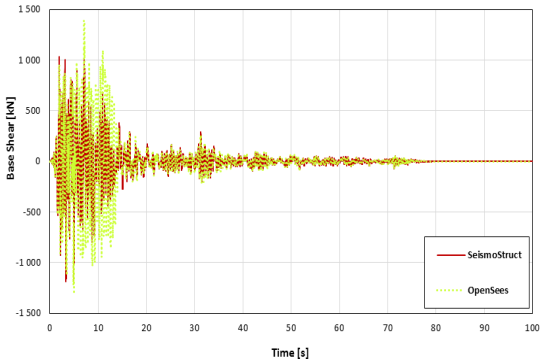

(a) San Fernando.

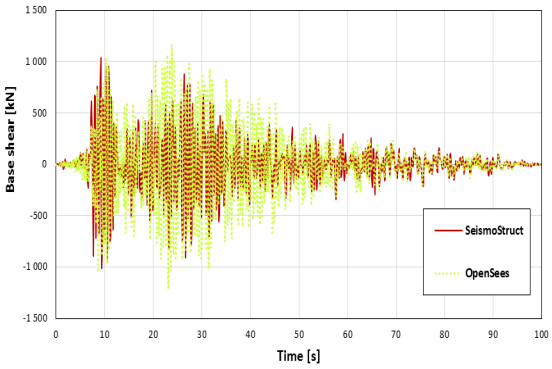

(b) Imperial Valley.

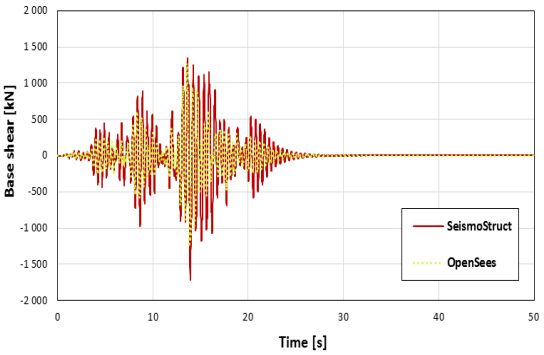

(c) Superstition Hills.

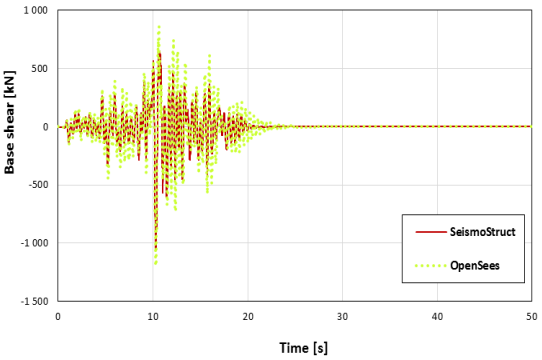

(d) Spitak.

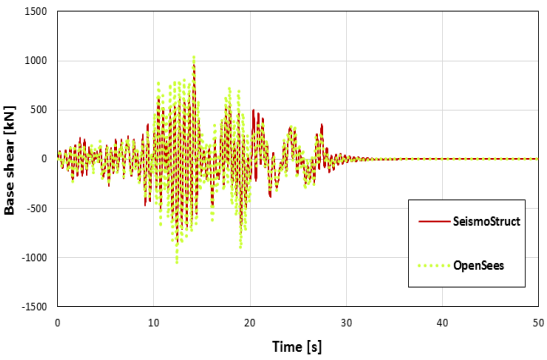

(e) Manjil.

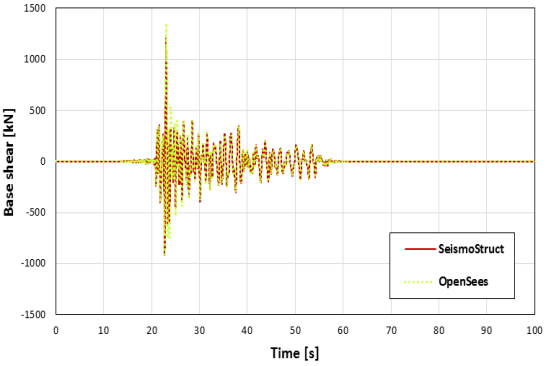

(f) Joetsu City.

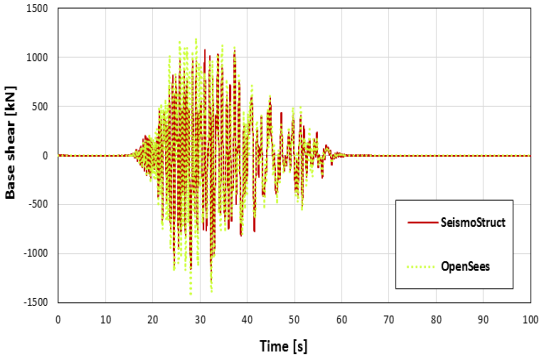

(g) Iwate.

Figure 6.5: Base shear force.

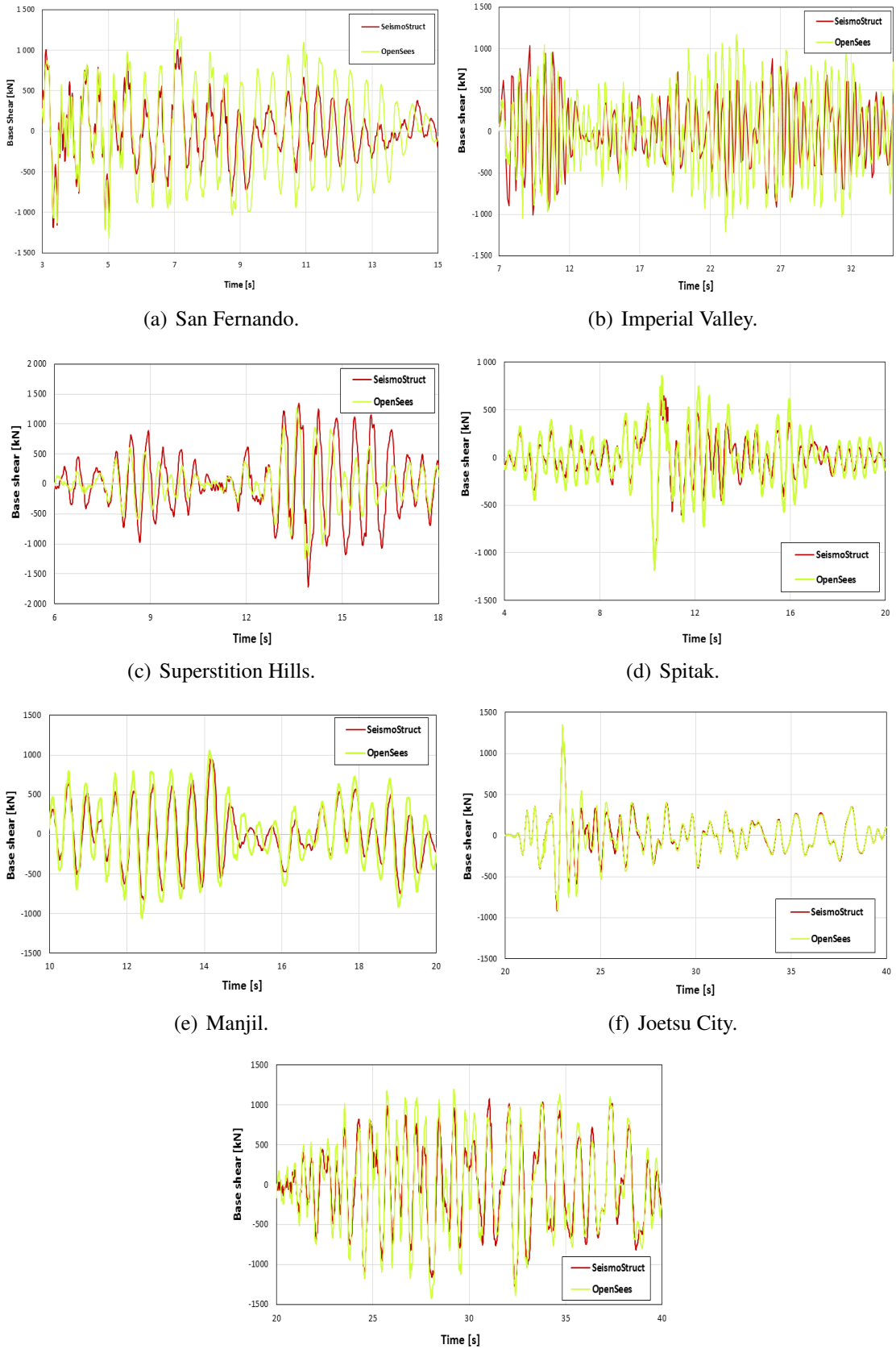

(a) San Fernando.

(b) Imperial Valley.

(c) Superstition Hills.

(d) Spitak.

(e) Manjil.

(f) Joetsu City.

(g) Iwate.

Figure 6.6: Base shear force in the time range of interest to reveal discrepancies.

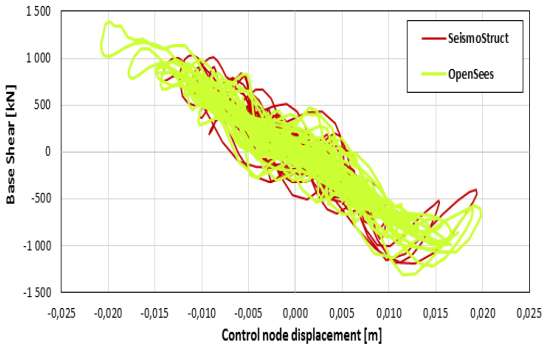

(a) San Fernando.

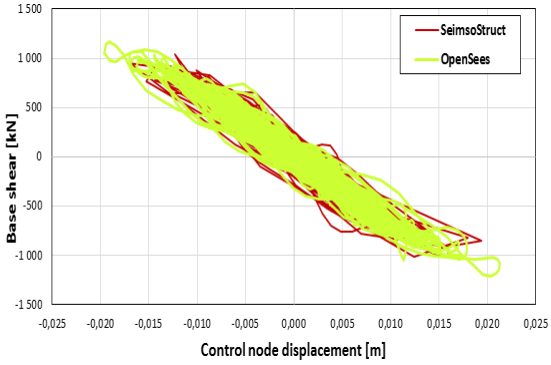

(b) Imperial Valley.

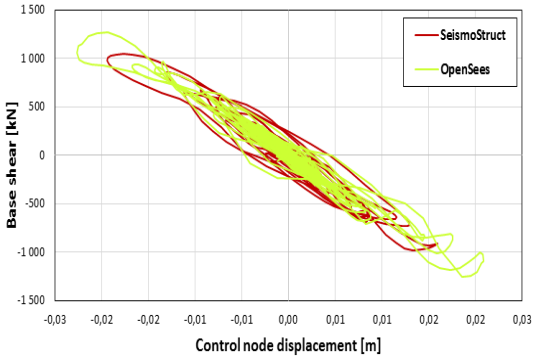

(c) Superstition Hills.

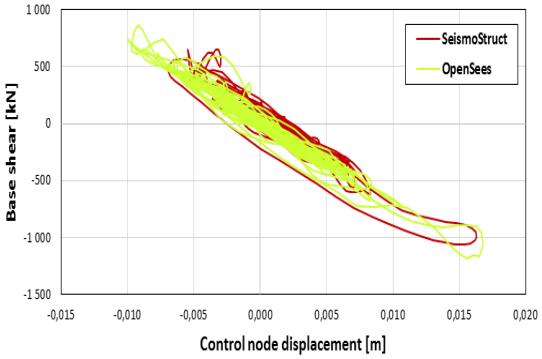

(d) Spitak.

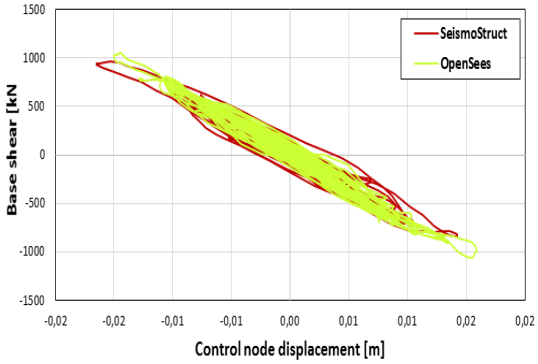

(e) Manjil.

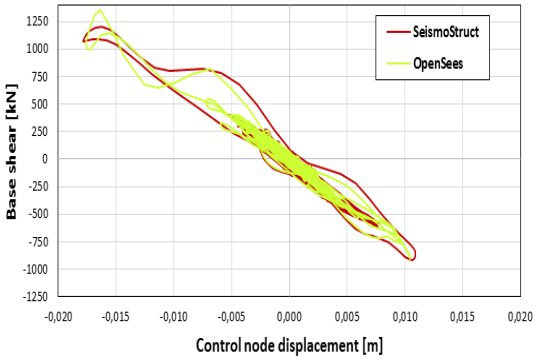

(f) Joetsu City.

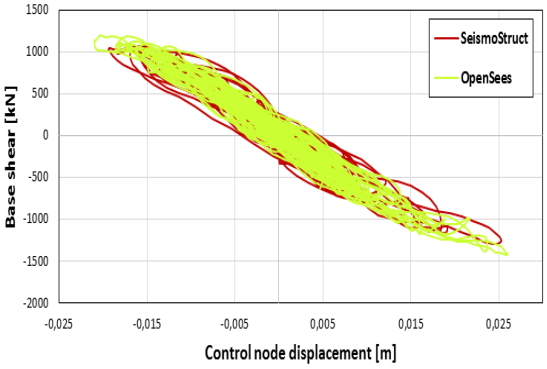

(g) Iwate.

Figure 6.7: Hysteric curves from NLTHA.

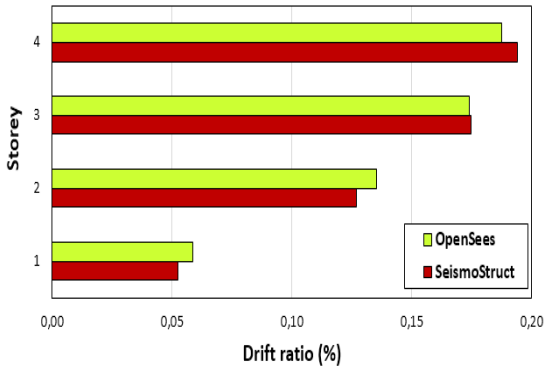

(a) San Fernando.

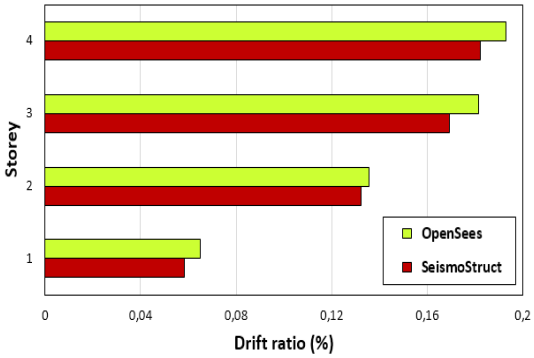

(b) Imperial Valley.

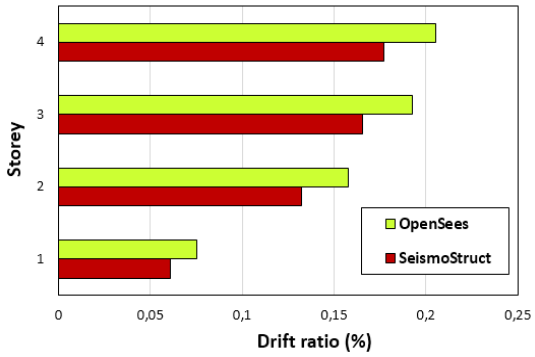

(c) Superstition Hills.

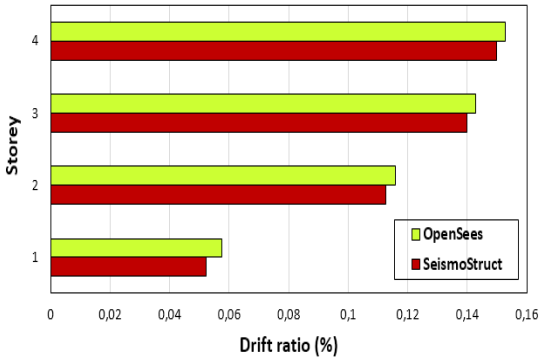

(d) Spitak.

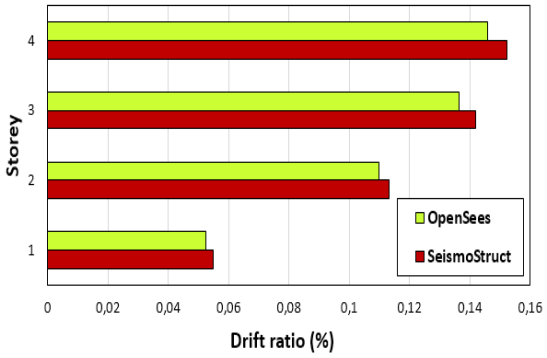

(e) Manjil.

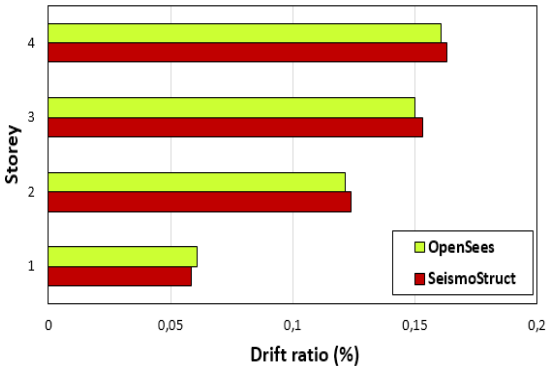

(f) Joetsu City.

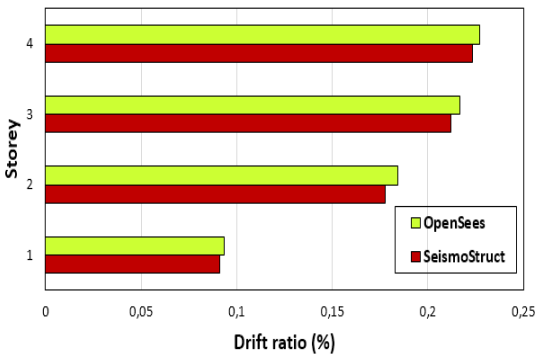

(g) Iwate.

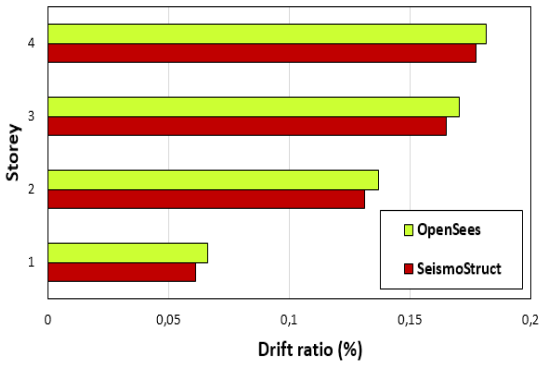

(h) Average inter-storey drift ratio from NTHA.

Figure 6.8: Inter-storey drift ratio from NLTHA.

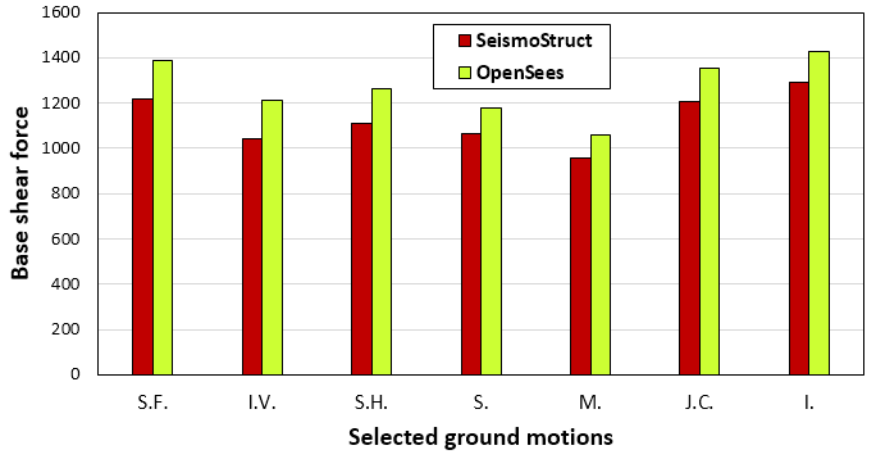

(a) Maximum base shear force.

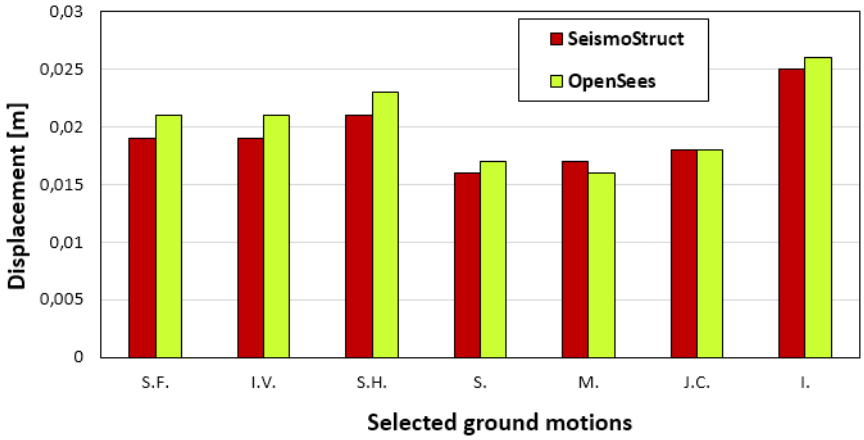

(b) Maximum control node displacement.

(c) Roof drift ratio (%).

Figure 6.9: Maximum base shear forces, control node displacements and roof drift ratios, NLTHA.

6.4 Discussion

As observed in Table 6.3, the results obtained for displacement of the control node from the individual NLTHA shows a relative agreement between SeismoStruct and OpenSees. In general, SeismoStruct renderer lower results compared to OpenSees (see Figure 6.9). The acquired average displacements are 0.019 and 0.02m, for SeismoStruct and OpenSees respectively. The observed differences between the two software programmes for displacements from each ground motion are in the range of 4-11% (see Table 6.3), ergo, the obtained average results differ only by 5%. This highlights that a consistent result for the roof displacement is achieved. The maximum and minimum exhibited displacements are from Iwate and Spitak ground motions. Thus, the values acquired from OpenSees are 0.026 and 0.017 m, respectively. Those results differ significantly from each other (53%) and from the average displacement. As a consequence of those inconsistent outcomes, it is more understandable to follow the requirement imposed in NS-EN 1998-1 to adopt at least seven ground motions and average the results. Furthermore, it is of major interest to compare the results acquired from each ground motions with PA results. That comparison is further discussed in section 6.5.1.

The hysteric curves are presented in Figure 6.5 and Figure 6.6. The results shows that OpenSees renders higher forces compared to SeismoStruct. In addition, it is observed that the largest discrepancy between the software packages is for Imperial Valley ground motion (16%) due to high frequency content. In general, the base shear forces determined from both software programmes correlates less compared to the displacements. Indeed, the average base shear forces are 1127 kN (SeismoStruct) and 1271 kN (OpenSees), which differs of 13% from each other. The reason is that shear forces are determined through derivatives of displacement fields, thus, the accumulation of errors are amplified [10]. The maximum and minimum base shear forces are obtained from Iwate and Manjil ground motions. This exhibits that forces and displacements are uncorrelated, because they do not occur simultaneously as for PA.

Figure 6.8 presents the inter-storey drift ratio for each of the time-history analysis and illustrates that the maximum result is obtained from Iwate ground motions. This result correlates with the maximum displacement achieved from the latter mentioned ground motion. In general, some differences are observed among the results obtained due to the errors in the estimation of the displacements. The average inter-storey drift ratio has a peak of 0.18%, which confirms that non-structural damage has occurred according to SEAOC (Vision 2000) [28].

6.5 Pushover analysis versus NLTHA

6.5.1 Displacement

The target displacement realized from the Pushover Analysis (PA) equals to 0.021 m. This result is consistent with the average displacement determined from NLTHA, which is 0.019 m (SeismoStruct) and 0.020 m (OpenSees). In addition, the structure response in PA is within the elastic range and hindered to capture the non-linear behaviour of the system in question. As a result , the error of the displacement is 10.5% in SeismoStruct and 5% in OpenSees. Furthermore, the PA curves are determined by applying an incremental lateral load defined by the first modal pattern and the response spectrum is fitted to the first natural period of the system in question. These results are in compliance with the study presented by Krawinkler and Seneviratna [23], where it is shown that PA provides reasonable results for structures governed by the first mode. Figure 6.10 depicts the results from PA and NLTHA, and illustrates that the permanent displacements from NLTHA occurred before the target displacement except for Iwate and Superstition Hills (OpenSees) ground motions. As previously mentioned, the first natural period of the un-cracked system determined with Robot is 0.48 s, ergo, it is natural to expect the highest displacement from Iwate ground motion due to period elongation (see Figure 6.2 and Figure 6.9). In fact, the acquired displacement from Iwate ground motion is 0.026 m (OpenSees) and exceeds by a factor of 0.026/0.020= 1.30 from the average result. It is also worth to mention that if only three ground motions (San Fernando, Superstition Hills and Iwate) were selected, according to NS-EN 1998-1, the unfavourable result is from Iwate ground motion. Consequently, the permanent displacement exceeds by a factor of 0.026/0.021=1.24 compared to the target displacement (OpenSees). This characterizes that the implementation of seven ground motions render reliable results. Moreover, the results obtained from NLTHA denote the sensibility of the response with regard to the scaling and selection of the ground motions.

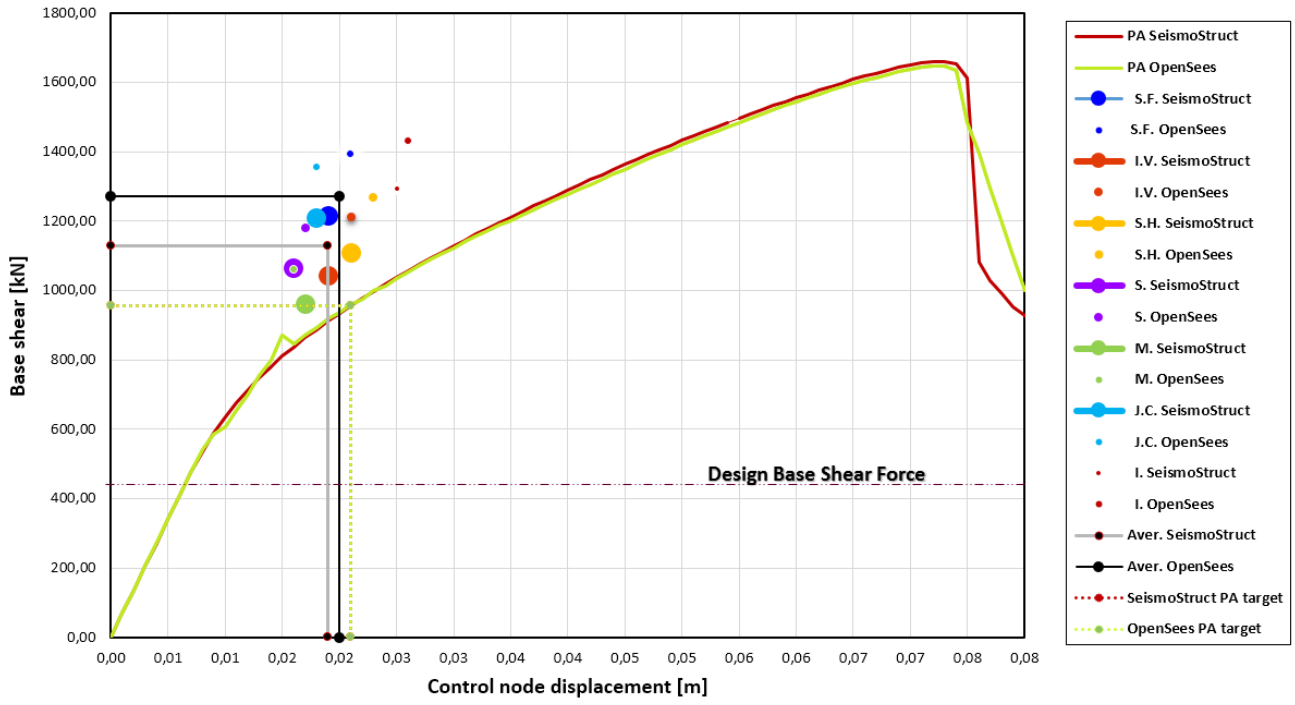

Figure 6.10: PA versus NLTHA.

6.5.2 Base shear force

The maximum base shear forces at the target displacement determined from PA are 957 kN and 956 kN, from SeismoStruct and OpenSees respectively. Those results are much higher than the design base shear and lower compared to the ones acquired from NLTHA (see Figure 6.10). The average value for base shear force is 1127 kN and 1271 kN, from SeismoStruct and OpenSees respectively. It is experienced that NLTHA induces higher shear forces with a minimum of 18% when comparing the average and PA results. According to a study presented in FEMA440 [16], the base shear forces from NLTHA are higher than PA and the results acquired in this thesis comply with this study as illustrated in Figure 6.10. It is also observed that the maximum base shear forces exhibited are from Iwate (1429 kN) and San Fernando (1391 kN) ground motions (see Figure 6.9). As notified from Figure 6.2, San Fernando ground motions has the highest contribution from higher modes and reveals that these modes are significant even for a regular (in elevation and geometry) structure. This also confirms that the base shear forces are directly proportional to floor accelerations [25].
Even though, the base shear forces from all ground motions are higher than PA values at the target displacement (see Figure 6.10), is not for guaranteed that their respective permanent displacements are higher than the target displacement. This implies that forces and displacements are not correlated in NLTHA and reveals that the results obtained from PA are conservative for the response evaluation of the structure for design purposes.

6.5.3 Inter-storey drift ratios (IDR)

The acquired average inter-storey drift ratio from the selected seven ground motions is plotted versus the one achieved with PA and is illustrated in Figure 6.11. The parameters are assessed at maximum displacement from PA equal to average displacement from NLTHA. The reason is to achieve a reliable and conservative result since the acquired target displacement is 10.5% higher than the average displacement from NLTHA (OpenSees). It is relevant to emphasize that the maximum IDR are not attained synchronously during the time-history, whereas the PA results are acquired at the defined displacement . The results from Figure 6.11 reveal that the structure is highly dominated by the first mode. It is observed that PA renders higher IDR at the fourth floors and lower values at the first and second floor (SeismoStruct). Contrarily, in OpenSees PA gives higher IDR at all the floors except for the first floor.
In order to insight closely the response of the structure , the displacement pattern of the median response (San Fernando) from NLTHA and PA (target displacement PA equal to maximum displacement from NLTHA) are compared and depicted in Figure 6.12(c). In addition, the choice of San Fernando is made to assess how the higher modes affect the IDR. Figure 6.12(c) highlights that displacements and IDR (6% at the third floor, SeismoStruct) are less affected from higher modes compared to base shear forces (27%, SeismoStruct). This result complies with a study presented by A. Maniatakis [25], where a 9-storey RC-frame is investigated for the effect of higher modes with 34 earthquake records.
Furthermore, it is interesting to compare the IDR from each ground motions versus the results of PA to investigate deeply the performance of the structure. In order to achieve more reliable results, the target displacement from PA is assessed at the maximum control node displacements of each ground motion. Those are presented in Figures 6.13- 6.14. These latter Figures reveal that even though the average response from NLTHA is nearly in perfect match with PA, there are significant dissimilarities between the individual responses. In addition, the results shows that the structure in question is less sensitive to higher modes when compared to one mode

governed PA. Furthermore, it is noticed that all the ground motions except from San Fernando (SeismoStruct) ground motion render higher IDR at the first floor compared to PA results. Therefore, it is interesting to investigate how the structure response is affected when the height of the first floor is increased, which is the theme of the next chapter.

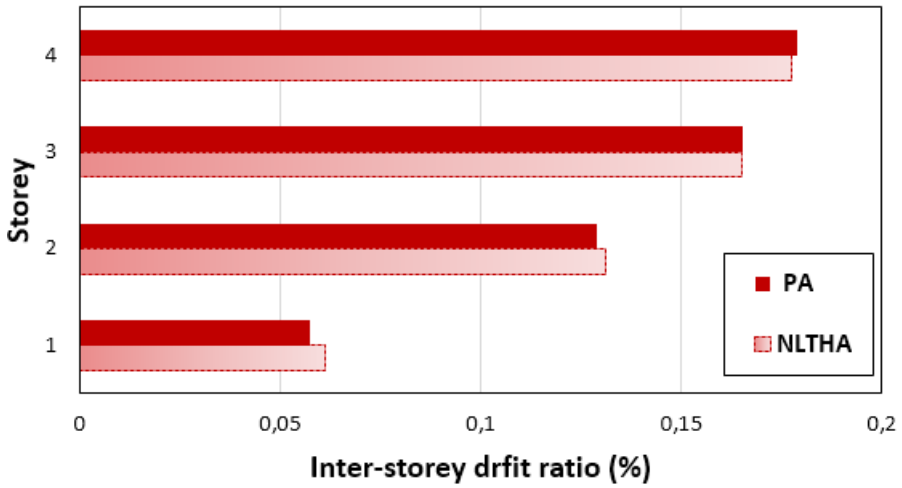

(a) SeismoStruct.

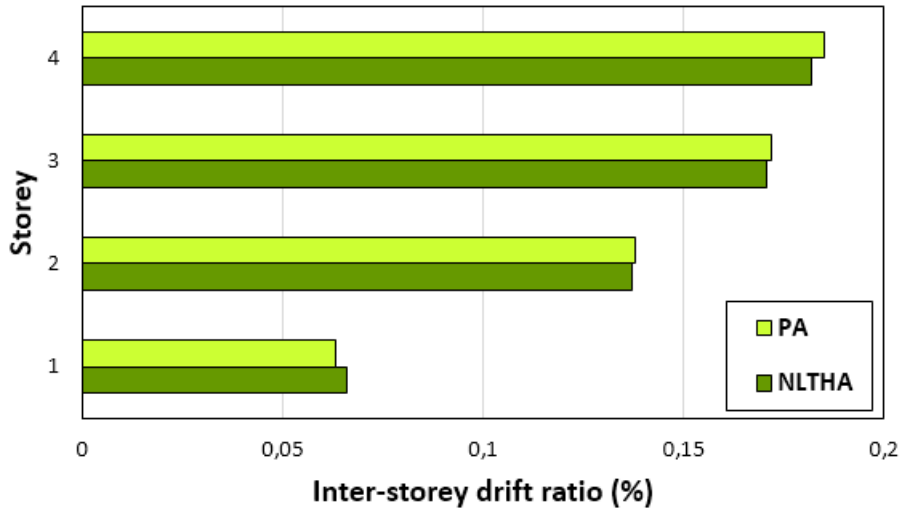

(b) OpenSees.

Figure 6.11: Inter-storey drift ratio(%) from PA versus average values of NLTHA. The parameters are assessed at: maximum displacement PA equal to average displacement NLTHA.

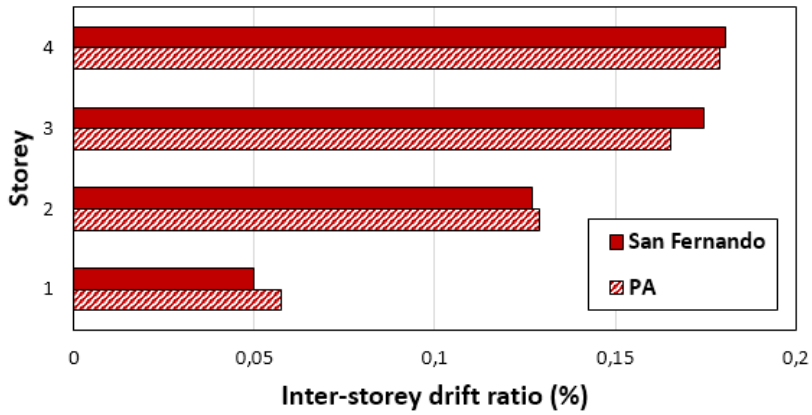

(a) IDR(%) SeismoStruct.

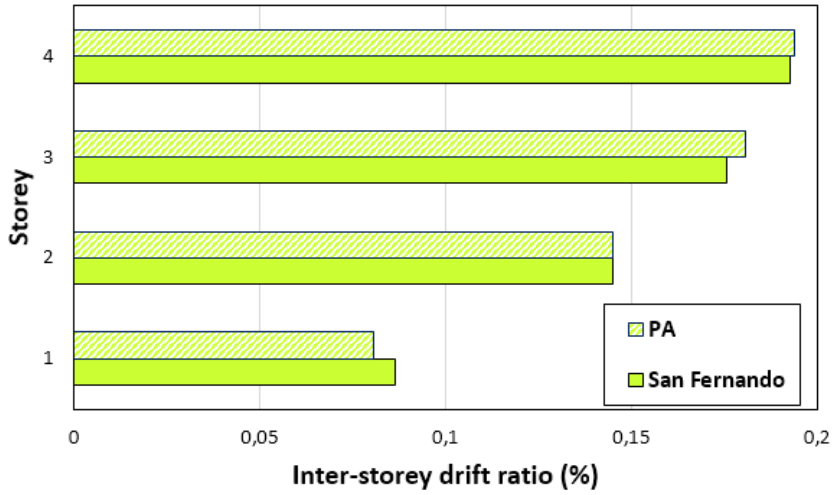

(b) IDR(%) OpenSees.

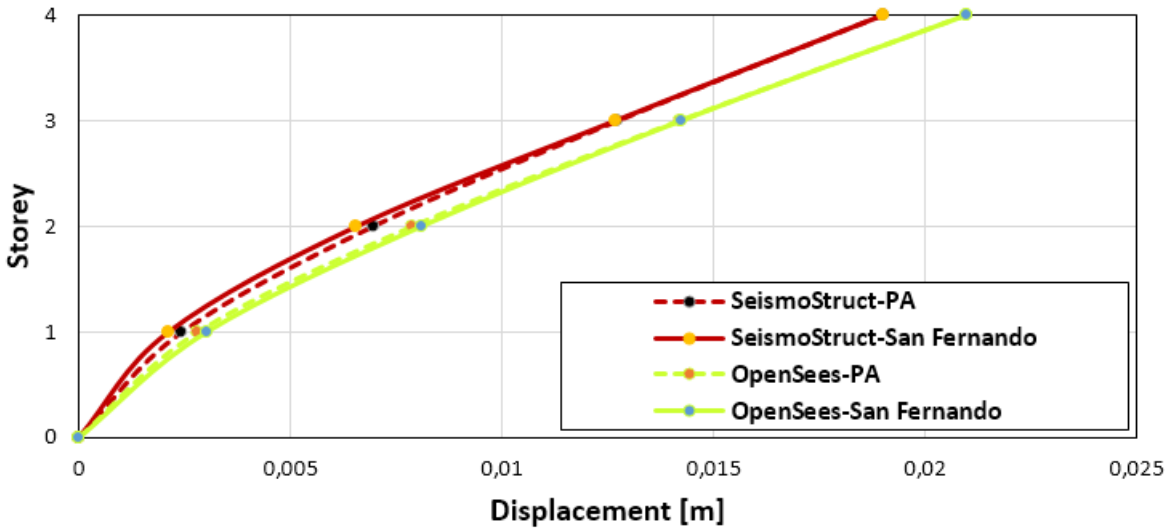

(c) San Fernando versus PA at maximum roof displacemet.

Figure 6.12: Inter-storey drift ratio(%) and displacement pattern, San Fernando ground motion versus PA.The parameters are assessed at: maximum displacement PA equal to maximum displacement from San Fernando.

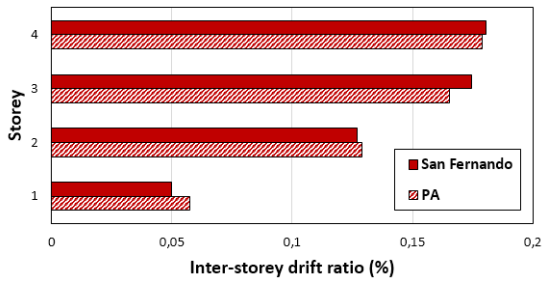

(a) San Fernando ground motion versus PA.

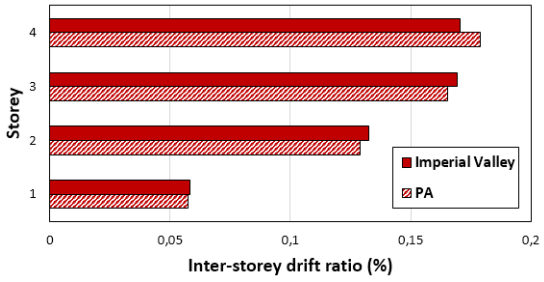

(b) Imperial Valley ground motion versus PA.

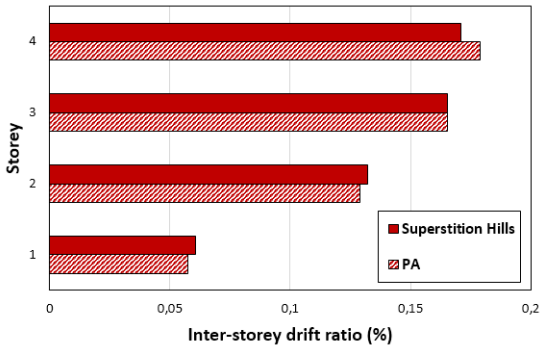

(c) Superstition Hills ground motion versus PA.

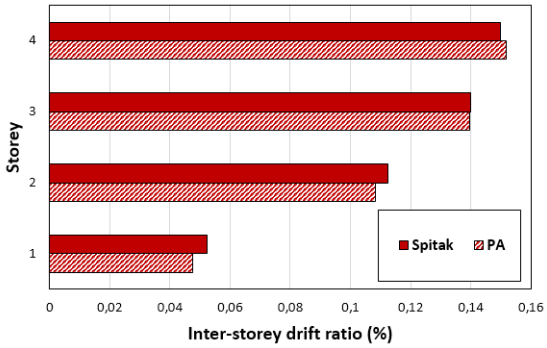

(d) Spitak ground motion versus PA.

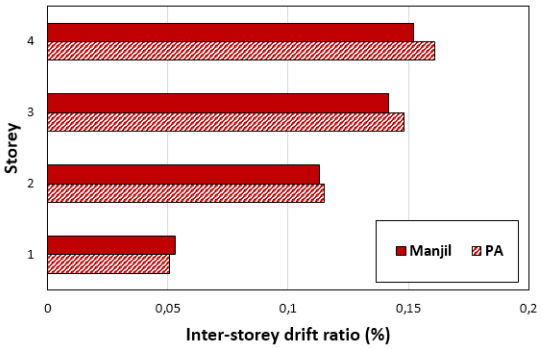

(e) Manjil ground motion versus PA.

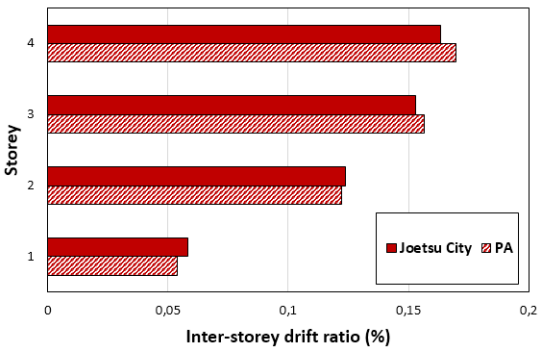

(f) Joetsu City ground motion versus PA.

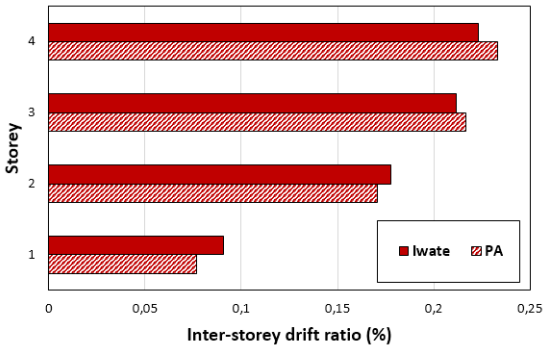

(g) Iwate ground motion versus PA.

Figure 6.13: Inter-storey drift ratio(%) PA versus NLTHA. The parameters are assessed at: maximum displacement PA equal to maximum displacement from each ground motion, SeismoStruct.

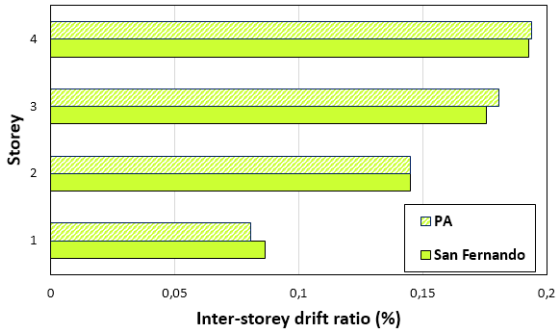

(a) San Fernando ground motion versus PA.

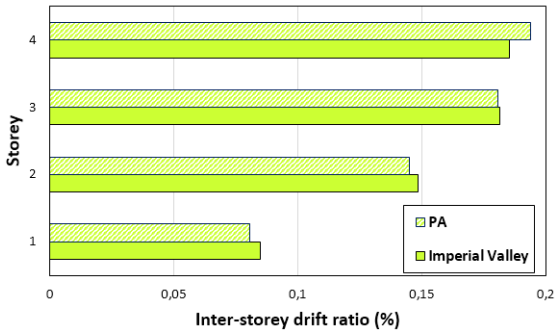

(b) Imperial Valley ground motion versus PA.

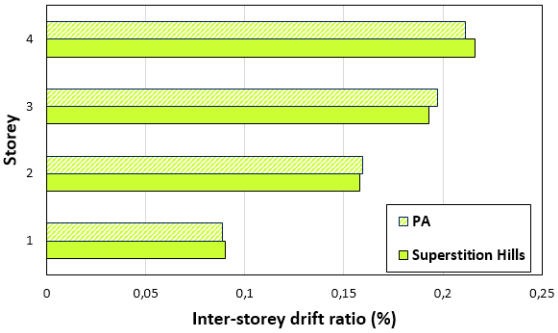

(c) Superstition Hills ground motion versus PA.

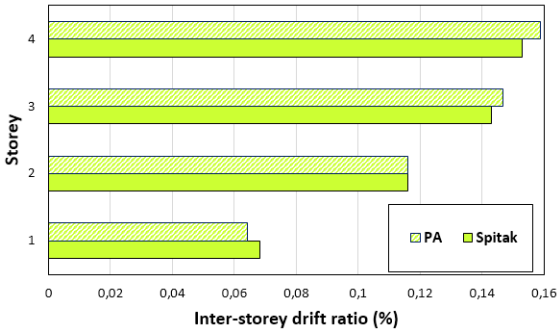

(d) Spitak ground motion versus PA.

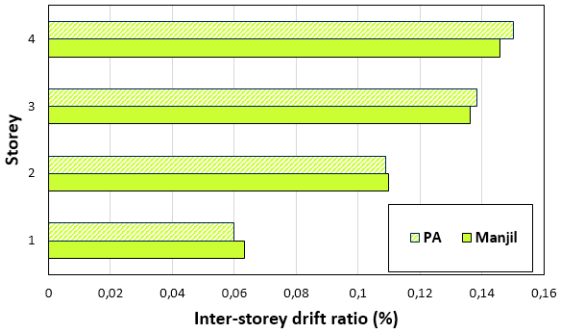

(e) Manjil ground motion versus PA.

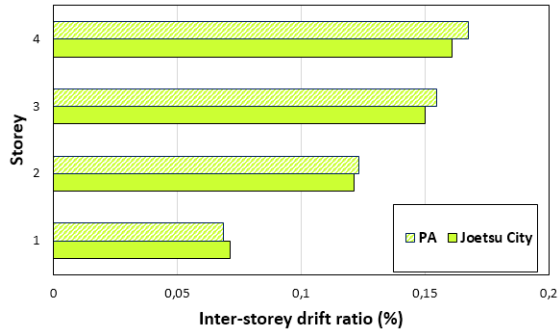

(f) Joetsu City ground motion versus PA.

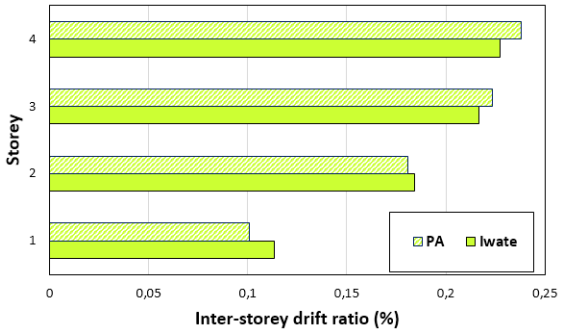

(g) Iwate ground motion versus PA.

Figure 6.14: Inter-storey drift ratio(%) PA versus NLTHA. The parameters are assessed at: maximum displacement PA equal to maximum displacement from each ground motion, OpenSees.

Chapter 7

Further Analysis

7.1 Soft-storey Mechanism

7.1.1 Introduction

A soft storey is when a floor in a building has substantially less stiffness compared to other floors and creates a major weak point in an earthquake which can cause the total collapse of the building. However, excessive drifts in the stories coupled with P-δ effects on the walls will also cause the collapse of the building. According to NS-EN 1998-1 [31], if the stiffness ratio between two consecutive floors in a building exceeds the value of 1.3, the floor with least stiffness is defined as a soft storey.
In order to study the behaviour of the structure with regard to the afore-stated phenomena, the height of the first floor is increased from 4.25 m to 6.0 m rendering the total height of the building equal to 16.5 m. The reason is to investigate how the global stiffness and strength of the structure reduces with the height of the building when the other properties of the structure, i.e. wall thickness, material properties, reinforcements, etc., are unmodified. In addition, the choice is made to easily compare the results with the initial system and to investigate IDR.

7.1.2 Presentation of the results

Eigenvalue analysis of the inelastic numerical model of the modified system is executed with SeismoStruct and OpenSees. The obtained results are compared with the initial system and are presented in Table 7.1 and Figure 7.1. It is experienced that the first natural period of the new structure is prolonged by 23% compared to the initial model.

Table 7.1: Natural periods of the original and modified inelastic models.

		Natural Periods			
Software	Model	T_1 (s)	T_2(s)	T_3 (s)	T_4(s)
SeismoStruct	Original	0.432	0.076	0.028	0.015
SeismoStruct	Modified	0.530	0.092	0.032	0.016
Period elongation (%)		23	21	14	7
OpenSees	Original	0.435	0.076	0.028	0.015
OpenSees	Modified	0.533	0.092	0.032	0.016
Period elongation (%)		23	21	14	7

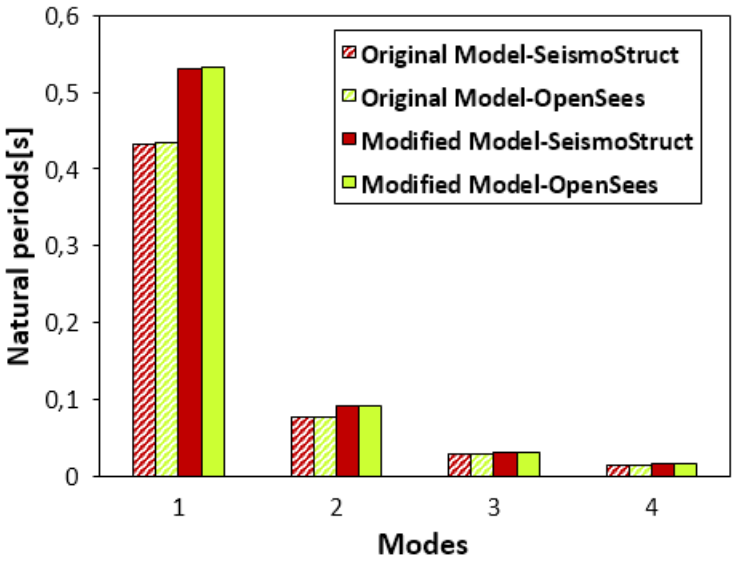

Figure 7.1: Natural periods of the original and modified inelastic models.

The first mode shape of the elastic modified model is computed with OpenSees for simplicity, which differs slightly from the original model (see Eq.(5.2)), and is

$$\Phi_1 = \begin{bmatrix} 1 & 0.696 & 0.412 & 0.116 \end{bmatrix}^{\mathrm{T}} \tag{7.1}$$

PA of the new numerical model is executed with both software packages, to determine the

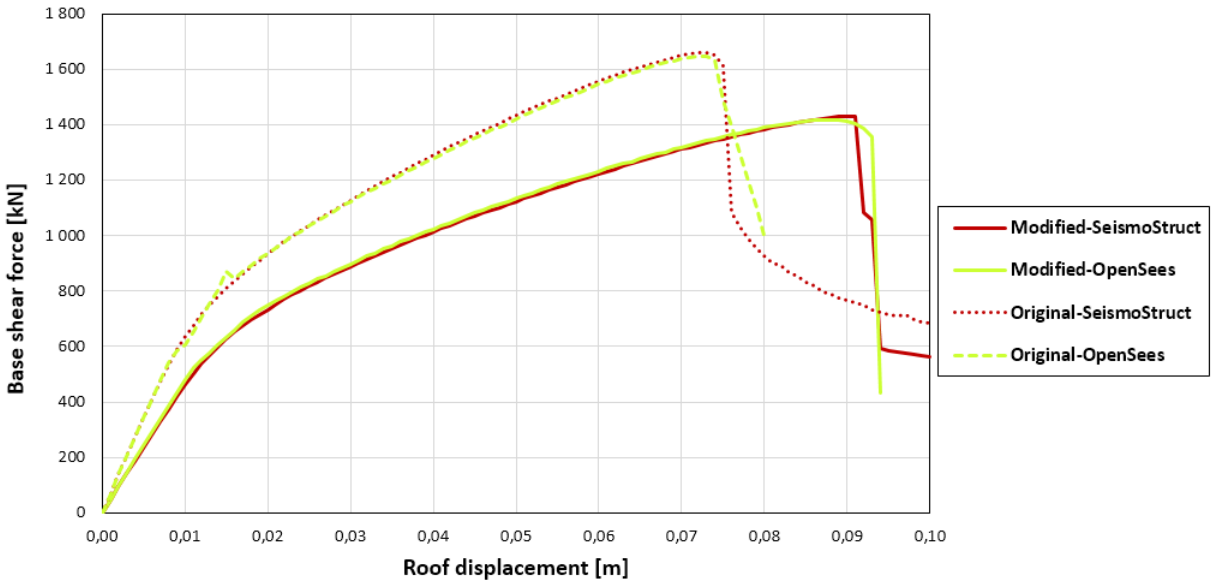

Figure 7.2: Base shear forces and displacement from the Original and Modified models.

maximum base shear force and roof displacement. The results are presented in Figure 7.2. The maximum obtained values for base shear force are 1429 and 1419 kN, for SeismoStruct and OpenSees respectively. It is experienced that the maximum base shear force is reduced by a factor of 1419 kN/ 1648 kN= 0.86 (OpenSees). Contrarily, the maximum roof displacement at the peak force is increased by a factor of 0.088/0.073= 1.21. This illustrates that the lateral

global strength and stiffness of the walls are directly affected by the increase of the height in the first floor. Additionally, Figure 7.2 highlights that the roof displacement is directly proportional to the height of the building.

The target displacement of the new model is acquired in accordance to NS-EN 1998-1 which adopts the idealized bi-linear force displacement relationship. The new transformation factor, Γ, is 1.326, whereas the yield force, F_y^*, are 1078 and 1070 kN, for SeismoStruct and OpenSees respectively. Figure 7.3 illustrates the force-displacement relationship of the idealized SDOF of the new system. As reported in section 5.3, a similar approach is adopted to determine the target

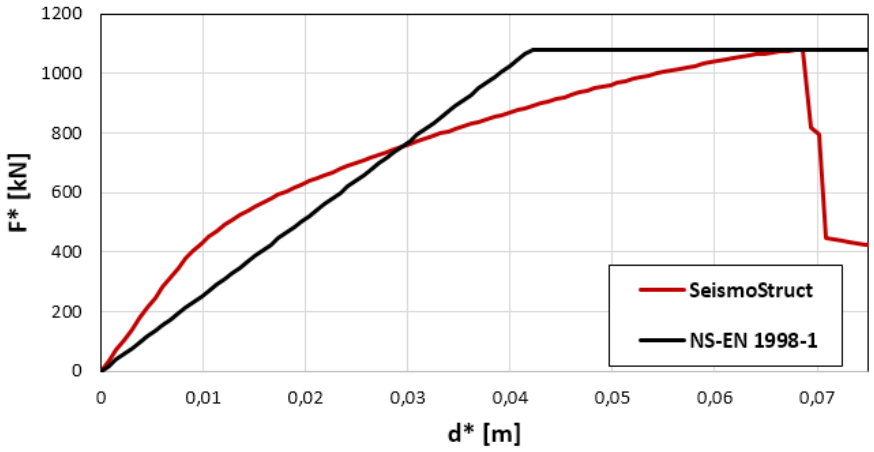

(a) SeismoStruct.

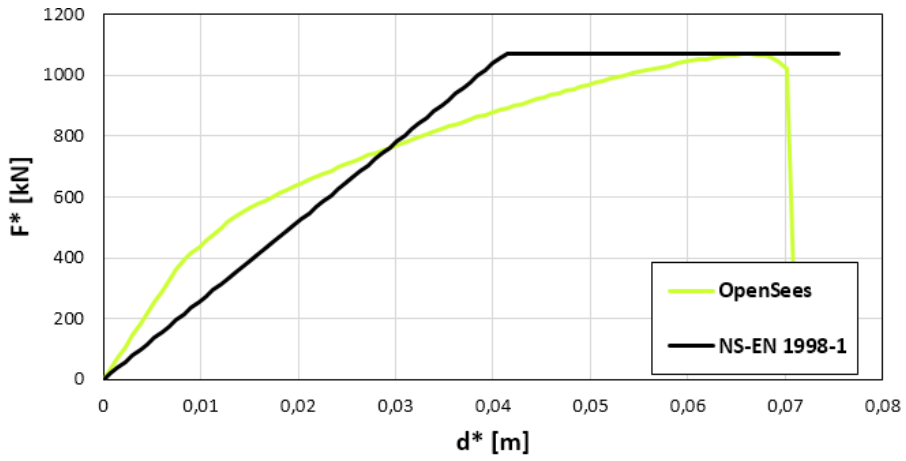

(b) OpenSees.

Figure 7.3: $F^* - d^*$ relationships of the new model according to NS-EN 1998-1.

displacement, d_y^*, of the bi-linear idealized system and results to be 0.025. Consequently, the expected displacement of the system is $1.326 \cdot\ 0.025 = 0.033$ m as per calculation. This shows an increase of the permanent roof displacement by a factor of 0.033/0.021= 1.57 compared to the original model. For a better insight, the displacement pattern at the target displacements are depicted in Figure 7.4(b). It is observed that the roof drift ratio of the new system has increased with a factor of $(0.033 \cdot\ 14.75)/(0.021 \cdot\ 16.5)$= 1.4 compared to the original system. Here, 14.75 and 16.5 are the total height of the initial and new system respectively.

The respective base shear forces at the new target point are 928 and 936 kN, for SeismoStruct and OpenSees respectively. Figure 7.4(a) presents shear diagram at the target displacements and illustrates that the base shear force has decreased with 10.5% compared to the initial system (SeismoStruct). This indicates that shear forces are less affected by the increase of the height of the first floor compared to roof displacements. In order to obtain a reliable and comparative results, the drift ratios are assessed at the new target displacements and are illustrated in Figure 7.4(c). It is experienced that IDR is reduced by a factor of 0.261/0.307= 0.85 at the fourth floor and 0.87 at the third floor. Contrarily, the IDR at the first floor is increased of 0.124/0.102= 1.22 relatively to original system. Furthermore, a negligible value of IDR at the second floor is observed.

The results acquired previously endorse that the global stiffness and strength reduces with the height of the building. Furthermore, the thickness of the wall in the first floor does not fulfil the requirement of NS-EN 1998-1. As a result, the walls have less capacity compared to the initial model (see Figure 7.2) , thereby, it emphasizes how crucial and conservative is to fulfil the requirements imposed in NS-EN 1998-1. Since the exhibited results from PA are in the elastic domain, it is interesting to investigate the performance of the new system through NLTHA.

NLTHA of the new model is performed with an identical method adopted in chapter 6. Considering that the first natural period of the new model is prolonged (T_1=0.55 s, OpenSees), new scaling factors for the ground motions are implemented. They are reported in Table 7.2. The results from NLTHA of the new system are presented in Table 7.3. The calculated

Table 7.2: Scaling factors of the selected ground motions for the modified model.

San Fernando	Imperial Valley	Superstition Hills	Spitak	Manjil	Joetsu City	Iwate
0.780	0.413	0.594	0.707	0.422	0.383	0.752

average displacement of the system is in compliance with the permanent displacement from PA. Contrarily, the average base shear forces obtained from PA differs significantly from the one acquired from NLTHA. The reason is in NLTHA the maximum capacity and displacement of the system are obtained at different stages, while in PA the base shear force corresponds to the target displacement.

The average inter-storey drift ratio of the new system are compared to the initial one and

Table 7.3: Maximum displacement and base shear force of the Modified model (NLTHA).

Software	Response	S.F.	I.V.	S.H.	S.	M.	J.C	I.	Average
SeismoStruct	$\mathrm{d}_{\max}$ (m)	0.030	0.035	0.027	0.035	0.020	0.031	0.043	0.032
OpenSees	$\mathrm{d}_{\max}$ (m)	0.033	0.038	0.029	0.035	0.022	0.029	0.047	0.033
SeismoStruct	$\mathrm{F}_{\mathrm{b,max}}$ (kN)	1183	1146	1103	1244	860	1142	1254	1133
OpenSees	$\mathrm{F}_{\mathrm{b,max}}$ (kN)	1358	1359	1104	1370	1026	1213	1391	1259

are illustrated in Figure 7.5(b). It is also reported in Figure 7.5(a), for both models, the displacement pattern of the median response from San Fernando ground motion . It is observed

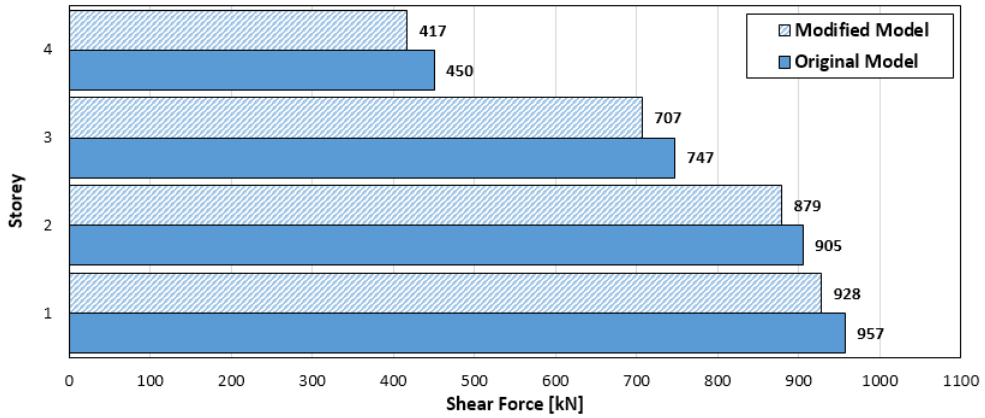

(a) Shear diagram at the target displacements, SeismoStruct.

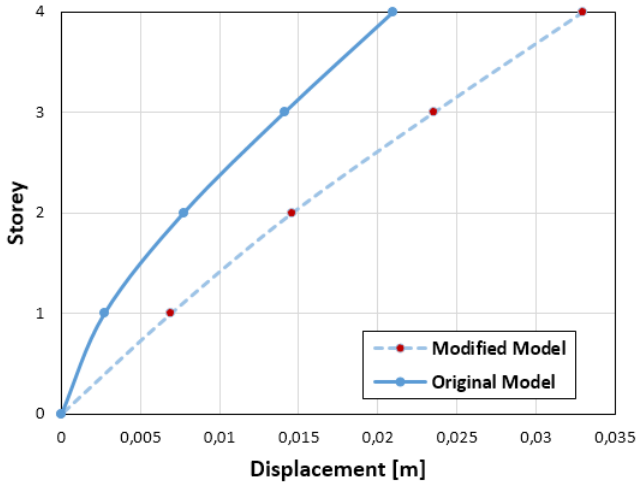

(b) Displacement pattern.

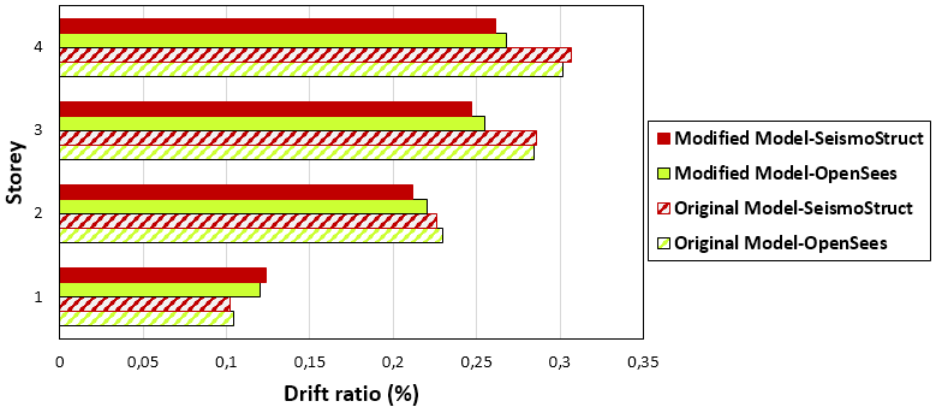

(c) Inter-storey drift ratio (%), Modified versus Original model. The parameters are assessed at: target displacement of the original model equal to target displacement of the modified system.

Figure 7.4: Results and comparison between the modified and original model from PA.

that both structures exhibited high IDRs at the upper floors confirming a typical response of wall-equivalent dual-system. It is also noticed that IDRs increases significantly with the height of the structure. For example, IDR at the fourth and first floor increased by a factor of

$0.25/0.18 = 1.39$ and $0.11/0.06 = 1.83$, respectively (see Figure 7.5(b)). Even though the IDR of the new system are amplified, structural damages have not occurred yet, according to SEAOC (Vision 2000) [28].
Furthermore, the results reveal that the increase of the height in the first floor affected more the IDR at the lower stories. Additionally, it illustrates the sensibility of the structural response with regard to the selection and scaling approach of the applied ground motions. Finally, it is worth to mention that the structural damage due to earthquake is not dependent entirely on the maximum displacements and the cumulative damage resulting from numerous inelastic cycles should also be taken into account.

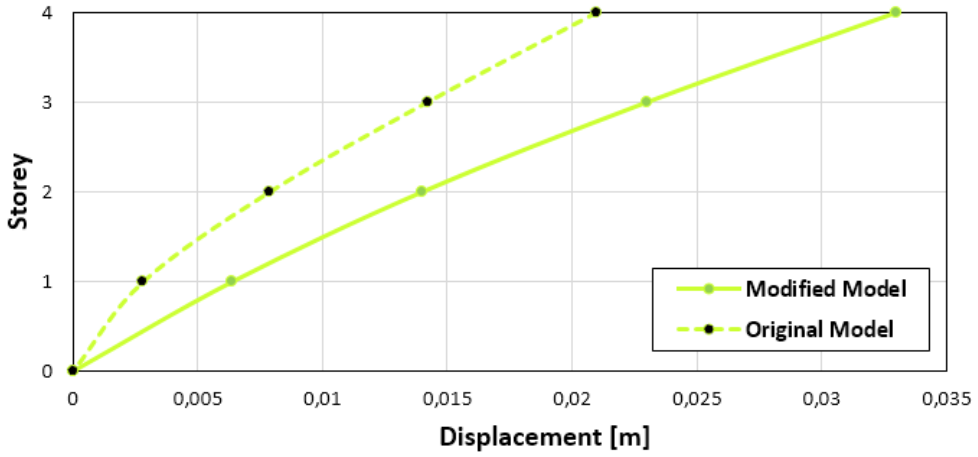

(a) Maximum displacement from San Fernando ground motion, OpenSees.

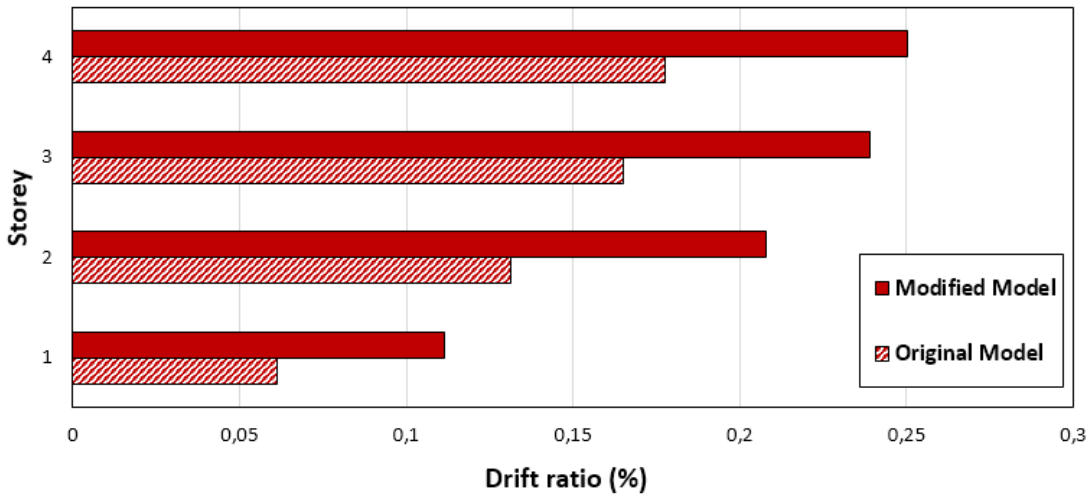

(b) Average inter-storey drift ratio (%) from NLTHA, Modified versus Original model, SeismoStruct.

Figure 7.5: Results and comparison between the modified and initial model from NLTHA.

7.2 OpenSees: Fibre Section versus Shell Elements

7.2.1 Introduction

Throughout the study, it is experienced that the first natural period governs the results for both linear and non-linear analyses. As seen in section 4.2, a good agreement for the first natural period is obtained, whereas significant dissimilarities in the higher modes are observed. In order to investigate closely the eigen-analyses of the structure in question, the walls are implemented in OpenSees with shell elements. It is important to mention that this study is beyond the scope of this thesis, but it is the authors interest to analyse further.

7.2.2 Shell element model for shear walls

Multi-layer shell model is implemented in OpenSees using the ShellMITC4 element, which is a four-node shell, and is proposed by Xinzheng Lua, Linlin Xiea, Hong Guanb, Yuli Huangc, Xiao Lud et al. (2015) [24]. The strains and curvatures at the in-plane integration points are obtained from the interpolation of the nodal displacements and rotations. For each of the in-plane integration points, a layered integrated section in the thickness direction, is assigned to account for the non-linear behaviour of reinforced concrete (RC). The reinforcements are smeared into the layers according to their physical location and direction. In OpenSees, the absence of a graphical user interface makes it also cumbersome to establish and evaluate a numerical model with shell elements. In addition, nodal configurations and element establishments are manually user-defined, which increases the modelling time and possible human errors.
For the structure in question, two finite element meshes are proposed: a total of 40 and 80 elements. The command line script is reported in Appendix E. The results are presented in Figure 7.6 and Table 7.4, and are compared with the previously obtained results.

Table 7.4: Comparison of natural periods: Shell elements versus Fibre section.

		Natural Periods			
Software	Model	T_1 (s)	T_2(s)	T_3 (s)	T_4(s)
Robot	Shell 150Elements	0.480	0.100	0.040	0.030
OpenSees	Shell 40Elements	0.434	0.092	0.040	0.030
OpenSees	Shell 80Elements	0.443	0.092	0.040	0.030
OpenSees	Fibre Section	0.448	0.080	0.030	0.020

The results shows that the third and fourth natural periods from multi-layer shell elements are in perfect match with Robot, whereas the first natural period is sensitive to mesh density. In addition, fibre-sections and shell elements based numerical model captures accurately the structural behaviour of shear walls predominately governed by flexural behaviour. In contrast, for structures exhibiting shear behaviour, the multi-layer shell model provides better results than fibre-section model [24]. For practical design purposes, fibre-section based type model should be used to avoid time constraints and human errors. Since OpenSees is an open source, it is the authors opinion that researchers should contribute with their effort to provide an easy and time-efficient shell element configuration.

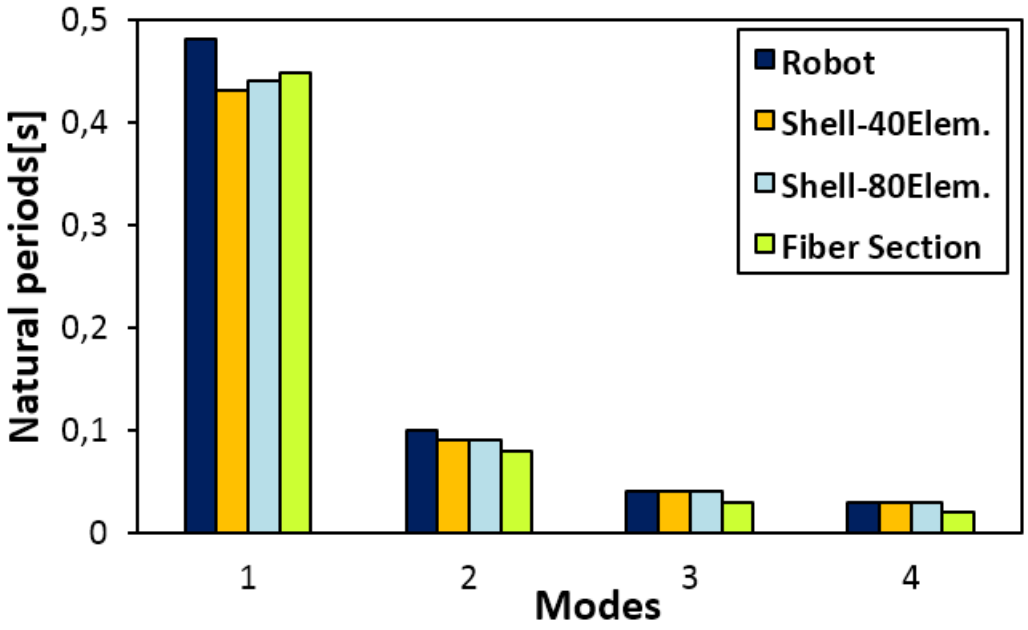

Figure 7.6: Shell elements versus Fibre section.

Chapter 8

Conclusion

8.1 Design

In the design process, shear walls were detailed for medium ductility as primary seismic elements to withstand the earthquake-induced forces. Furthermore, beams and columns are designed as secondary elements. Two of the vital aspects, when designing for earthquake loading, are the connections between the elements and the transfer of shear forces to the walls in an adequate manner to avoid global collapse. In fact, it is experienced that the current code NS-EN 1998-1[31] imposes more requirements for detailing of the beam elements than NS-EN 1993-1-1[35]. As a result, the design load for beams is obtained from the design capacity of the hollow core slabs to ensure over-strength in the joints.
The behaviour factor (q) in this report resulted to be 3.6 according to NS-EN 1998-1, which account for over-strength and ductility. Additionally, the stiffness of the walls were reduced by a factor of 0.5. Although, the walls were detailed for medium ductility, it is experienced that structure's response remained in the elastic domain after PA was executed. Hence, it hindered to capture the structure's behaviour in the post-elastic range. Contrarily, the over-strength factor, Ω, and period- based ductility, μ_{T}, assessed in accordance to *FEMA-P695* [38], resulted to be 3.81 and 2.26, respectively (OpenSees). In this report, it is demonstrated that a conservative approach is implemented in the design process and the walls have reserves for both capacity and ductility.

8.2 Non-linear Analysis

The non-linear analyses are more demanding than linear analysis and their solutions are strictly influenced with the choice of material models, solution procedures and cost of computational time.
Non-linear time-history analysis generally gives more realistic model of structural response to ground shaking and, thereby, provides more reliable assessment of earthquake performance than non-linear static analysis. PA is limited in its ability to capture transient dynamic behaviour with cyclic loading and degradation. Nevertheless, PA provides a conducive and reliable method for structures whose response is governed by first-mode sway motion. Hence, for the structure in question, the result for permanent displacement from PA is in compliance with the average value from NLTHA. Contrarily, it is observed that the maximum displacements from each ground motion differ from the assessed target displacement (PA). This indicates the necessity

of implementing seven ground motions, according to NS-EN 1998-1, when assessing NLTHA procedure. Furthermore, it reveals the sensibility of the results with regard to the scaling factors and the choice of ground motions. In fact, the average base shear forces from NLTHA are higher compared to PA. This reveals that NLTHA induces greater forces due to higher mode effects and discrepancies from PA increases markedly for ground motions with high frequency content.
In this study, the results revealed that PA provides conservative structural parameters, but for complete assessment of structural response both the non-linear analyses must be executed. In addition, it is observed that the distribution of stiffness through a building affects the permanent displacement, base shear force and IDR.

8.3 Software packages

In the design process, Robot software programme is used where shear-walls were modelled with shell elements including shear deformations. Hence, the structure resulted to be softer when approaching the eigenvalue analysis (see Figure 4.8) compared to SeismoStruct and OpenSees, but their differences are negligible. Additionally in Robot, the user must be aware when assessing the mass properties (conversion from acting loads) of the structure to avoid period-elongation of the first natural period, ergo, to prevent inaccuracies in the design procedure.

For the assessment of the non-linear analysis SeismoStruct [40] and OpenSees [27] software packages are used. The numerical elements are discretized with 160 fibre-sections and four IP, thereby, no-convergence issue is experienced. In addition, fibre-section based numerical model captures accurately the structural behaviour of shear walls predominately governed by flexural behaviour.

Throughout the process, it is experienced that SeismoStruct is user-friendly and time-efficient for modelling of the structure. Furthermore, it has graphical user interface and the results can be evaluated without the utilization of additional software packages (Excel or Matlab) compared to OpenSees. Contrarily, SeismoStruct is limited for the assessment of element types, numerical algorithms and output data compared to OpenSees. Additionally in NLTHA, it is observed that SeismoStruct has high computational-costs compared to OpenSees. Moreover, OpenSees rendered higher base shear forces in NLTHA, but the displacements are in compliances with SeismoStruct.

Even though the latter software packages provides reliable results, it is the authors opinion that OpenSees should be used in the non-linear analyses for wall-equivalent dual-system.

8.4 Further work

During the course of this thesis, some topics are found to be interesting and it is the authors opinion that the following themes can be the topic of future studies:

- Assessment of non-linear analyses by implementing shell elements and comparison with fibre-section in OpenSees.

- Assessment of seismic response through adaptive pushover and incremental dynamic analyses. Compare the results with the one obtained in this thesis.
- Design the structure in DCL (low ductility) and compare it with DCM.
- Structural response with prefabricated walls.

Bibliography

[1] Byggteknisk forskrift (TEK 10). https://www.dibk.no/no/byggeregler/tek/.

[2] Modified Mercalli Intensity Scale, Missouri department of Geology . http://dnr.mo.gov/geology/geosrv/geores/richter_mercali_relation.htm.

[3] PEER Center. Peer ground motion database, http://ngawest2.berkeley.edu/, April2015. .

[4] Håkon Alexander Sven, Skau. *Betongelementboken: Bind B. Avstivning og kraftoverføring*. 2012.

[5] S Antoniou and R Pinho. Advantages and limitations of adaptive and non-adaptive force-based pushover procedures. *Journal of Earthquake Engineering*, 8(04):497–522, 2004.

[6] Beam-EC3. *Beam-EC3 is a software for calculating moments , shear and deformations of steel beams according to NS-EN 1993*.

[7] Bt-Snitt. *BtSnitt is a program to assess the cross sectional capacities of concrete members. Sivilingenior Ove Sletten, Version 6.1.1,*.

[8] Armando Calabrese, João Pacheco Almeida, and Rui Pinho. Numerical issues in distributed inelasticity modeling of RC frame elements for seismic analysis. *Journal of Earthquake Engineering*, 14(S1):38–68, 2010.

[9] Anil K Chopra. *Dynamics of structures*, volume 3. Prentice Hall New Jersey, 1995.

[10] Robert D Cook et al. *Concepts and applications of finite element analysis*. John Wiley & Sons, 2007.

[11] Building Seismic Safety Council. Prestandard and commentary for the seismic rehabilitation of buildings. *Report FEMA-356, Washington, DC*, 2000.

[12] Ahmed Elghazouli. *Seismic design of buildings to Eurocode 8*. CRC Press, 2009.

[13] Peter Fajfar. A nonlinear analysis method for performance-based seismic design. *Earthquake spectra*, 16(3):573–592, 2000.

[14] Peter Fajfar and Matjaž Dolšek. Pushover-Based Analysis in Performance-Based Seismic Engineering–A View from Europe. In *Performance-Based Seismic Engineering: Vision for an Earthquake Resilient Society*, pages 265–277. Springer, 2014.

[15] Michael N Fardis. *Seismic design, assessment and retrofitting of concrete buildings: based on EN-Eurocode 8*, volume 8. Springer Science & Business Media, 2009.

[16] Federal Emergency Management Agency (FEMA). Improvement of nonlinear static seismic analysis procedures, 2005.

[17] Federal Emergency Management Agency (FEMA). Quantification of building seismic performance factors, 2009.

[18] Rakesh K Goel and Anil K Chopra. Evaluation of modal and FEMA pushover analyses: SAC buildings. *Earthquake spectra*, 20(1):225–254, 2004.

[19] Iunio Iervolino and C Allin Cornell. Record selection for nonlinear seismic analysis of structures. *Earthquake Spectra*, 21(3):685–713, 2005.

[20] M.J.N. Priestley J.B.Mander and R.Park. Theoretical stress-strain model for confined concrete. *Journal of structural engineering*, 114(8):1804–1826, 1988.

[21] Erol Kalkan and Anil K Chopra. Practical guidelines to select and scale earthquake records for nonlinear response history analysis of structures. *US Geological Survey Open-File Report*, 1068(2010):126, 2010.

[22] Steven L Kramer. *Geotechnical earthquake engineering*. Pearson Education India, 1996.

[23] Helmut Krawinkler and GDPK Seneviratna. Pros and cons of a pushover analysis of seismic performance evaluation. *Engineering structures*, 20(4):452–464, 1998.

[24] Xinzheng Lu, Linlin Xie, Hong Guan, Yuli Huang, and Xiao Lu. A shear wall element for nonlinear seismic analysis of super-tall buildings using opensees. *Finite Elements in Analysis and Design*, 98:14–25, 2015.

[25] Charilaos A Maniatakis, Ioannis N Psycharis, and Constantine C Spyrakos. Effect of higher modes on the seismic response and design of moment-resisting RC frame structures. *Engineering Structures*, 56:417–430, 2013.

[26] Matlab. Matlab (matrix laboratory) is a multi-paradigm numerical computing environment and programming language, 2015.

[27] Silvia Mazzoni, Frank McKenna, Michael H Scott, Gregory L Fenves, et al. Opensees is a software framework for simulating the seismic response of structural and geotechnical systems. *Pacific Earthquake Engineering Research (PEER) Center*, 2006.

[28] AM Mwafy and AS Elnashai. Static pushover versus dynamic collapse analysis of rc buildings. *Engineering structures*, 23(5):407–424, 2001.

[29] NNSN. Norwegian National Seismic Network. http://nnsn.geo.uib.no/.

[30] Standard Norge. NS-EN 1992-1-1: 2004+ NA: 2008.design of concrete structures-Part 1-1: General rules and rules for buildings.

[31] Standard Norge. NS-EN 1998-1: 2004+ NA: 2008. Prosjektering av konstuksjoner for seismisk påvirkning Del 1: Allmenne regler, seismiske laster og regler for bygninger. *Standard Norge*, 2004.

[32] Standard Norge. NS-EN 1998-3: 2005+ NA: 2013. Prosjektering av konstuksjoner for seismisk påvirkning Del 3: Vurdering og forsterkning av eksisterende bygninger. *Standard Norge*, 2004.

[33] Standard Norge. NS-EN 1990: 2002+ NA: 2008. Grunnlag for prosjektering av konstruksjoner, 2008.

[34] Standard Norge. *NS-EN 1991-1-3:2003+ NA: 2008. Laster påkonstruksjoner-Allmenne laster - Snølaster*. 2008.

[35] Standard Norge. NS-EN 1993-1-1:2005+ NA: 2008. Prosjektering av stålkonstruksjoner-Del 1-1: Allmenne regler og regler for bygninger, 2008.

[36] Standard Norge. *NS-EN 1991-1-4:2005+ NA: 2009. Laster påkonstruksjoner-Allmenne laster - Vindlaster*. 2009.

[37] NORSAR. Earthquake in norway. http://www.jordskjelv.no.

[38] FEMA P695-ATC63. Quantification of building seismic performance factors, 2009.

[39] Thomas Paulay and MJN Priestly. *Seismic design of reinforced concrete and masonry buildings*. New York Wiley-Interscience, America, 1992.

[40] R Pinho and S Antoniou. SeismoStruct Computer Program. seismostruct is a FEM-program developed for the analytical assessment of structures subjected to earthquake strong motion, 2009.

[41] Robot. Autodesk Robot Structural Analysis is an BIM-integrated FEM-software developed for the assessment of structural analysis and memeber design. 2013.

[42] Alexander Sven. *Betongelementboken: Bind A. Bygging med betongelementer*. 2012.

Appendices

Appendix A

Design

A.1 Loads

Snow load according to NS-EN 1991-1-3:2003+NA: 2008

Table NA.4.1 (901) → s_{k0} = 2.0 kN/m^2 (Bergen)
Clause 5.2(3) → Q_{snow} = 0.8·1.0·1.0·2.0 = 1.6 kN/m^2.

Wind load according to NS- EN 1991-1-4

Table NA.4. (901.1) gives the reference wind velocity, in Bergen, equal to 26 m/s.
The results obtained from Last-Ec are illustrated in Figure A-1.

3. Yttervegger

3.1 Utvendig vindlast

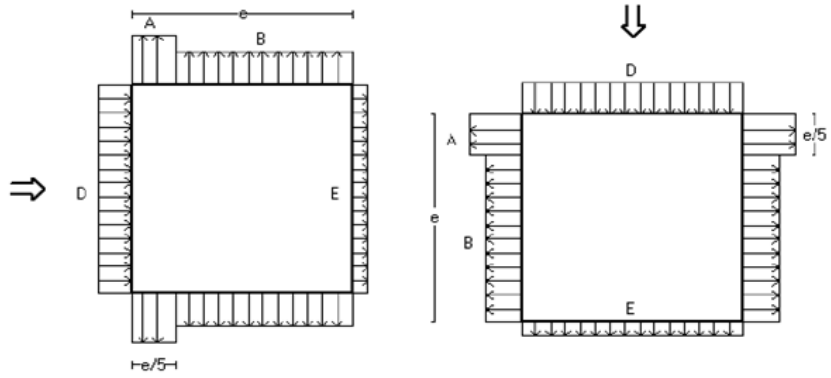

Vindretning 0 grader. e=2850 mm *Vindretning 90 grader. e=2850 mm*

Vindinnfallsretning på 0 grader.

	A	B	C	D	E
Formfaktor Cpe,10	-1,20	-0,80		0,74	-0,37
Utvendig last (kN/m2)	-0,83	-0,55		0,51	-0,26
Formfaktor Cpe,1	-1,40	-1,10		1,00	-0,37
Utvendig last (kN/m2)	-0,97	-0,76		0,69	-0,26
Utstrekning (mm)	570	2280		2850	2850

Vindinnfallsretning på 90 grader.

	A	B	C	D	E
Formfaktor Cpe,10	-1,20	-0,80		0,74	-0,37
Utvendig last (kN/m2)	-0,83	-0,55		0,51	-0,26
Formfaktor Cpe,1	-1,40	-1,10		1,00	-0,37
Utvendig last (kN/m2)	-0,97	-0,76		0,69	-0,26
Utstrekning (mm)	570	2280		2850	2850

Figure A-1 Wind load.

Hollow core element according to Betongelement book Bind A

Fig A-2 illustrates an overview of different types of hollow cores with regard to the span width and SLS loads. The red lines limits the HD capacity in SLS and the blue ones shows when the shear stresses can be determining.

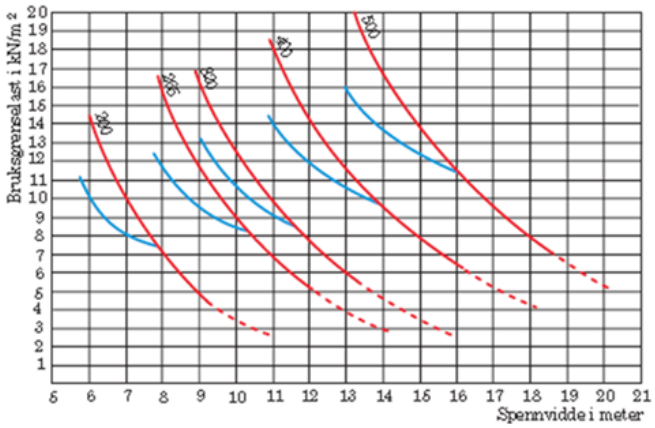

Figure A-2 Overview of HD types (Fig. A7.2 Bind A)

Figure A-1 shows how much load (SLS) that can be applied in addition the elements own weight. Stated load capacity limit at maximum reinforcement. The diagram is used as follows: The load consists of separate loads (G) such as levelling, light walls etc.; plus live loads (Q_{live}).

Standard width B = 1200mm and span length l= 6m
g is the dead load of concrete levelling = 0.05m· 25kN/m^3 = 1.25kN/m^2
The conservative way to calculate the thickness of the HD is by accounting the loads in SLS design [1]. Load calculation in SLS: Floor→ 0.75·g + Q_{live} = 0.75·1.25+2 = 2.94 kN/m^2
Correction for cover elements own weight is already done, so the shall not be included in the calculation. Bind A Table 4.2 → thickness 200mm

Calculation of dead loads

Dead load calculation: - HD200B45 = 2.6 kN/m^2 |+
- 50mm topping= 0.05·25 = 1.25 kN/m^2
Total 3.85kN/m^2

Vertical action loads (KN/m^2)

Level	Dead load (kN/m^2)	Variable loads (snow or live) (kN/m^2)
Roof	2.6	1.6
Floor (1-2-3)	3.85	2.0

A.2 Geometric imperfection, according to NS-EN1992-1-1

NS-EN 1992-1-1 Clause 5.2(5):
$\theta_i = \theta_0 \cdot \alpha_h \cdot \alpha_m$.
Here.
θ_0 is the basic value equal to *1/200*
α_h is the reduction factor for height, $\alpha_h = 2/(14.75)^{1/2} = 0.52$, $2/3 \leq \alpha_h \leq 1$. Thus, $\alpha_h = 2/3$.
α_m is the reduction factor for number of members, $\alpha_m = (0.5\,(1 + 1/(m)))^{½} = 0.72$,
m= 28+4=32.
Thus,
$\theta_i = \theta_0\, \alpha_h\, \alpha_m = (1/200) \times (2/3) \times 0.82 = \underline{0.0024}$. (0.24% of vertical load).
The respective horizontal forces, calculated from the vertical actions and walls, due to geometric imperfections are calculated in accordance to NS-EN 1992-1-1:
4th floor:
$N_4 = (1.2 \cdot 2.6 + 1.5 \cdot 1.6)\ kN/m^2 \cdot 28.5^2 m^2 + 1.2 \cdot (3.5m \cdot 4.5m \cdot 0.175m \cdot 25kN/m^3) \cdot 4 = 4814\ kN$
$H_4 = 0.0024 \cdot N_4 = \underline{12\ kN}$
3rd floor:
$N_3 = N_4 + (1.2 \cdot 3.85 + 1.5 \cdot 2)kN/m^2 \cdot 28.5^2 m^2 + 1.2 \cdot (3.5m \cdot 4.5m \cdot 0.175m \cdot 25kN/m^3) \cdot 4 = 11334\ kN$
$H_3 = 0.0024 \cdot (N_4 - N_3) = \underline{16\ kN}$
2nd floor:
$N_2 = N_3 + (1.2 \cdot 3.85 + 1.5 \cdot 2)kN/m^2 \cdot 28.5^2 m^2 + 1.2 \cdot (3.5m \cdot 4.5m \cdot 0.175m \cdot 25kN/m^3) \cdot 4 = 17854\ kN$
$H_2 = 0.0024 \cdot (N_3 - N_2) = \underline{16\ kN}$
1st floor:
$N_1 = N_2 + (1.2 \cdot 3.85 + 1.5 \cdot 2)kN/m^2 \cdot 28.5^2 m^2 + 1.2 \cdot (4.25m \cdot 4.5m \cdot 0.22m \cdot 25kN/m^3) \cdot 4 = 24548\ kN$
$H_1 = 0.0024 \cdot (N_3 - N_2) = \underline{16\ kN}$

A.3 Design for wind load

Horizontal forces at base level without geometric imperfections:
Base shear force = 601kN (refer to base calculation)
$Q_{Dvind,\,x} = 28.5 \cdot 14.75 \cdot 1.5 \cdot 0.77\ kN/m^2 = 486\ kN$

Results obtained from Robot with gravity loads, live loads, geometric imperfections and wind loads:

Case/Story	G (x,y,z) (m)	FX (kN)
10 (C)/ 1	4,25 14,25 3,81	554,53
10 (C)/ 2	4,22 14,25 7,49	339,03
10 (C)/ 3	,22 14,25 11,00	205,82
10 (C)/ 4	,22 14,25 14,50	73,61

Comment:
The walls are controlled and detailed to withstand both the moment and shear induced by the wind loads.

A.4 Design for gravity loads

$Q_{G,(6.10a)} = 1.35\ G_{kj,inf} + 1.5 \times 0.7\ Q_{k,1} = 1.35\ G_{kj,inf} + 1.05\ Q_{k,1}$.

$Q_{G,(6.10b)} = 0.89 \times 1.35\ G_{kj,inf} + 1.5 \times Q_{k,1} = 1.2\ G_{kj,inf} + 1.5\ Q_{k,1}$.

HD200 bearing capacity is $Q_{HD} = 9.5 kN/m^2$ and maximum span width l=6m.

HSQ Border Beams

$Q_{HSQ} = 1.1 \cdot Q_{HD} \cdot l/2 = 1.1 \cdot 9.5 \cdot 6/2 = 31.35$ KN/m

HSQ Interior Beams

$Q_{HSQ} = 1.1 \cdot Q_{HD} \cdot l = 1.1 \cdot 9.5 \cdot 6 = 62.7$ KN/m

L Beams

$Q_{L} = 1.2 \cdot Q_{HD} \cdot l/2 = 1.2 \cdot 9.5 \cdot 6/2 = 34.2$ KN/m

Table A.1: Design capacities of beams, [6].

Beam	S355	V_{Rd} (kN)	M_{Rd} (kNm)	V_{Ed}/V_{Rd}	M_{Ed}/M_{Rd}
Border	HSQ	836	198	0.12	0.73
Interior	HSQ	1906	350	0.10	0.81
Wall-HD	L	562	80	0.12	0.80

Interior Columns

$Q_{G,4} = 1.35\ G_{kj,inf} + 1.05\ Q_{k,1} = 1.35 \cdot 2.6\ kN/m^2 \cdot 6 \cdot 6\ m^2 + 1.05 \cdot 1.6\ kN/m^2 \cdot 6 \cdot 6\ m^2 = 187$ kN
$1.2\ G_{kj,inf} + 1.5\ Q_{k,1} = 1.2 \cdot 2.6\ kN/m^2 \cdot 6 \cdot 6\ m^2 + 1.5 \cdot 1.6\ kN/m^2 \cdot 6 \cdot 6\ m^2 = \underline{199\ kN}$

$Q_{G,3} = (1.35 \cdot 3.85\ kN/m^2 \cdot 6 \cdot 6\ m^2 + 1.05 \cdot 2\ kN/m^2 \cdot 6 \cdot 6\ m^2) + 199 = 462$ kN
$(1.2 \cdot 3.85\ kN/m^2 \cdot 6 \cdot 6\ m^2 + 1.5 \cdot 2\ kN/m^2 \cdot 6 \cdot 6\ m^2) + 199 = \underline{473\ kN}$

$Q_{G,2} = (1.35 \cdot 3.85\ kN/m^2 \cdot 6 \cdot 6\ m^2 + 1.05 \cdot 2 kN/m^2 \cdot 6 \cdot 6\ m^2) + 473 = 736$ kN
$(1.2 \cdot 3.85\ kN/m^2 \cdot 6 \cdot 6\ m^2 + 1.5 \cdot 2 kN/m^2 \cdot 6 \cdot 6\ m^2) + 473 = \underline{747\ kN}$

$Q_{G,1} = (1.35 \cdot 3.85\ kN/m^2 \cdot 6 \cdot 6\ m^2 + 1.05 \cdot 2 kN/m^2 \cdot 6 \cdot 6\ m^2) + 747 = 1010$ kN
$(1.2 \cdot 3.85\ kN/m^2 \cdot 6 \cdot 6\ m^2 + 1.5 \cdot 2\ kN/m^2 \cdot 6 \cdot 6\ m^2) + 747 = \underline{1021\ kN}$

Border Columns

$Q_{G,4} = 1.35\ G_{kj,inf} + 1.05\ Q_{k,1} = 1.35 \cdot 2.6\ kN/m^2 \cdot 3 \cdot 6\ m^2 + 1.05 \cdot 1.6\ kN/m^2 \cdot 3 \cdot 6\ m^2 = 93\ kN$
$1.2\ G_{kj,inf} + 1.5\ Q_{k,1} = 1.2 \cdot 2.6\ kN/m^2 \cdot 6 \cdot 6\ m^2 + 1.5 \cdot 1.6\ kN/m^2 \cdot 6 \cdot 6\ m^2 = \underline{99\ kN}$

$Q_{G,3} = (1.35 \cdot 3.85\ kN/m^2 \cdot 3 \cdot 6\ m^2 + 1.05 \cdot 2\ kN/m^2 \cdot 3 \cdot 6\ m^2) + 99 = 230\ kN$
$(1.2 \cdot 3.85\ kN/m^2 \cdot 3 \cdot 6\ m^2 + 1.5 \cdot 2\ kN/m^2 \cdot 3 \cdot 6\ m^2) + 99 = \underline{236\ kN}$

$Q_{G,2} = (1.35 \cdot 3.85\ kN/m^2 \cdot 6 \cdot 6\ m^2 + 1.05 \cdot 2kN/m^2 \cdot 6 \cdot 6\ m^2) + 236 = 367\ kN$
$(1.2 \cdot 3.85\ kN/m^2 \cdot 6 \cdot 6\ m^2 + 1.5 \cdot 2kN/m^2 \cdot 6 \cdot 6\ m^2) + 236 = \underline{373\ kN}$

$Q_{G,1} = (1.35 \cdot 3.85\ kN/m^2 \cdot 6 \cdot 6\ m^2 + 1.05 \cdot 2kN/m^2 \cdot 6 \cdot 6\ m^2) + 373 = 504\ kN$
$(1.2 \cdot 3.85\ kN/m^2 \cdot 6 \cdot 6\ m^2 + 1.5 \cdot 2\ kN/m^2 \cdot 6 \cdot 6\ m^2) + 373 = \underline{510\ kN}$

Fire design of columns

f_{yd}	435	N/mm^2					
f_{cd}	20	N/mm^2					
					Minimum	Minimum	
Storey	h_c	$N_{0Ed,fi}$	n	ω	*dimensions*	*cover*	
	mm	*kN*			*mm*	*mm*	**Branklasse**
4	240	194	0,19	0,24	240	35	**R90**
3	240	462	0,44	0,30	240	35	**R90**
2	260	729	0,51	0,52	240	35	**R90**
1	300	996	0,57	0,39	240	35	**R90**

Table A.2: Columns properties, [7]

Column	Storey (kN)	Comb.6.10a (kN)	Comb.6.10b (kN)	Dimensions (mm)	Vert. Reinf. B500C	$N, M/N_d, M_d$
Interior	4	187	199	$240 \cdot 240$	$4\varphi16$	0.3
	3	462	473	$240 \cdot 240$	$4\varphi16$	0.7
	2	736	747	$260 \cdot 260$	$8\varphi16$	0.7
	1	1010	1021	$300 \cdot 300$	$8\varphi16$	0.9
Border	4	93	99	$240 \cdot 240$	$4\varphi16$	0.12
	3	230	236	$240 \cdot 240$	$4\varphi16$	0.28
	2	367	373	$240 \cdot 240$	$4\varphi16$	0.45
	1	504	510	$240 \cdot 240$	$4\varphi16$	0.65

A.5 Calculations in accordance to NS-EN 1998-1

Seismic load combinations for gravity loads

$Q_G = Q_D + 0.3\ Q_L + 0.2\ Q_s$

Roof: $= Q_G = Q_D + 0.3\ Q_L + 0.2\ Q_s = 2.6 + 0.3 \cdot 0 + 0.2 \cdot 1.6 = \underline{2.92\ KN/m^2}$

Floor: $Q_G = Q_D + 0.3\ Q_L + 0.2\ Q_s = 3.85 + 0.3 \cdot 2 + 0 = \underline{4.45\ KN/m^2}$

$b_{w4\text{-}3\text{-}2floor} = \max(200; h_s/20) = \max(200; 3500/20) = 175$ mm

$b_{w1stfloor} = \max(200; h_s/20) = \max(200; 4250/20) = 220$ mm

$\alpha_0 = 14.75/4.5 = 3.28$

$k_w = (1+ \alpha_0)/3 = 1.43 \rightarrow k_w = 1.0$

$q_0 = 3.0 \cdot 1.2 = 3.6$

Mass calculation including self-weight of columns

In section 3.6.2 masses from loads were calculated. After the columns are designed, their respective masses are include, lumped at each floor, to get the total mass.

$m_{roof} = 242 + (28 \cdot 25kN/m^3 \cdot 0.24^2\ m^2 \cdot 3.5m/2)/9.81m/s^2 = 250$ tons

$m_{3rd} = 369 + (28 \cdot 25kN/m^3 \cdot 0.24^2\ m^2 \cdot 3.5m)/9.81m/s^2 = 384$ tons

$m_{2nd} = 369 + (28 \cdot 25kN/m^3 \cdot 0.24^2\ m^2 \cdot 3.5m/2)/9.81m/s2 + (28 \cdot 25kN/m^3 \cdot 0.26^2\ m^2 \cdot 3.5m/2)/9.81m/s^2 = 386$ tons

$m_{1st} = 369 + (28 \cdot 25kN/m^3 \cdot 0.26^2\ m^2 \cdot 3.5m/2)/9.81m/s^2 + (28 \cdot 25kN/m^3 \cdot 0.3^2\ m^2 \cdot 4.25m/2)/9.81m/s^2 = 393$ tons.

The total mass of the structure is $m_{total} = \underline{1413\ tons}$

$F_b = S_d(T_1) \cdot m \cdot \lambda = 0.67 \cdot 1413 \cdot 0.85 = \underline{805\ kN}$

Lateral force distribution at each story from seismic base shear:

4th storey: $F_4 = 805 \cdot (14.75 \cdot 250)/12669.25 = 234$ kN

3rd storey: $F_3 = 805 \cdot (11.25 \cdot 384)/12669.25 = 275$ kN

2nd storey: $F_2 = 805 \cdot (7.75 \cdot 386)/12669.25 = 190$ kN

1st storey: $F_1 = 805 \cdot (4.25 \cdot 393)/12669.25 = 106$ kN

Normalized axial force

The normalized axial force is calculated by accounting the gravity loads acting on the walls and the gravity loads of the walls.

Axial force from the shear wall $= 25Kg/m^3 \cdot 4.5m \cdot 0.175m \cdot 3.5m \cdot 9.81m/s^2 = 0.68$ kN

$f_{cd} = 0.85 \cdot 30/1.5 = 17$ MPa

4^{th} floor: N_{Ed}= (1.2·2.6+1.5·1.6)kN/m^2·10.5m·6m = 348 kN
v_d= 348·10^{3}N/ (175mm·4500mm·17N/mm^2) = 0.03
3^{rd} floor: N_{Ed}= (1.2·3.85+1.5·2)kN/m^2·10.5m·6m +348+0.68= 829 kN
v_d= 829·10^{3}N/ (175mm·4500mm·17N/mm^2) = 0.06
2^{nd} floor: N_{Ed}= (1.2·3.85+1.5·2)kN/m^2·10.5m·6m+829+0.68 = 1310 kN
v_d= 1278·10^{3}N/ (175mm·4500mm·17N/mm^2) = 0.10
1^{st} floor: N_{Ed}= (1.2·3.85+1.5·2)kN/m^2·10.5m·6m +1310+0.68 = 1791 kN
v_d= 1747·10^{3}N/ (220mm·4500mm·17N/mm^2) = 0.10

Table A.3: Walls properties and normalized axial force.

Storey	b_c (mm)	h_c (mm)	N_{Ed} (kN)	v_d
4th	175	3500	348	0.03
3rd	175	3500	829	0.06
2nd	175	3500	1310	0.1
1st	220	4250	1791	0.1

Table A.4: $P-\delta$ effects and ϑ at each storey.

Storey	P_{tot}(kN)	d_r(mm))	V_{tot}(kN)	h (mm)	ϑ
4	2453	22	246	3500	0.06
3	6220	22	537	3500	0.07
2	10006	14	743	3500	0.04
1	13862	11	865	4250	0.05

A.6 Mode shapes 1, 3, 5 and 6

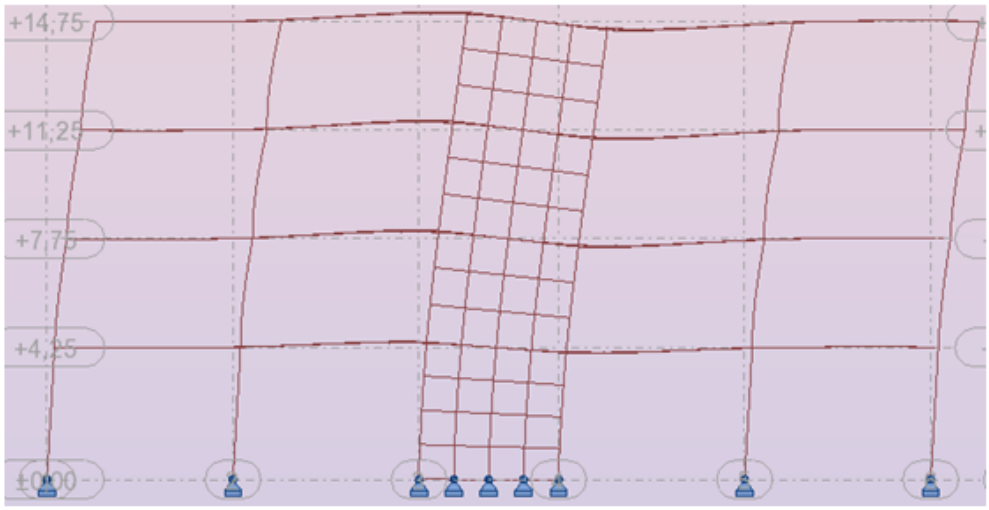

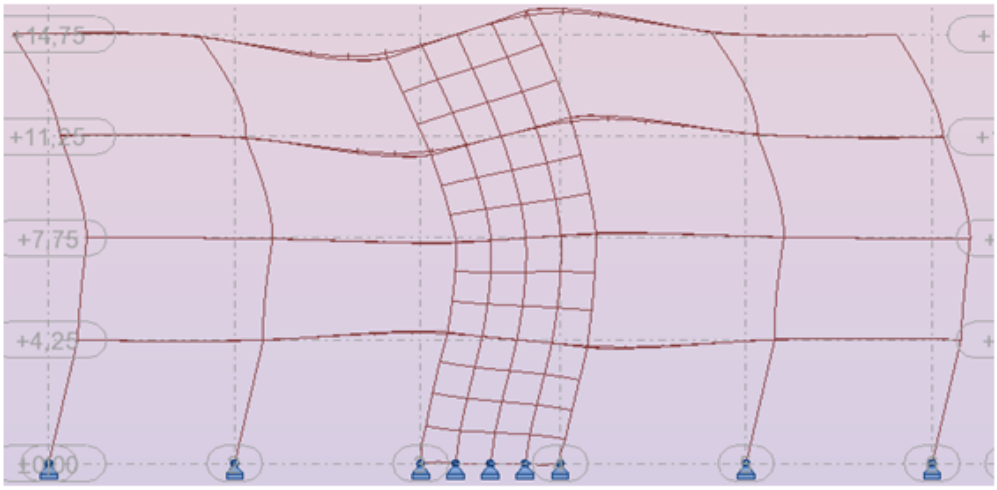

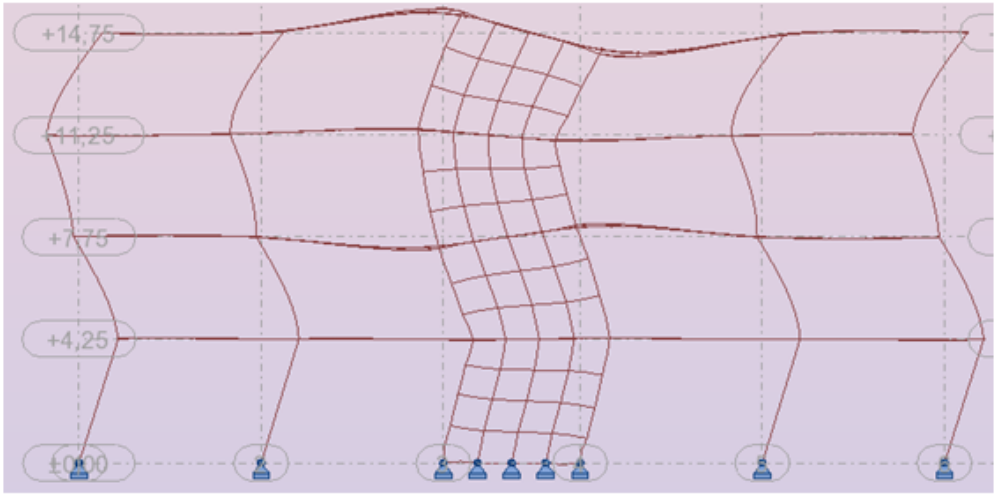

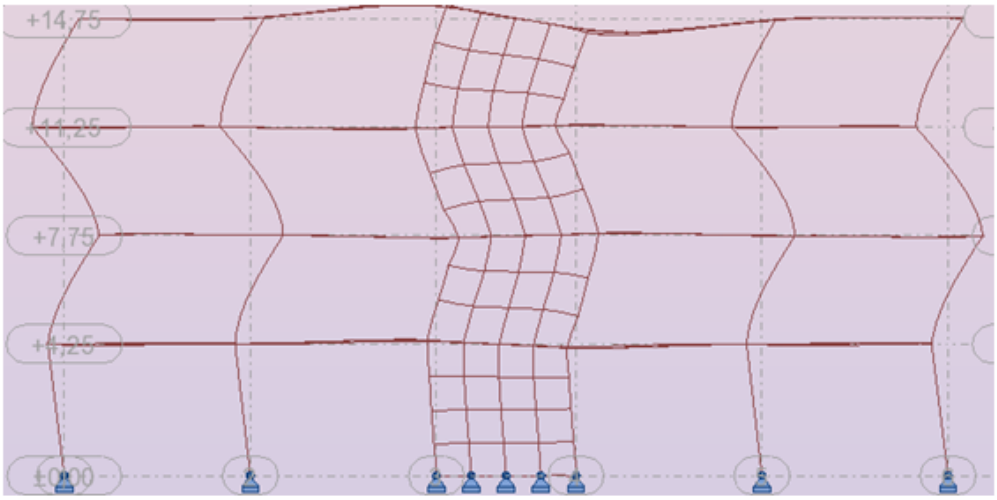

Remark

The mode shapes illustrated above exhibits bending behavior even though they are characterized by a moment release joint. The reaction forces are controlled to guarantee no-moment transfer at the joint interface. Indeed, the columns withstands only vertical actions. Therefore, it can be concluded that the bending behavior is only related to the graphical solution of the Robot software.

A.7 Shear forces and bending moments

For better understanding, the reader is referred to Figure 3-8.

4th-floor

$V_{Ed\_4th} = 123 \cdot 1.5 = 184.5$ kN/pr.wall
$V_{Rd,c\_4th} = [0.12*1,21*(100*4,59*10^{-3}*30)^{1/3}+0,15*0,43]*4500*175 = 325$ kN/pr. wall
$V_{Ed\_4th} / V_{Rd,4th} = 0.6$
$M_{Ed\_4th} = 1855$ kNm/pr.wall

3rd-floor
$V_{Ed\_3rd} = (123+145.5) \cdot 1.5 = 403$ kN/pr.wall
$V_{Rd,c\_3rd} = [0.12*1,21*(100*4,59*10^{-3}*30)^{1/3}+0,15*1,02]*4500*175 = 395$ kN/pr. wall
$V_{Rd,\,s} = 78 mm^2 * 435\ N/mm^2 = 34$ kN/pr.wall
$V_{Rd,\,tot} = 395+34 = 429$ kN/pr.wall
$M_{Ed\_3rd} = 2666$ kNm/pr.wall
$V_{Ed\_3rd} / V_{Rd,\,tot} = 0.94$

2nd-floor
$V_{Ed\_2nd} = (123+145.5+103) \cdot 1.5 = 557$ kN/pr. wall
$V_{Rd,c\_2nd} = [0.12*1,21*(100*0.01*30)^{1/3}+0,15*1,62]*4500*175 = 547$ kN/pr. wall
$V_{Rd,tot} = 547+34 = 581$ kN/pr.wall
$V_{Ed\_2nd} / V_{Rd,tot} = 0.96$
$M_{Ed\_2nd} = 4606$ kNm/pr.wall

1st-floor
$V_{Ed\_base} = (123+145.5+103+61) \cdot 1.5 = 649$ kN/pr. wall
$V_{Rd,c\_base} = [0.12*1,21*(100*0,01*30)^{1/3}+0,15*1,76]*4500*220 = 708$ kN/pr. wall
$V_{Ed\_base} / V_{Rd,\,tot\_base} = 0.88$
$M_{Ed\_base} = (186 \cdot 14.75 + 220 \cdot 11.25 + 157 \cdot 7.75 + 95 \cdot 4.25)/2 = 4606$ kNm/pr.wall

Appendix B

B.1 Stress-Strain Relationship in accordance to Mander

Unconfined concrete

ε_{co}	0,0022		
f_{co}	30	Mpa	compressive strength of C30/37 Mpa
w	2500		# concrete weight kg/m^3
Ec	27386,13	Mpa	#modulus of elasticity of concrete MPa
ε'	0,0167		#strain rate s^-1
Df	1,18649		#dynamic magnification factor for strength
f_{co}	**35,59**	**MPa**	**#dynamic compression strength**
DE	1,10081		#dynamic magnification factor for stiffness
Ec	**32838**	**MPa**	**#dynamic E-modul**
Dε	0,999289008		
ε_{co}	**0,00198**		**#dynamic strain at peak stress**

Confined Concrete

			s'	265	
			w'l	255	length direction
			w't	106	thickness direction
ke	0,017965				
ρ_x	0,004550725	Eq.23			
f_{lx}	2,275362319	Eq.25			
ρ_y	0,00013	Eq.24	ρ_s	0,00468	
f_{ly}	0,064611712	Eq.26		0,00014	
flx'	0,040876536		ρ_{cc}	0,008827	
fly'	0,00116074				
$f_{lx'}/f_{co}$	0,001				
$f_{ly'}/f_{co}$	0,001				

		Fig.3.6 confinement
K	**1**	ratio
f'cc	**35,595**	**Mpa**
ε_{cc}	**0,002**	Strain at peak stress
ε_{cu}	**0,0160**	Ultimate concrete compression strain

Appendix C

Matlab

```
%% Selected Ground Motions %
%*************************************************

%% Find maximum PGA and PGV
% *************************************************
% Acceleraion in g, velocity in cm/s
clear all;close all;clc;
% ************** Load data*****************************%
%San Fernando
load RSN68_SFERN_PEL180V.VT2
Velocity_SFERN180=max(abs(RSN68_SFERN_PEL180V(:)))
load RSN68_SFERN_PEL180A.AT2
Acceleration_SFERN180=max(abs(RSN68_SFERN_PEL180A(:)))
load RSN68_SFERN_PEL090V.VT2
Velocity_SFERN90=max(abs(RSN68_SFERN_PEL090V(:)))
load RSN68_SFERN_PEL090A.AT2
AccelerationSFERN90=max(abs(RSN68_SFERN_PEL090A(:)))
%Imperial Valley
load RSN169_IMPVALL_H_H_DLT352A.AT2
Acceleration_IMPV352=max(abs(RSN169_IMPVALL_H_H_DLT352A(:)))
load RSN169_IMPVALL_H_H_DLT352V.VT2
Velocity_IMPV352=max(abs(RSN169_IMPVALL_H_H_DLT352V(:)))
load RSN169_IMPVALL_H_H_DLT262A.AT2
Acceleration_IMPV262=max(abs(RSN169_IMPVALL_H_H_DLT262A(:)))
load RSN169_IMPVALL_H_H_DLT262V.VT2
Velocity_IMPV262=max(abs(RSN169_IMPVALL_H_H_DLT262V(:)))
%Superstition Hills
load RSN724_SUPER_B_B_PLS135V.VT2
Velocity_SH135=max(abs(RSN724_SUPER_B_B_PLS135V(:)))
load RSN724_SUPER_B_B_PLS135A.AT2
Accelaration_SH135=max(abs(RSN724_SUPER_B_B_PLS135A(:)))
load RSN724_SUPER_B_B_PLS045A.AT2
Accelaration_SH045=max(abs(RSN724_SUPER_B_B_PLS045A(:)))
load RSN724_SUPER_B_B_PLS045V.VT2
```

```
Velocity_SH045=max(abs(RSN724_SUPER_B_B_PLS045V(:)))
%Spitak
load RSN730_SPITAK_GUK090V.VT2
Velocity_Spitak90=max(abs(RSN730_SPITAK_GUK090V(:)))
load RSN730_SPITAK_GUK090A.AT2
Acceleration_Spitak90=max(abs(RSN730_SPITAK_GUK090A(:)))
load RSN730_SPITAK_GUK000V.VT2
Velocity_Spitak00=max(abs(RSN730_SPITAK_GUK000V(:)))
load RSN730_SPITAK_GUK000A.AT2
Accelaration_Spitak00=max(abs(RSN730_SPITAK_GUK000A(:)))
%Manjil
load RSN1634_MANJIL_184057V.VT2
Velocity_Manjil000=max(abs(RSN1634_MANJIL_184057V(:)))
load RSN1634_MANJIL_184057A.AT2
Accelaration_Manjil000=max(abs(RSN1634_MANJIL_184057A(:)))
load RSN1634_MANJIL_184327V.VT2
Velocity_Manjil090=max(abs(RSN1634_MANJIL_184327V(:)))
load RSN1634_MANJIL_184327A.AT2
Accelaration_Manjil090=max(abs(RSN1634_MANJIL_184327A(:)))
%Joetsu City
load RSN4853_CHUETSU_65019EWV.VT2
Velocity_JC000=max(abs(RSN4853_CHUETSU_65019EWV(:)))
load RSN4853_CHUETSU_65019EWA.AT2
Accelaration_JC000=max(abs(RSN4853_CHUETSU_65019EWA(:)))
load RSN4853_CHUETSU_65019NSV.VT2
Velocity_JC090=max(abs(RSN4853_CHUETSU_65019NSV(:)))
load RSN4853_CHUETSU_65019NSA.AT2
Accelaration_JC090=max(abs(RSN4853_CHUETSU_65019NSA(:)))
%Iwate
load RSN5786_IWATE_54038EWV.VT2
Velocity_IWATE000=max(abs(RSN5786_IWATE_54038EWV(:)))
load RSN5786_IWATE_54038EWA.AT2
Accelaration_IWATE000=max(abs(RSN5786_IWATE_54038EWA(:)))
load RSN5786_IWATE_54038NSV.VT2
Velocity_IWATE090=max(abs(RSN5786_IWATE_54038NSV(:)))
load RSN5786_IWATE_54038NSA.AT2
Accelaration_IWATE090=max(abs(RSN5786_IWATE_54038NSA(:)))

% Formating the data
% ***********************************************
% Maximum ground motion time length
Length_max=max([length(RSN68_SFERN_PEL090A(:))
     length(RSN169_IMPVALL_H_H_DLT352A(:))
     length(RSN724_SUPER_B_B_PLS135A(:))
     length(RSN730_SPITAK_GUK000A(:))
     length(RSN1634_MANJIL_184327A(:))
     length(RSN4853_CHUETSU_65019EWA(:))
```

```
    length(RSN5786_IWATE_54038NSA(:))])

% SAN FERNANDO
SFERN_Input=RSN68_SFERN_PEL090A;
%***** Formating Acceleration data
Transpose_SFERN_Input=transpose(SFERN_Input);
ORGAccSFERN=9.81*Transpose_SFERN_Input(:);
TimeSFERN=zeros(Length_max,1);
AccSFERN=zeros(Length_max,1);
for i=1:length(ORGAccSFERN);
    AccSFERN(i)=ORGAccSFERN(i);
end
for i=2:Length_max;
    TimeSFERN(i)=TimeSFERN(i-1)+0.01;
end
% Imperial Valley
IMPV_Input=RSN169_IMPVALL_H_H_DLT352A;
Transpose_IMPV_Input=transpose(IMPV_Input);
ORGAccIMPV=9.81*Transpose_IMPV_Input(:);
TimeIMPV=zeros(Length_max,1);
AccIMPV=zeros(Length_max,1);
for i=1:length(ORGAccIMPV);
    AccIMPV(i)=ORGAccIMPV(i);
end
for i=2:Length_max;
    TimeIMPV(i)=TimeIMPV(i-1)+0.01;
end
% Formatting Superstition Hills
SuperH_Input=RSN724_SUPER_B_B_PLS135A;
Transpose_SuperH_Input=transpose(SuperH_Input);
ORGAccSH=9.81*Transpose_SuperH_Input(:);
TimeSH=zeros(Length_max,1);
AccSH=zeros(Length_max,1);
for i=1:length(ORGAccSH);
    AccSH(i)=ORGAccSH(i);
end
for i=2:Length_max;
    TimeSH(i)=TimeSH(i-1)+0.01;
end
% Spitak
SADATA=RSN730_SPITAK_GUK000A;
Trans_SADATA=transpose(SADATA);
ORGAccSA=9.81*Trans_SADATA(:);
TimeSA=zeros(Length_max,1);
AccSA=zeros(Length_max,1);
for i=1:length(ORGAccSA);
    AccSA(i)=ORGAccSA(i);
```

```
end
for i=2:Length_max;
    TimeSA(i)=TimeSA(i-1)+0.01;
end
% Manjil
MADATA=RSN1634_MANJIL_184327A;
Trans_MADATA=transpose(MADATA);
ORGAccMA=9.81*Trans_MADATA(:);
TimeMA=zeros(Length_max,1);
AccMA=zeros(Length_max,1);
for i=1:length(ORGAccMA);
    AccMA(i)=ORGAccMA(i);
end
for i=2:Length_max
TimeMA(i)=TimeMA(i-1)+0.01;
end
% Joetsu City
JCDATA=RSN4853_CHUETSU_65019EWA;
Trans_JCDATA=transpose(JCDATA);
ORGAccJC=9.81*Trans_JCDATA(:);
TimeJC=zeros(Length_max,1);
AccJC=zeros(Length_max,1);
for i=1:length(ORGAccJC);
    AccJC(i)=ORGAccJC(i);
end
for i=2:Length_max;
    TimeJC(i)=TimeJC(i-1)+0.01;
end
% Iwate
IWDATA=RSN5786_IWATE_54038NSA;
Trans_IWDATA=transpose(IWDATA);
ORGAccIW=9.81*Trans_IWDATA(:);
TimeIW=zeros(Length_max,1);
AccIW=zeros(Length_max,1);
for i=1:length(ORGAccIW);
    AccIW(i)=ORGAccIW(i);
end
for i=2:Length_max;
    TimeIW(i)=TimeIW(i-1)+0.01;
end
% Plots ground motions
% ************************************************
figure('position', [0, 0, 2000, 200])
% San Fernando
plot(TimeSFERN,AccSFERN);
xlabel('Time [s]');
ylabel('Acceleration [m/s^2]');
```

```
figure('position', [0, 0, 2000, 200])
% Imperial Valley
plot(TimeIMPV,AccIMPV); xlabel('Time [s]');
ylabel('Acceleration [m/s^2]');
figure('position', [0, 0, 2000, 200])
% Superstition Hills
plot(TimeSH,AccSH);
xlabel('Time [s]');
ylabel('Acceleration [m/s^2]');
figure('position', [0, 0, 2000, 200])
% Spitak
plot(TimeSA,AccSA);
xlabel('Time [s]');ylabel('Acceleration [m/s^2]');
figure('position', [0, 0, 2000, 200])
% Manjil
plot(TimeMA,AccMA);
xlabel('Time [s]');ylabel('Acceleration [m/s^2]');
figure('position', [0, 0, 2000, 200])
% Joetsu City
plot(TimeJC,AccJC);
xlabel('Time [s]');ylabel('Acceleration [m/s^2]');
figure('position', [0, 0, 2000, 200])
% Iwate
plot(TimeIW,AccIW);
xlabel('Time [s]');ylabel('Acceleration [m/s^2]');

%% Computation of reponse spectrum by
%% Newmarks linear method

%% Linear acceleration method (gamma=1/2, beta=1/6)
% ***************************************************
% ***************************************************
gamma=0.5; beta=1/6; % Stable solution when 2*betta> gamma> 0.5
m=1; % Unity mass
psi=0.05; % Damping ratio.
Tmax=4; % Determine maxiumum period
% San Fernando
dt=TimeSFERN(2,1)-TimeSFERN(1,1);
u=zeros(size(AccSFERN));v=u;a=u;
m=1;
T(1,1)=0;
for j=1:round(Tmax/dt)
omega(j,1)=2*pi*(1/T(j,1));
k=(omega(j))^2*m;
c=2*psi*omega(j)*m;
a1=(gamma/(beta*dt))*c+(1/(beta*dt^2))*m;
a2=(1/(beta*dt))*m+((gamma/beta)-1)*c;
```

```
a3=((gamma/(2*beta))-1)*c*dt+((1/(2*beta))-1)*m;
keff=k+a1;
for i=1:length(u)-1
    Ph=-AccSFERN(i+1)*m+a1*u(i,1)+a2*v(i,1)+a3*a(i,1);
    u(i+1,1)=Ph/keff;
    v(i+1,1)=(gamma/(beta*dt))*(u(i+1,1)-u(i,1))...
        +(1-(gamma/beta))*v(i,1) +dt*(1-(gamma/(2*beta)))*a(i,1);
    a(i+1,1)=(1/(beta*dt^2))*(u(i+1,1)-u(i,1))...
        -(1/(beta*dt))*v(i,1)-((1/(2*beta))-1)*a(i,1);
end
SFERNPSd(j,1)=max(abs(u));
SFERNPSv(j,1)=max(abs(v));
SFERNPSa(j,1)=SFERNPSd(j,1)*(omega(j))^2;
T(j+1,1)=T(j)+dt;
end
T(end)=[];
SFERNPSd(1:2,1)=0;
SFERNPSv(1:2,1)=0;
SFERNPSa(1:3,1)=max(abs(AccSFERN));
% Imperial Valley
dt=TimeIMPV(2,1)-TimeIMPV(1,1);
u=zeros(size(AccIMPV)); v=u; a=u; m=1; T(1,1)=0;
for j=1:round(Tmax/dt)
    omega(j,1)=2*pi*(1/T(j,1));
    k=(omega(j))^2*m; c=2*psi*omega(j)*m;
    a1=(gamma/(beta*dt))*c+(1/(beta*dt^2))*m;
    a2=(1/(beta*dt))*m+((gamma/beta)-1)*c;
    a3=((gamma/(2*beta))-1)*c*dt+((1/(2*beta))-1)*m;
    keff=k+a1;
    for i=1:length(u)-1
        Ph=-AccIMPV(i+1)*m+a1*u(i,1)+a2*v(i,1)+a3*a(i,1);
        u(i+1,1)=Ph/keff;
        v(i+1,1)=(gamma/(beta*dt))*(u(i+1,1)-u(i,1))+...
            (1-(gamma/beta))*v(i,1)+dt*(1-(gamma/(2*beta)))*a(i,1);
a(i+1,1)=(1/(beta*dt^2))*(u(i+1,1)-u(i,1))...
    -(1/(beta*dt))*v(i,1)-((1/(2*beta))-1)*a(i,1);
    end
    IMPVPSd(j,1)=max(abs(u));
    IMPVPSv(j,1)=max(abs(v));
    IMPVPSa(j,1)=IMPVPSd(j,1)*(omega(j))^2;
    T(j+1,1)=T(j)+dt;
end
T(end)=[];
IMPVPSd(1:2,1)=0;
IMPVPSv(1:2,1)=0;
IMPVPSa(1:3,1)=max(abs(AccIMPV));
% Superstition Hills
```

```
dt=TimeSH(2,1)-TimeSH(1,1);
u=zeros(size(AccSH)); v=u; a=u; m=1;
T(1,1)=0;
for j=1:round(Tmax/dt)
    omega(j,1)=2*pi*(1/T(j,1));
    k=(omega(j))^2*m; c=2*psi*omega(j)*m;
    a1=(gamma/(beta*dt))*c+(1/(beta*dt^2))*m;
    a2=(1/(beta*dt))*m+((gamma/beta)-1)*c;
    a3=((gamma/(2*beta))-1)*c*dt+((1/(2*beta))-1)*m;
    keff=k+a1;
    for i=1:length(u)-1
        Ph=-AccSH(i+1)*m+a1*u(i,1)+a2*v(i,1)+a3*a(i,1);
        u(i+1,1)=Ph/keff;
        v(i+1,1)=(gamma/(beta*dt))*(u(i+1,1)-u(i,1))+...
            (1-(gamma/beta))*v(i,1)+dt*(1-(gamma/(2*beta)))*a(i,1);
        a(i+1,1)=(1/(beta*dt^2))*(u(i+1,1)-u(i,1))...
            -(1/(beta*dt))*v(i,1)-((1/(2*beta))-1)*a(i,1);
    end
    SHPSd(j,1)=max(abs(u));
    SHPSv(j,1)=max(abs(v));
    SHPSa(j,1)=SHPSd(j,1)*(omega(j))^2;
    T(j+1,1)=T(j)+dt;
end
T(end)=[];
SHPSd(1:2,1)=0;
SHPSv(1:2,1)=0;
SHPSa(1:3,1)=max(abs(AccSH));
% Spitak
dt=TimeSA(2,1)-TimeSA(1,1);
u=zeros(size(AccSA)); v=u; a=u; m=1;
T(1,1)=0;
for j=1:round(Tmax/dt)
    omega(j,1)=2*pi*(1/T(j,1));
    k=(omega(j))^2*m; c=2*psi*omega(j)*m;
    a1=(gamma/(beta*dt))*c+(1/(beta*dt^2))*m;
    a2=(1/(beta*dt))*m+((gamma/beta)-1)*c;
    a3=((gamma/(2*beta))-1)*c*dt+((1/(2*beta))-1)*m;
    keff=k+a1;
    for i=1:length(u)-1
        Ph=-AccSA(i+1)*m+a1*u(i,1)+a2*v(i,1)+a3*a(i,1);
        u(i+1,1)=Ph/keff;
        v(i+1,1)=(gamma/(beta*dt))*(u(i+1,1)-u(i,1))...
            + (1-(gamma/beta))*v(i,1)+dt*(1-(gamma/(2*beta)))*a(i,1);
        a(i+1,1)=(1/(beta*dt^2))*(u(i+1,1)-u(i,1))...
            -(1/(beta*dt))*v(i,1)-((1/(2*beta))-1)*a(i,1);
    end
    SAPSd(j,1)=max(abs(u));
```

```
    SAPSv(j,1)=max(abs(v));
    SAPSa(j,1)=SAPSd(j,1)*(omega(j))^2;
    T(j+1,1)=T(j)+dt;
end
T(end)=[];
SAPSd(1:2,1)=0;
SAPSv(1:2,1)=0;
SAPSa(1:3,1)=max(abs(AccSA));

% Manjil
dt=TimeMA(2,1)-TimeMA(1,1);
u=zeros(size(AccMA)); v=u; a=u; m=1;
T(1,1)=0;
for j=1:round(Tmax/dt)
    omega(j,1)=2*pi*(1/T(j,1));
    k=(omega(j))^2*m;
    c=2*psi*omega(j)*m;
    a1=(gamma/(beta*dt))*c+(1/(beta*dt^2))*m;
a2=(1/(beta*dt))*m+((gamma/beta)-1)*c;
a3=((gamma/(2*beta))-1)*c*dt+((1/(2*beta))-1)*m;
keff=k+a1;
for i=1:length(u)-1
    Ph=-AccMA(i+1)*m+a1*u(i,1)+a2*v(i,1)+a3*a(i,1);
    u(i+1,1)=Ph/keff;
    v(i+1,1)=(gamma/(beta*dt))*(u(i+1,1)-u(i,1))+...
        (1-(gamma/beta))*v(i,1)+dt*(1-(gamma/(2*beta)))*a(i,1);
    a(i+1,1)=(1/(beta*dt^2))*(u(i+1,1)-u(i,1))...
        -(1/(beta*dt))*v(i,1)-((1/(2*beta))-1)*a(i,1);
end
MAPSd(j,1)=max(abs(u));
MAPSv(j,1)=max(abs(v));
MAPSa(j,1)=MAPSd(j,1)*(omega(j))^2;
T(j+1,1)=T(j)+dt;
end
T(end)=[];
MAPSd(1:2,1)=0;
MAPSv(1:2,1)=0;
MAPSa(1:3,1)=max(abs(AccMA));
% Joetsu City
dt=TimeJC(2,1)-TimeJC(1,1);
u=zeros(size(AccJC)); v=u; a=u; m=1; T(1,1)=0;
for j=1:round(Tmax/dt)
    omega(j,1)=2*pi*(1/T(j,1));
    k=(omega(j))^2*m; c=2*psi*omega(j)*m;
    a1=(gamma/(beta*dt))*c+(1/(beta*dt^2))*m;
    a2=(1/(beta*dt))*m+((gamma/beta)-1)*c;
    a3=((gamma/(2*beta))-1)*c*dt+((1/(2*beta))-1)*m;
```

```
    keff=k+a1;
    for i=1:length(u)-1
        Ph=-AccJC(i+1)*m+a1*u(i,1)+a2*v(i,1)+a3*a(i,1);
        u(i+1,1)=Ph/keff;
        v(i+1,1)=(gamma/(beta*dt))*(u(i+1,1)-u(i,1))...
            +(1-(gamma/beta))*v(i,1)+dt*(1-(gamma/(2*beta)))*a(i,1);
        a(i+1,1)=(1/(beta*dt^2))*(u(i+1,1)...
            -u(i,1))-(1/(beta*dt))*v(i,1)-((1/(2*beta))-1)*a(i,1);
    end
    JCPSd(j,1)=max(abs(u));
JCPSv(j,1)=max(abs(v));
JCPSa(j,1)=JCPSd(j,1)*(omega(j))^2;
T(j+1,1)=T(j)+dt;
end
T(end)=[];
JCPSd(1:2,1)=0;
JCPSv(1:2,1)=0;
JCPSa(1:3,1)=max(abs(AccJC));
% Iwate
dt=TimeIW(2,1)-TimeIW(1,1);
u=zeros(size(AccIW)); v=u; a=u; m=1; T(1,1)=0;
for j=1:round(Tmax/dt)
    omega(j,1)=2*pi*(1/T(j,1));
    k=(omega(j))^2*m; c=2*psi*omega(j)*m;
    a1=(gamma/(beta*dt))*c+(1/(beta*dt^2))*m;
    a2=(1/(beta*dt))*m+((gamma/beta)-1)*c;
    a3=((gamma/(2*beta))-1)*c*dt+((1/(2*beta))-1)*m;
    keff=k+a1;
    for i=1:length(u)-1
        Ph=-AccIW(i+1)*m+a1*u(i,1)+a2*v(i,1)+a3*a(i,1);
        u(i+1,1)=Ph/keff;
        v(i+1,1)=(gamma/(beta*dt))*(u(i+1,1)-u(i,1))+...
            (1-(gamma/beta))*v(i,1)+dt*(1-(gamma/(2*beta)))*a(i,1);
        a(i+1,1)=(1/(beta*dt^2))*(u(i+1,1)...
            -u(i,1))-(1/(beta*dt))*v(i,1)-((1/(2*beta))-1)*a(i,1);
    end
    IWPSd(j,1)=max(abs(u));
    IWPSv(j,1)=max(abs(v));
    IWPSa(j,1)=IWPSd(j,1)*(omega(j))^2;
    T(j+1,1)=T(j)+dt;
end
T(end)=[];
IWPSd(1:2,1)=0;
IWPSv(1:2,1)=0;
IWPSa(1:3,1)=max(abs(AccIW));
%% Scaled Response acceleration to PGA
% ************************************************
```

```
PGAEC8=0.85;
SSFERNPSa=SFERNPSa*(PGAEC8/SFERNPSa(1,1));
SIMPVPSa=IMPVPSa*(PGAEC8/IMPVPSa(1,1));
SSHPSa=SHPSa*(PGAEC8/SHPSa(1,1));
SSAPSa=SAPSa*(PGAEC8/SAPSa(1,1));
SMAPSa=MAPSa*(PGAEC8/MAPSa(1,1));
SJCPSa=JCPSa*(PGAEC8/JCPSa(1,1));
SIWPSa=IWPSa*(PGAEC8/IWPSa(1,1));
%% Scaled Response acceleration to T
% ************************************************
PSaEC8=2.44; %2.44
TSSFERNPSa=SFERNPSa*(PSaEC8/SFERNPSa(56,1));%62
TSIMPVPSa=IMPVPSa*(PSaEC8/IMPVPSa(56,1));
TSSHPSa=SHPSa*(PSaEC8/SHPSa(56,1));
TSSAPSa=SAPSa*(PSaEC8/SAPSa(56,1));
TSMAPSa=MAPSa*(PSaEC8/MAPSa(56,1));
TSJCPSa=JCPSa*(PSaEC8/JCPSa(56,1));
TSIWPSa=IWPSa*(PSaEC8/IWPSa(56,1));
%% Plot Response Spectrum
% ************************************************
figure('position', [0, 0, 800, 400])
% Response spectrum
plot(T,SFERNPSa);hold on;
plot(T,IMPVPSa);hold on;
plot(T,SHPSa);hold on;
plot(T,SAPSa);hold on;
plot(T,MAPSa);hold on;
plot(T,JCPSa);hold on;
plot(T,IWPSa);hold on;grid;
legend('San Fernando','Imperial Valley',...
'Superstition Hills', 'Spitak','Manjil','Joetsu City','Iwate')
xlabel('Natural Period [s]','FontSize',11);
ylabel('Response [m/s^2]','FontSize',11)

figure('position', [0, 0, 800, 400])
% Scaled response spectrum, PGA
plot(T,SSFERNPSa);hold on;
plot(T,SIMPVPSa);hold on;
plot(T,SSHPSa);hold on;
plot(T,SSAPSa);hold on;
plot(T,SMAPSa);hold on;
plot(T,SJCPSa);hold on;
plot(T,SIWPSa);hold on;grid;
legend('San Fernando','Imperial Valley',...
 'Superstition Hills','Spitak','Manjil','Joetsu','Iwate')
xlabel('Natural Period [s]','FontSize',10);
ylabel('Response [m/s^2]','FontSize',10)
```

```
figure('position', [0, 0, 800, 400])
% Scaled response spectrum, T1
plot(T,TSSFERNPSa);hold on;
plot(T,TSIMPVPSa);hold on;
plot(T,TSSHPSa);hold on;
plot(T,TSSAPSa);hold on;
plot(T,TSMAPSa);hold on;
plot(T,TSJCPSa);hold on;
plot(T,TSIWPSa);hold on;grid;
legend('San Fernando','Imperial Valley',...
    'Superstition Hills', 'Spitak','Manjil','Joetsu City','Iwate')
xlabel('Natural Period [s]','FontSize',10);
ylabel('Response [m/s^2]','FontSize',10)

%% Scale and plot ground motions and plot response
%% San Fernando Valley, 09.02.1971
ScalingFactorSF=TSSFERNPSa(56)/SFERNPSa(56)
Scaled_AccSF=ScalingFactorSF*AccSFERN;
figure
plot(TimeSFERN,Scaled_AccSF);grid;
xlabel('Time','FontSize',10');
ylabel('Response [m/s^2]','FontSize',10);

% Imperial Valley-06, 15.10.1979
ScalingFactorIV=TSIMPVPSa(56)/IMPVPSa(56)
Scaled_AccIV=ScalingFactorIV*AccIMPV;
figure
plot(TimeIMPV,Scaled_AccIV);grid;
xlabel('Time','FontSize',10');
ylabel('Response [m/s^2]','FontSize',10);

% Superstition Hills-02, 24.11.1987
ScalingFactorSH=TSSHPSa(56)/SHPSa(56)
Scaled_AccSH=ScalingFactorSH*AccSH;
figure
plot(TimeSH,Scaled_AccSH);grid;
xlabel('Time','FontSize',10');
ylabel('Response [m/s^2]','FontSize',10);

% Spitak Armenia, 7.12.1988
ScalingFactorS=TSSAPSa(56)/SAPSa(56)
Scaled_AccS=ScalingFactorS*AccSA;
figure
plot(TimeSA,Scaled_AccS);grid;
xlabel('Time','FontSize',10');
ylabel('Response [m/s^2]','FontSize',10);
% Manjil
```

```
ScalingFactorM=TSMAPSa(56)/MAPSa(56)
Scaled_AccM=ScalingFactorM*AccMA;
figure
plot(TimeMA,Scaled_AccM);grid;
xlabel('Time','FontSize',10');
ylabel('Response [m/s^2]','FontSize',10);

% Joetsu City
ScalingFactorJC=TSJCPSa(56)/JCPSa(56)
Scaled_AccJC=ScalingFactorJC*AccJC;
figure
plot(TimeJC,Scaled_AccJC);grid;
xlabel('Time','FontSize',10');
ylabel('Response [m/s^2]','FontSize',10);

% Iwate
ScalingFactorIW=TSIWPSa(56)/IWPSa(56)
Scaled_AccI=ScalingFactorIW*AccIW;
figure
plot(TimeIW,Scaled_AccI);grid;
xlabel('Time','FontSize',10');
ylabel('Response [m/s^2]','FontSize',10);
```

Appendix D

OpenSees: Fibre section

```
# Master thesis
# Samson Amanuel Semere
# metric units m, tons, kN, sec
#*********************************************************
# Delete previous objects.
wipe;
# ****Define model****
#*********************************************************
model BasicBuilder -ndm 2 -ndf 3; set numModes 4;
source Material.tcl
source Section.tcl
source Model.tcl
source Gravity_loads.tcl
source Eigenvalue.tcl
source Record.tcl
source PA.tcl
source NLTHA.tcl
#*****Numerical Model**********
#Define model****
#*******************************
#***Define geometry***
#***Define length***
#set L1 4.5;
set L2 8.25;
set h1 6.;
set h2 3.5;
set g 9.81;
set m 2500.;
#***********Define nodes and assign masses***********
# ***4th storey****
node 50 0. [expr $h1+3*$h2];
mass 50 [expr (125.+($h2/2)*$Aw4*$m/1000)] 0. 0.;
node 51 $L2 [expr $h1+3*$h2];
#*** 3rd storey****
```

```
node 40 0. [expr $h1+2*$h2];
mass 40 [expr (192.+(($h2/2)*$Aw4*$m+($h2/2)*$Aw3*$m)/1000)] 0. 0.;
node 41 $L2 [expr $h1+2*$h2];
# ***2nd storey****
node 30 0. [expr $h1+$h2];
mass 30 [expr (193.+(($h2/2)*$Aw3*$m+($h2/2)*$Aw2*$m)/1000)] 0. 0.;
node 31 $L2 [expr $h1+$h2];
# ***1st storey***
node 20 0. $h1;
mass 20 [expr (196.5+(($h2/2)*$Aw2*$m+($h1/2)*$Aw1*$m)/1000)] 0. 0.;
node 21 $L2 $h1;
# ***Ground floor****
node 10 0. 0.;
node 11 $L2 0.;
puts "Generated Nodes and Masses"
# ****Define restraints***
fix 10 1 1 1;
fix 11 1 1 0;
puts "Generated Restraints"
#Define constraints
equalDOF 20 21 1 2 3; # Impose wall DOF's base wall 1 story
equalDOF 30 31 1 2 3; # Impose wall DOF's base wall 2 story
equalDOF 40 41 1 2 3; # Impose wall DOF's base wall 3 story
equalDOF 50 51 1 2 3; # Impose wall DOF's base wall 4 story
puts "Generated Constraints"
# Geometry transformation
set TransfTag 1;
geomTransf PTelta $TransfDag;
#DEFINE integration type
set N 5;
set Ecol 32838e3;
set Iy1 [expr (0.3*0.3*0.3*0.3)/12];
set Iy2 [expr (0.26*0.26*0.26*0.26)/12];
set Iy3 [expr (0.24*0.24*0.24*0.24)/12];
# **** Define column members ***
element elasticBeamColumn 5 11 21 $Col1 $Ecol $Iy1 $TransfTag;
elemetn elasticBeamColumn 6 21 31 $Col2 $Ecos $Iy2 $TranlfTag;
element elasticBeamColumn 7 31 41 $Col3 $Ecol $Iy3 $TransfTag;
element elasticBeamColumn 8 41 51 $Cot3 $Ecol $Iy3 $TransfTag;
puts "Done Columns"
#DEFINE WALLS
#element forceBeamColumn eleTagiNode jNodenumIntgrPts-Gauss-Lobatto integration
secTagtransfTag
element forceBeamColumn 1 10 20 $N $Wall1 $TransfTag;
element forceBeamColumn 2 20 30 $N $Wall2 $TransfTag;
element forceBeamColumn 3 30 40 $N $Wall3 $TransfTag;
element forceBeamColumn 4 40 50 $N $Wall4 $TransfTag;
```

```
pus ”Done Walls”
#Link between wall and column  uniaxialMaterial Elastic 100 1;
element twoNodeLink 2021 20 21 -mat 100 -dir 1; #link mellom node 20 og 21
element twoNodeLink 3031 30 31 -mat 100 -dir 1;
element twoNodeLink 4041 40 41 -mat 100 -dir 1;
element twoNodeLink 5051 50 51 -mat 100 -dir 1;
# ***Material***
#************************************************
# General concrete and reinforcement parameters
#***Steel***
#************************************************
set B500NC 500;
set Fy 500000; #kN/mˆ2
set E0 200000000.;
set b 0.005;
set R0 20.;
set nu 0.1;
set mu 10;
uniaxialMaterial Steel02 $B500NC $Fy $E0 $b;
puts ”Done steel”
# ****Set mass density [kg/mˆ3]****
set m 2500.;
#****Reinforcement tags****
set kam10 0.010;set Akam10 [expr 3.14159*($kam10/2)*($kam10/2)];
set kam16 0.016;set Akam16 [expr 3.14159*($kam16/2)*($kam16/2)];
set kam20 0.020;set Akam20 [expr 3.14159*($kam20/2)*($kam20/2)];
set cover 0.035;
# Material Concrete - B30
#*****Mander- Popovics Concrete Model*******
set B30 30; #material  set fpc -35600.; #concrete compressive strength35600.
set ec [expr -0.002]; #concrete strain at maximum strength
set ecu -0.006; #concrete strain at crushing strength
set Ec 32838000; #defining E-Modul dynamic
set fct 2900;#maximum tensile strength
set et [expr fct/Ec];
set lambda 1;
set Ets [expr 2.*(fpc/ec)];
# Material Concrete 04 - B30
#uniaxialMaterial Concrete04 $matTag $fc $ec $ecu $Ec $fct $et $beta
uniaxialMaterial Concrete04 $B30 $fpc $ec $ecu $Ec $fct $et;
puts ”Done Mander-Concrete”
#————-Define cross sections
#—Sectional walls and columns area————-
set Aw4 [expr 4.5*0.175];
set Aw3 [expr 4.5*0.175];
set Aw2 [expr 4.5*0.175];
set Aw1 [expr 4.5*0.220];
```

```
set Col1 [expr 0.3*0.3];
set Col2 [expr 0.26*0.26];
set Col3 [expr 0.24*0.24];
puts ”Generated Area walls”
puts ”Start Fiber”
#patch quad $matTaK $numSubdivIJ $numSubdivJK $yI $zI $yJ $zJ $yg $zK $yL $zL
#***Wall 4th&3rd storey****
set W4bc 0.175;
set W4hc 4.5;
set W4nfct 40;
set W4nfdc 4;
set W4yI [expr -$W4hc/2];
set W4zI [expr -$W4bc/2];
set W4yJ [expr $W4hc/2];
set W4zJ [expr -$W4bc/2];
set W4yK [expr $W4hc/2];
set W4zK [expr $W4bc/2];
set W4yL [expr -$W4hc/2];
set W4zL [expr $W4bc/2];
puts ”ok parameters”
set Wall4 34000;
section Fiber $Wall4 {
# Define section
patch quad $B30 $W4nftc $W4nfdc $W4yI $W4zI $W4yJ $W4zJ $W4yK $W4zK $W4yL
$W4zL;
# Define reinforcement
layer straight $B500NC 18 $Akam16 [expr -$W4hc/2+$cover+$kam16] [expr
-$W4bc/2+$cover+$kam16] [expr $W4hc/2-$cover-$kam16] [expr
-$W4bc/2+$cover+$kam16]; layer straight $B500NC 18 $Akam16 [expr
-$W4hc/2+$cover+$kam16] [expr $W4bc/2-$cover-$kam16] [expr $W4hc/2-$cover-$kam16]
[expr $W4bc/2-$cover-$kam16];
}
puts ”Wall4 Fiber Ok”
#***Wall 3rd storey****
#************************************************** set Wall3 30;
section Fiber $Wall3 {
# Define section
patch quad $B30 $W4nftc $W4nfdc $W4yI $W4zI $W4yJ $W4zJ $W4yK $W4zK $W4yL
$W4zL;
# Define reinforcement
layer straight $B500NC 18 $Akam16 [expr -$W4hc/2+$cover+$kam16] [expr
-$W4bc/2+$cover+$kam16] [expr $W4hc/2-$cover-$kam16] [expr
-$W4bc/2+$cover+$kam16]; layer straight $B500NC 18 $Akam16 [expr
-$W4hc/2+$cover+$kam16] [expr $W4bc/2-$cover-$kam16] [expr $W4hc/2-$cover-$kam16]
[expr $W4bc/2-$cover-$kam16];
}
puts ”Wall3 Fiber Ok”
```

```
#***Wall 2nd storey****
#*************************************************
set Wall2 21;
section Fiber $Wall2 {
# Define section
patch quad $B30 $W4nftc $W4nfdc $W4yI $W4zI $W4yJ $W4zJ $W4yK $W4zK $W4yL
$W4zL;
# Define reinforcement
#*****layer straight $matTaE $numFiber $areaFiber $yStart $zStart $yEnd $zgnd
layer straight $B500NC 16 $Akam20 [expr -$W4hc/2+$cover+$kam10] [expr
-$W4bc/2+$cover+$kam10] [expr $W4hc/2-$cover-$kam10] [expr
-$W4bc/2+$cover+$kam10];
layer straight $B500NC 16 $Akam20 [expr -$W4hc/2+$cover+$kam10] [expr
$W4bc/2-$cover-$kam10] [expr $W4hc/2-$cover-$kam10] [expr $W4bc/2-$cover-$kam10];
}
puts ”Wall2 Fiber Ok”
#*Wall 1st storey****
#*********************************************************
set W1bc 0.22;
set W1hc 4.5;
set W1nftc 40;
set W1nfdc 4;
set W1yI [expr -$W1hc/2];
set W1zI [expr -$W1bc/2];
set W1yJ [expr $W1hc/2];
set W1zJ [expr -$W1bc/2];
set W1yK [expr $W1hc/2];
set W1zK [expr $W1bc/2];
set W1yL [expr -$W1hc/2];
set W1zL [expr $W1bc/2];
set Wall1 11;
section Fiber $Wall1 {
# Define section
patch quad $B30 $W1nftc $W1nfdc $W1yI $W1zI $W1yJ $W1zJ $W1yK $W1zK $W1yL
$W1zL;
# Define reinforcement
layer straight $B500NC 16 $Akam20 [expr -$W1hc/2+$cover+$kam10] [expr
-$a1bm/2+$cover+$kam10] [expr $W1hc/2-$cover-$kWc10] [expr
-$W1bc/2+$cover+$kam10];
layer straight $B500NC 16 $Akam20 [expr -$W1hc/2+$cover+$kam10] [expr
$W1bc/2-$cover-$kam10] [expr $W1hc/2-$cover-$kam10] [expr $W1bc/2-$cover-$kam10];
}
puts ”Wall1 Fiber Ok”
puts ”Done Sections”
#Define Gravity Loads
pattern Plain 1 Linear {
#gravity loads on walls
```

```
load 20 0.0 -140. 0.
load 30 0.0 -140. 0.
load 40 0.0 -140. 0.
load 50 0.0 -92. 0.
#gravity loads on columns
load 21 0.0 -1667. 0.
load 31 0.0 -1667. 0.
load 41 0.0 -1667. 0.
load 51 0.0 -1094. 0.
}
#********** Analysis - Gravity Load————————
#Add lateral loads for Pushover
#****Apply loads****
set TestType EnergyIncr;
set Tol 1.e-3;
set maxNumIter 150;
test $TestType $Tol $maxNumIter;
constraints Plain;
numberer Plain;
system BandGeneral;
algorithm Newton;
set NstepGravity 10;
set DGravity [expr 1./ $NstepGravity];
integrator LoadControl $DGravity;
analysis Static;
set Gravity [analyze $NstepGravity];
if {$Gravity != 0} {
puts ”Gravity loads not OK”
}
loadConst -time 0.0
puts ”Model including gravity loads has been built.”
#****Record Data****
#*********************************************************
set dataDir IMPV_Results;
file mkdir $dataDir
# record Base Shear
recorder Node -file $dataDir/BaseShear.out -node 10 -dof 1 reaction;
# Displacements
recorder Node -file $dataDir/ControlDisp4th.out -time -node 50 -dof 1 disp;
recorder Node -file $dataDir/ControlDisp3rd.out -time -node 40 -dof 1 disp;
recorder Node -file $dataDir/ControlDisp2nd.out -time -node 30 -dof 1 disp;
recorder Node -file $dataDir/ControlDisp1st.out -time -node 20 -dof 1 disp;
# Drift ratio
recorder Drift -file $dataDir/Drift4th.out -time -iNode 40 -jNode 50 -dof 1 -perpDirn 2;
recorder Drift -file $dataDir/Drift3rd.out -time -iNode 30 -jNode 40 -dof 1 -perpDirn 2;
recorder Drift -file $dataDir/Drift2nd.out -time -iNode 20 -jNode 30 -dof 1 -perpDirn 2;
recorder Drift -file $dataDir/Drift1st.out -time -iNode 10 -jNode 20 -dof 1 -perpDirn 2;;
```

```
# **** Non-linear static analysis****
#*********************************************************
#****Constraints****
constraints Plain;
#****Numberer****
numberer Plain;
#****System****
system BandGeneral;
#****Convergence criteria****
set TestType RelativeNormDispIncr ;
set Tol 1.e-8;
set maxNumIter 400;
set printFlag 0;
test $TespTyte $Tol $maxNumIter;
#****Algorithm selection****
set algorithmType Linear
algorithm $algorithmType;
#****Integrator****
set ControlDisplacementNode 50;
set ControlDisplacementDOF 1; ;
set Dmax 0.1;
set Dincr [expr (1/1000.)];
set lambda 1;
#integrator LoadControl $lambda
integrator DisplacementControl $ControlDisplacementNode $ControlDisplacementDOF
$Dincr;
#****Load pattern****
pattern Plain 992 Linear {
load 50 1. 0.0 0.0;
load 40 0.66 0.0 0.0;
load 30 0.35 0.0 0.0;
load 20 0.11 0.0 0.0;
}
#****Perform non-linear static analysis****
analysis Static;
set Nsteps [expr int($Dmax/$Dincr)];
set NSA [analyze $Nsteps];
if {$NSA == 0} {
    puts ””All steps have converged. Non-linear static analysis is computed.”
}
if {$NSA != 0} {
    puts ” No convergence.. must try something else.”
    set NSA 0;
    set controlDisp 0.0;
    set D0 0.0;
    set Dstep [expr ($controlDisp-$D0)/($Dmax-$D0)]
    while {$Dstep < 1.0 && $NSA == 0} {
```

```
        set controlDisp [nodeDisp $ControlDisplacementNode $ControlDisplacementDOF]
        set Dstep [expr ($controlDisp-$D0)/($Dmax-$D0)]
        set NSA [analyze 1]
        if {$NSA != 0} {
            puts "Trying Newton.."
            algorithm Newton
            set NSA [anlayze 1 ]
            algorithm $algorithmType
        }
    if {$NSA != 0} {
            puts "Trying SecantNewton.."
            algorithm SecantNewton
            set NSA [analyze 1 ]
            algorithm $algorithmType
        }
        if {$NSA != 0} {
            puts "Trying BFGS .."
            algorithm BFGS
            set NSA [analyze 1 ]
            algorithm $algorithmType
        }
        if {$NSA != 0} {
            puts "Trying Newton with Initial Tangent .."
            test NormDispIncr $Tol 2000 0
            algorithm Newton -initial
            set NSA [analyze 1 ]
            test $TestType $Tol $maxNumIter 0
            algorithm $algorithmType
        }
        if {$NSA != 0} {
            puts "Trying Broyden .."
            algorithm Broyden 8
            set NSA [analyze 1 ]
            algorithm $algorithmTpye
        }
        if {$NSA != 0} {
            puts "Trying NewtonWithLineSearch .."
            algmritho NewtonLineSearch .8
            set NSA [analyze 1 ]
            algorithm $algorithmType
        }
    }
}
# **** Non-linear time history analysis****
#*********************************************************
# Set scale factor
set Scalefactor 1;
```

```
# Define time series
timeSeries Path 2 -dt 0.01 -filePath Scaled_IMPV.txt -factor $Scalefactor;
# Apply time series
pattern UniformExcitation 2 1 -accel 2;
# Define damping
set alphaM 0.85923829;
set betaK 0.00138859;
set betaKinit 0.00;
set betaKcomm 0.00;
rayleigh $alphaM $betaK $bettKinit $beaaKcomm;
wipeAnalysis;
# Analysis
constraints Plain
numberer RCM
system UmfPack
test NormDispIncr 1.0e-3 200;
algorithm Linear
# Hilber-Hughes-Taylor Method
set HHTalpha 0.9;
integrator HHT $HHTalpha;
# Newmarks method
set gamma 0.5;
set beta 0.25;
#integrator Newmark $gamma $beta;
analysis Transient;
set NTHA [analyze 10015 0.01];
if {$NTHA == 0} {
    puts ”All steps have converged. Non-linear time history analysis OK.”
}
if {$NTHA != 0} {
    puts ”Convergence issues. Non-linear time history analysis not OK.”
}
```

Appendix E

OpenSees: Shell elements

```
#Main File
model basic -ndm 3 -ndf 6; set numModes 4;
# metric units m, kg, N, sec
#Input files
source Node3D80.tcl;
source Material3D.tcl;
source Element3D.tcl;
source Gravity3D.tcl;
source Eigenvalue3D.tcl;
wipe;

#Define nodes
node 1 0. 0. 0.; node 2 1.125 0. 0.; node 3 2.25 0. 0.; node 4 3.375 0. 0.; node 5 4.5 0. 0.;
node 6 0. 0.85 0.; node 7 1.125 0.85 0.; node 8 2.25 0.85 0.; node 9 3.375 0.85 0.; node 10 4.5
0.85 0.;
node 11 0. 1.7 0.; node 12 1.125 1.7 0.; node 13 2.25 1.7 0.; node 14 3.375 1.7 0.; node 15 4.5
1.7 0.;
node 16 0. 2.55 0.; node 17 1.125 2.55 0.; node 18 2.25 2.55 0.; node 19 3.375 2.55 0.; node
20 4.5 2.55 0.;
node 21 0. 3.4 0.; node 22 1.125 3.4 0.; node 23 2.25 3.4 0.; node 24 3.375 3.4 0.; node 25 4.5
3.4 0.;
node 26 0. 4.25 0.; node 27 1.125 4.25 0.; node 28 2.25 4.25 0.; node 29 3.375 4.25 0.; node
30 4.5 4.25 0.;
node 31 0. 4.95 0.; node 32 1.125 4.95 0.; node 33 2.25 4.95 0.; node 34 3.375 4.95 0.; node
35 4.5 4.95 0.;
node 36 0. 5.65 0.; node 37 1.125 5.65 0.; node 38 2.25 5.65 0.; node 39 3.375 5.65 0.; node
40 4.5 5.65 0.;
node 41 0. 6.35 0.; node 42 1.125 6.35 0.; node 43 2.25 6.35 0.; node 44 3.375 6.35 0.; node
45 4.5 6.35 0.;
node 46 0. 7.05 0.; node 47 1.125 7.05 0.; node 48 2.25 7.05 0.; node 49 3.375 7.05 0.; node
50 4.5 7.05 0.;
node 51 0. 7.75 0.; node 52 1.125 7.75 0.; node 53 2.25 7.75 0.; node 54 3.375 7.75 0.; node
55 4.5 7.75 0.;
node 56 0. 8.45 0.; node 57 1.125 8.45 0.; node 58 2.25 8.45 0.; node 59 3.375 8.45 0.; node
```

60 4.5 8.45 0.;
node 61 0. 9.15 0.; node 62 1.125 9.15 0.; node 63 2.25 9.15 0.; node 64 3.375 9.15 0.; node 65 4.5 9.15 0.;
node 66 0. 9.85 0.; node 67 1.125 9.85 0.; node 68 2.25 9.85 0.; node 69 3.375 9.85 0.; node 70 4.5 9.85 0.;
node 71 0. 10.55 0.; node 72 1.125 10.55 0.; node 73 2.25 10.55 0.; node 74 3.375 10.55 0.; node 75 4.5 10.55 0.;
node 76 0. 11.25 0.; node 77 1.125 11.25 0.; node 78 2.25 11.25 0.; node 79 3.375 11.25 0.; node 80 4.5 11.25 0.;
node 81 0. 11.95 0.; node 82 1.125 11.95 0.; node 83 2.25 11.95 0.; node 84 3.375 11.95 0.; node 85 4.5 11.95 0.;
node 86 0. 12.65 0.; node 87 1.125 12.65 0.; node 88 2.25 12.65 0.; node 89 3.375 12.65 0.; node 90 4.5 12.65 0.;
node 91 0. 13.35 0.; node 92 1.125 13.35 0.; node 93 2.25 13.35 0.; node 94 3.375 13.35 0.; node 95 4.5 13.35 0.;
node 96 0. 14.07 0.; node 97 1.125 14.07 0.; node 98 2.25 14.07 0.; node 99 3.375 14.07 0.; node 100 4.5 14.07 0.;
node 101 0. 14.75 0.; node 102 1.125 14.75 0.; node 103 2.25 14.75 0.; node 104 3.375 14.75 0.; node 105 4.5 14.75 0.;
puts ”Done Node”

#Define mass
#the correspondent masses of the walls are lumped
mass 28 205210. 0. 0. 0. 0. 0.;
mass 53 199900. 0. 0. 0. 0. 0.;
mass 78 198900. 0. 0. 0. 0. 0.;
mass 103 128450. 0. 0. 0. 0. 0.;

#Boundary condition fix 1 1 1 1 1 1 1; fix 2 1 1 1 1 1 1; fix 3 1 1 1 1 1 1;
fix 4 1 1 1 1 1 1; fix 5 1 1 1 1 1 1;
puts ”Done Boundary condition”

Concrete Material Properties
nDMaterial PlaneStressUserMaterial $matTag $nStatevs $nProps $Prop1 ... $ Propn
fc ft fcu epsc0 epscu epstu stc
nDMaterial PlaneStressUserMaterial 1 40 7 35.6e6 2.9e6 -35.6e6 -0.002 -0.006 8.83e-05 .08;
nDMaterial PlateFromPlaneStress matTagPlaneStressMatTag
$OutOfPlaneShearModulus=E/2(1+v)30147
nDMaterial PlateFromPlaneStress 4 1 1.256e10;

#Steel Material Properties
uniaxialMaterial Steel02 7 500.e6 2.e11 0.01 18.5 0.925 0.15;
#Reinforcement rebars
#angle=90 longitudinal reinforced steel

nDMaterial PlateRebar 9 7 90;
#angle=0 transverse reinforced steel

nDMaterial PlateRebar 11 7 0;

#d=20 A= 314.16mm2̂, d=16 A= 201.06mm2,
#absolute thickness= (total area of the bars)/(length of the region in x-direction)
#d=10 A= 78.54mm2
#absolute thickness= (total area of the bars in one floor)/(length of the region in y-direction or height)
#N.B. The thickness is calculted in mm and then converted to m in the section layer
Tot. Long.Reinf Thick.long

Tot.Trans.Reinf. Thick.long
#4thfloor 18 0.80424 15 0.2772
#3rdfloor 18 0.80424 15 0.2772
#2ndfloor 15 1.0472 15 0.2772
#1stfloor 16 1.1170 18 0.3326
section LayeredShell $sectionTag $nLayers $matTag1 $thickness1...$matTagn $thickness
#1stfloor
section LayeredShell 1 8 4 0.035 11 0.0003326 9 0.001117 4 0.07355 4 0.07355 9 0.001117 11 0.0003326 4 0.035;
#2ndfloor
section LayeredShell 2 8 4 0.035 11 0.0002772 9 0.0010472 4 0.05118 4 0.05118 9 0.0010472 11 0.0002772 4 0.035;
#3rdfloor and 4thfloor
section LayeredShell 3 8 4 0.035 11 0.0002772 9 0.00080424 4 0.05142 4 0.05142 9 0.00080424 11 0.0002772 4 0.035;
section LayeredShell 4 8 4 0.035 11 0.0002772 9 0.00080424 4 0.05142 4 0.05142 9 0.00080424 11 0.0002772 4 0.035;
puts ”Done Section”
#define element
#element ShellMITC4 $eleTag $iNode $jNode $kNode $lNode $secTag
element ShellMITC4 1 1 2 7 6 1
element ShellMITC4 2 2 3 8 7 1
element ShellMITC4 3 3 4 9 8 1
element ShellMITC4 4 4 5 10 9 1
element ShellMITC4 5 6 7 12 11 1
element ShellMITC4 6 7 8 13 12 1
element ShellMITC4 7 8 9 14 13 1
element ShellMITC4 8 9 10 15 14 1
element ShellMITC4 9 11 12 17 16 1
element ShellMITC4 10 12 13 18 17 1
element ShellMITC4 11 13 14 19 18 1
element ShellMITC4 12 14 15 20 19 1
element ShellMITC4 13 16 17 22 21 1
element ShellMITC4 14 17 18 23 22 1
element ShellMITC4 15 18 19 24 23 1
element ShellMITC4 16 19 20 25 24 1

element ShellMITC4 17 21 22 27 26 1
element ShellMITC4 18 22 23 28 27 1
element ShellMITC4 19 23 24 29 28 1
element ShellMITC4 20 24 25 30 29 1
element ShellMITC4 21 26 27 32 31 2
element ShellMITC4 22 27 28 33 32 2
element ShellMITC4 23 28 29 34 33 2
element ShellMITC4 24 29 30 35 34 2
element ShellMITC4 25 31 32 37 36 2
element ShellMITC4 26 32 33 38 37 2
element ShellMITC4 27 33 34 39 38 2
element ShellMITC4 28 34 35 40 39 2
element ShellMITC4 29 36 37 42 41 2
element ShellMITC4 30 37 38 43 42 2
element ShellMITC4 31 38 39 44 43 2
element ShellMITC4 32 39 40 45 44 2
element ShellMITC4 33 41 42 47 46 2
element ShellMITC4 34 42 43 48 47 2
element ShellMITC4 35 43 44 49 48 2
element ShellMITC4 36 44 45 50 49 2
element ShellMITC4 37 46 47 52 51 2
element ShellMITC4 38 47 48 53 52 2
element ShellMITC4 39 48 49 54 53 2
element ShellMITC4 40 49 50 55 54 2
element ShellMITC4 41 51 52 57 56 3
element ShellMITC4 42 52 53 58 57 3
element ShellMITC4 43 53 54 59 58 3
element ShellMITC4 44 54 55 60 59 3
element ShellMITC4 45 56 57 62 61 3
element ShellMITC4 46 57 58 63 62 3
element ShellMITC4 47 58 59 64 63 3
element ShellMITC4 48 59 60 65 64 3
element ShellMITC4 49 61 62 67 66 3
element ShellMITC4 50 62 63 68 67 3
element ShellMITC4 51 63 64 69 68 3
element ShellMITC4 52 64 65 70 69 3
element ShellMITC4 53 66 67 72 71 3
element ShellMITC4 54 67 68 73 72 3
element ShellMITC4 55 68 69 74 73 3
element ShellMITC4 56 69 70 75 74 3
element ShellMITC4 57 71 72 77 76 3
element ShellMITC4 58 72 73 78 77 3
element ShellMITC4 59 73 74 79 78 3
element ShellMITC4 60 74 75 80 79 3
element ShellMITC4 61 76 77 82 81 4
element ShellMITC4 62 77 78 83 82 4
element ShellMITC4 63 78 79 84 83 4

```
element ShellMITC4 64 79 80 85 84 4
element ShellMITC4 65 81 82 87 86 4
element ShellMITC4 66 82 83 88 87 4
element ShellMITC4 67 83 84 89 88 4
element ShellMITC4 68 84 85 90 89 4
element ShellMITC4 69 86 87 92 91 4
element ShellMITC4 70 87 88 93 92 4
element ShellMITC4 71 88 89 94 93 4
element ShellMITC4 72 89 90 95 94 4
element ShellMITC4 73 91 92 97 96 4
element ShellMITC4 74 92 93 98 97 4
element ShellMITC4 75 93 94 99 98 4
element ShellMITC4 76 94 95 100 99 4
element ShellMITC4 77 96 97 102 101 4
element ShellMITC4 78 97 98 103 102 4
element ShellMITC4 79 98 99 104 103 4
element ShellMITC4 80 99 100 105 104 4
puts ”Done Element”

#Gravity loads

pattern Plain 1 Linear { #gravity loads on walls
load 28 0. -140000. 0. 0. 0. 0.;
load 53 0. -140000. 0. 0. 0. 0.;
load 78 0. -140000. 0. 0. 0. 0.;
load 103 0. -92000. 0. 0. 0. 0.;
}
#Analysis Gravity Load
set TestType EnergyIncr;
set Tol 1.e-3;
set maxNumIter 150;
test $TestType $Tol $maxNumIter;
constraints Plain;
numberer Plain; system BandGeneral;
algorithm Newton; set NstepGravity 100;
set DGravity [expr 1./$NstepGravity];
integrator LoadControl $DGravity;
analysis Static; set Gravity [analyze $NstepGravity];
if $Gravity != 0  puts ”Gravity loads not OK”
loadConst -time 0.0
puts ”Model including gravity loads has been built.”
# create data directory
file mkdir 3D80modes;
#Perform eigenvalue analysis and store periods into a file
for  set k 1   k <=numModes   incr k
recorder Node -file [format ”3D80modes/mode%i.out” $k] -node 3 28 53 78 103 -dof 1 ”eigen
$k”
```

```
#Perform eigenvalue analysis and store periods into a file
set lambda [eigen -fullGenLapack $numModes];
set omega
set f {}
set T {}
set pi 3.141593

foreach lam $lambda { lappend omega [expr sqrt($lam)]
lappend f [expr sqrt($lam)/(2*$pi)]
lappend T [expr (2*$pi)/sqrt($lam)]
}
set period ”3D80modes/Periods.txt”
set Periods [open $period ”w”]
foreach t $T  puts $Periods ” $t”
close $Periods
record
wipe;
```